# REPORT DOCUMENTATION PAGE

AFRL-SR-BL-TR-99-

0217



| 1. AGENCY USE ONLY (Leave blank) | 2. REPORT DATE | 3. REPORT TYPE AND DATES COVERED |
|---|---|---|
| | 23 August 1999 | Technical 1 June 1998 - 31 May 1999 |

**4. TITLE AND SUBTITLE**
(U) ARO and AFOSR Contractors Meeting in Chemical Propulsion

**5. FUNDING NUMBERS**
PE - 61102A
61102F

**6. AUTHORS**
David M. Mann and Julian M. Tishkoff

**7. PERFORMING ORGANIZATION NAME(S) AND ADDRESS(ES)**
Army Research Office
Research Triangle Park NC 27709-2211

Air Force Office of Scientific Research
Arlington VA 22203-1977

**8. PERFORMING ORGANIZATION REPORT NUMBER**

**9. SPONSORING / MONITORING AGENCY NAME(S) AND ADDRESS(ES)**

**10. SPONSORING / MONITORING AGENCY REPORT NUMBER**

**11. SUPPLEMENTARY NOTES**

**12a. DISTRIBUTION / AVAILABILITY STATEMENT**
Approved for public release; distribution is unlimited

**12b. DISTRIBUTION CODE**

**13. ABSTRACT** *(Maximum 200 Words)*

Abstracts are given for 6.1 basic research in chemical propulsion supported by the Army Research Office and the Air Force Office of Scientific Research.

19990927 129

**14. SUBJECT TERMS**
Flames, Propulsion, Gas Turbines, Diesel Engines, Scramjets, Ram Accelerators, Turbulence, Diagnostics, Simulation

**15. NUMBER OF PAGES**
179

**16. PRICE CODE**

| 17. SECURITY CLASSIFICATION OF REPORT | 18. SECURITY CLASSIFICATION OF THIS PAGE | 19. SECURITY CLASSIFICATION OF ABSTRACT | 20. LIMITATION OF ABSTRACT |
|---|---|---|---|
| Unclassified | Unclassified | Unclassified | UL |

# ARO/AFOSR CONTRACTORS' MEETING

## IN

# CHEMICAL PROPULSION

**Holiday Inn Sunspree Resort**
**Bar Harbor, ME**
**13-16 June 1999**

## SUNDAY, 13 JUNE

2:00 - 5:00 OPEN DISCUSSIONS – Dr. Mann and Dr. Tishkoff will be available for informal interactions

## MONDAY, 14 JUNE

8:00 – 8:15 Air Force Welcome and Introduction – Julian Tishkoff

8:15 - 8:30 Army Welcome and Introduction – David Mann

Session Chairman: Dr. Tim Edwards, AFRL/PRSF

Topic: High Speed Propulsion/Energetic Materials

8:30 - 9:00 High Resolution Measurements of Supersonic Mixing and Combustion in Coflowing Turbulent Jets
W.J.A. Dahm and J.F. Driscoll, The University of Michigan

9:00 - 9:30 Reacting, Compressible Flow Research
T.A. Jackson, AFRL/PRSS

9:30 - 10:15 Chemical Reactions in Turbulent Mixing Flows
P.E. Dimotakis and A. Leonard, California Institute of Technology

10:15 – 10:45 BREAK

10:45 – 11:15 Shock Tube Studies of Ram Accelerator Phenomena
R.K. Hanson, Stanford University

| | |
|---|---|
| 11:15 – 11:45 | Flame Structure of Combusting Liquid Gun Propellants<br>K. Kuo, The Pennsylvania State University |
| 11:45 – 12:15 | Experimental Study of Plasma/Propellant Interactions<br>S. Thynell, The Pennsylvania State University |
| 12:15 – 12:45 | Modeling of Physical Processes<br>J. Buckmaster, University of Illinois – Urbana-Champaign |
| 12:45 - 7:30 | Open Interactions |
| 7:30 - 9:30 | DISCUSSION – The Future of Combustion Research |

## TUESDAY, 15 JUNE

| | |
|---|---|
| 8:15 - 8:30 | Announcements |

Session Chairman: Dr. Gabriel Roy, Office of Naval Reserach

Topic: Turbulent Reacting Flow

| | |
|---|---|
| 8:30 - 9:00 | Combustion Research<br>W.M. Roquemore, AFRL/PRSC |
| 9:00 - 9:30 | Mixing Studies for Gas Turbine Combustors<br>A. Glezer, J. Jagoda, G. Seitzman, and B.T. Zinn,<br>Georgia Institute of Technology |
| 9:30 - 10:00 | Chemically Reacting Shear Layer I: An Experimental Study Using Hydrogen Fuels<br>J. Ghandhi, University of Wisconsin-Madison |
| 10:00 - 10:30 | BREAK |
| 10:30 - 11:00 | Two- and Three-Dimensional Measurements in Flames<br>M. B. Long, Yale University |
| 11:00 - 11:45 | Studies on High Pressure and Unsteady Flame Phenomena<br>C.K. Law, Princeton University |
| 11:45 - 12:15 | Particle Image Velocity Measurements of In-Cylinder Flows and Correlation With Engine Combustion Behavior<br>J. Martin, University of Wisconsin-Madison |

12:15 - 1:30 LUNCH

TOPIC: Computational Combustion

1:30 - 2:00 Modeling Mixing and Reaction in Turbulent Combustion
S.B. Pope, Cornell University

2:00 - 2:30 Chemically Reacting Shear Layer II: A DNS Study of Turbulent Transport
C. Rutland, University of Wisconsin-Madison

2:30 - 3:00 Evaluation of Closure Models for Turbulent Diffusion Flames
G. Kosaly and J.J. Riley, University of Washington

3:00 - 3:30 BREAK

3:30 - 4:00 LES Simulations of Gas Turbine Combustors
S. Menon, Georgia Institute of Technology

4:00 - 4:30 Compressible Turbulent Reactive Flows
F.A. Williams, P.A. Libby, and S. Sarkar
University of California, San Diego

## WEDNESDAY, 16 JUNE

8:15 - 8:30 Announcements

Topic: Diesel Engine Combustion

8:30 - 9:00 Large Eddy Simulations of Diesel Combustion
I.B. Celik, West Virginia University

9:00 - 9:30 Direct Injection Diesel Emissions and Performance Modeling
A. M. Mellor, Vanderbilt University

9:30 - 10:00 Advanced Engine Control for Military Diesel Engines
C. Atkinson, West Virginia University

10:00 – 10:30 BREAK

| | |
|---|---|
| 10:30 – 11:00 | BUSINESS SESSION - Contractors in Dr. Mann's Program Only |
| 11:00 – 12:00 | BUSINESS SESSION - Contractors in Dr. Tishkoff's Program Only |
| 12:00 | ADJOURN |

# AFOSR SPONSORED RESEARCH IN COMBUSTION AND DIAGNOSTICS


## PROGRAM MANAGER: JULIAN M. TISHKOFF

**AFOSR/NA**
**801 North Randolph Street, Room 732**
**Arlington VA 22203-1977**



**SUMMARY/OVERVIEW**: The Air Force Office of Scientific Research (AFOSR) program in combustion and diagnostics currently is focused on six areas of study: supersonic combustion, turbulent combustion, soot, sprays, kinetics, and supercritical fuel behavior. An assessment of major research needs in each of these areas is presented.


## TECHNICAL DISCUSSION

AFOSR is the single manager for Air Force basic research, including efforts based on external proposals and in-house work at the Air Force Research Laboratory (AFRL). Combustion and Diagnostics is assigned to the AFOSR Directorate of Aerospace and Materials Sciences along with programs in rocket and space propulsion, fluid and solid mechanics, and structural materials.

Interests of the AFOSR Combustion and Diagnostics subarea are given in the SUMMARY section above. Many achievements can be cited for these interests, yet imposing fundamental research challenges remain. The objective of the program is publications in the refereed scientific literature describing significant new understanding of multiphase turbulent reacting flow. Incremental improvements to existing scientific approaches, hardware development, and computer codes fall outside the scope of this objective.

Decisions on support for research proposals are based on scientific opportunities and technology needs. Proposals are submitted for panel review. Therefore, researchers interested in submitting proposals should contact Dr. Tishkoff for information on time constraints associated with proposal evaluations. Further information on research interests and proposal preparation can be found on the AFOSR web site, http://www.afosr.af.mil.

The Combustion and Diagnostics subarea reflects a new Air Force commitment to support space science and technology. Accordingly, the research in this subarea will address research issues related to chemical propulsion for all Air Force aerospace missions, including combined cycle propulsion for access to space. This program will complement related research activities in space propulsion and energetic materials.

Future airbreathing propulsion systems will require fuels to absorb substantial thermal energy, raising fuel temperatures to supercritical thermodynamic conditions. Understanding and controlling fuel properties at these conditions will be crucial for avoiding thermal degradation and for optimizing subsequent processes within the combustor. Environmental concerns and the availability of petroleum supplies also will contribute to future propulsion system design and operational needs.

Designing propulsion systems that will offer reliability, maintainability and long service life represents a new motivation for propulsion research. Future budgets likely will dictate the acquisition of reduced quantities of new operational aerospace vehicles, with a corresponding increase in requirements for durability. Research topics such as soot and supercritical fuel behavior will be relevant to these new service constraints.

Beginning in fiscal year 1997 AFOSR and the Air Force Scientific Advisory Board established priority research areas to support future Air Force Technology under the New World Vistas (NWV) program. One of the research topics in New World Vistas is Hypersonics. Specific thrusts in Hypersonics address the impact of weakly ionized flows on hypersonic vehicle performance, including combustion, and the utilization of hydrocarbon fuels. Another NWV topic involving propulsion is Family of UAV (uninhabited aerial vehicles).

The availability funds places a major constraint on program redirection and growth. Figure 1 shows the recent trend of funding for basic research in combustion and diagnostics from Air Force and DOD sources. Funding in the next fiscal year (FY 2000) is expected to be roughly the same as that for FY 1999. Funding reductions are expected in the following year, F Y2001.

The purpose of this abstract has been to communicate AFOSR perceptions of research trends to the university and industrial research communities. However, communication from those communities back to AFOSR also is desirable and essential for creating new research opportunities. Therefore, all proposals and inquiries for fundamental research are encouraged even if the content does not fall within the areas of emphasis described herein. Comments and criticisms of current AFOSR programs also are welcome.

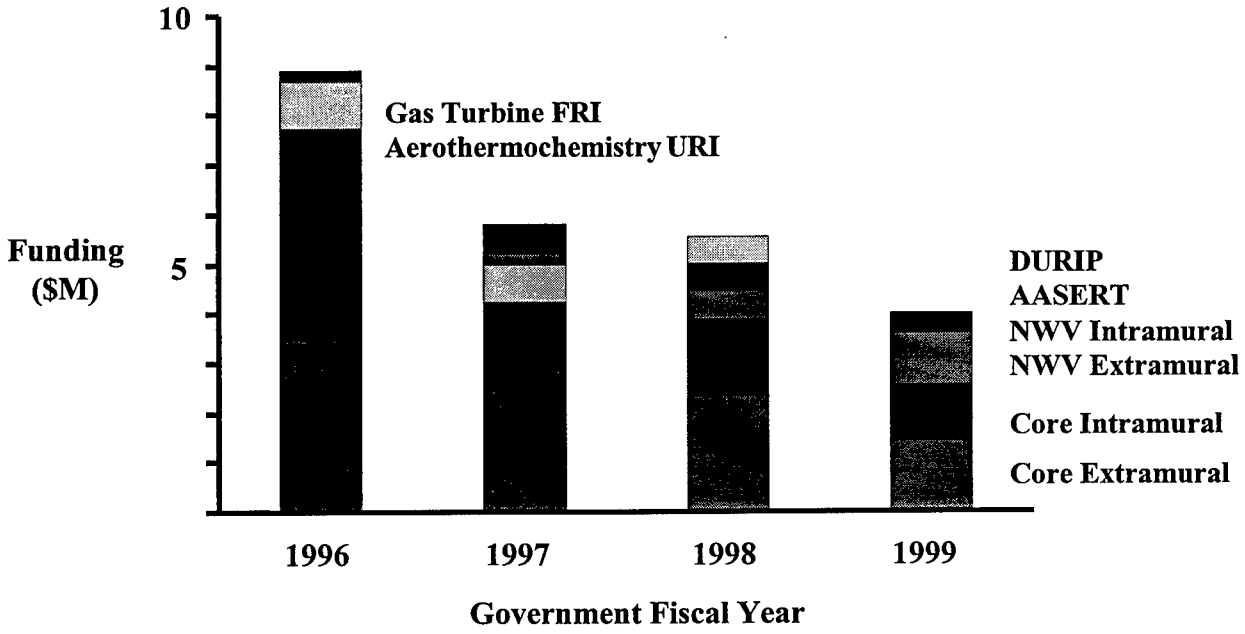


Figure 1. Research Funding History

## US Army Research Office
## COMBUSTION AND PROPULSION RESEARCH

David M. Mann
Associate Director, Engineering Sciences Directorate
Mechanics and Environmental Sciences Division

Combustion and propulsion research supports the Army's need for higher performance propulsion systems. These systems must also provide reduced logistics burden (lower fuel/propellant usage) and longer life than today's systems. Fundamental to this area are the extraction of stored, chemical energy and the conversion of that energy into useful work, for vehicle and projectile propulsion. In view of the high temperature and pressure environments encountered in these combustion systems, it is important to advance current understanding of fundamental processes as well as to advance the ability to make accurate, detailed measurements for the understanding of the dominant physical processes and the validation of predictive models. Thus, research in this area is characterized by a focus on high pressure, high temperature combustion processes and on the peculiarities of combustion behavior in systems of Army interest.

Ground and air vehicle propulsion relies on reciprocating (Diesel) and gas turbine engines. These engines must be capable of delivering high power with high fuel efficiency. These thrusts, power density and efficiency, are the heart of the Army's initiative for a Fuel Efficient Army After Next. The development of reliable, predictive models for vehicle engines will require advances in understanding fundamental processes, such as turbulent flame structure, heat transfer, and chemical kinetics, as well as understanding and control of the complex chain of fuel injection-atomization-ignition-combustion processes. An additional complication is presented by the high pressure/temperature environment, encountered in Diesel engines, which influences liquid behavior and combustion processes at near-critical and super-critical conditions. It should be noted that over 95% of Army vehicles are diesel-powered and that the Army desires the capability to use a single, logistics fuel in all engines, both diesel and turbine.

Gun propulsion relies on the rapid, controlled release of energy from high energy density propellants, which exhibit unique combustion characteristics. Modern composite, solid propellants are characterized by a complex, multi dimensional flame structure, with solid, liquid, liquid-gas, and gas phase reaction zones. The small scales of the combustion zones, typically on the order of tens of microns, and the high pressures, up to 100,000 psi, present formidable challenges for combustion diagnostics. There are systems whose future development requires new directions in combustion research. Among these is the electrothermal-chemical (ETC) gun, in which the ignition, and potentially combustion control, of solid propellant is achieved by high temperature plasmas. An underlying concern with all high energy density systems is the hazard and system vulnerability posed by the propellant. Thus, research is also needed to determine the response of these materials to inadvertent ignition stimuli and factors controlling undesired combustion behavior, such as pressure oscillations.

A recent, Army-wide Mechanics Research Coordinating Group report recommended the following areas of emphasis for the Army's research program:

Turbine Engine Propulsion Research
- Critical Processes for Small Gas Turbine Engines
- Active Control of Combustion and Dynamics in Small Turbine Engines

Reciprocating Engine Research
- Thermal Management in Ultra-Low Heat Rejection Combustion Environments
- Active Air/Fuel Management
- Cold Start Phenomena

Solid Gun Propulsion
- Ignition and Combustion Dynamics of Solid Gun Propellants
- High Performance Solid Propellant Charge Concepts

Alternative Gun Propulsion
- Novel Approaches
- Liquid Propulsion (LP)

Copies of the report, providing more detail on each of the above areas, are available from the Army Research Office.

# HIGH RESOLUTION MEASUREMENTS OF SUPERSONIC SHEAR FLOW MIXING AND COMBUSTION

AFOSR Grant No. F49620-98-1-0003

Werner J.A. Dahm and James F. Driscoll

*Laboratory for Turbulence & Combustion (LTC)*
*Department of Aerospace Engineering*
*The University of Michigan*
*Ann Arbor, MI 48109-2140*

## Summary/Overview

Achieving supersonic mixing and combustion while maintaining acceptable flame stability characteristics and emissions of trace chemical species are key to the development of improved airbreathing propulsion systems. The present investigation contributes to this objective by making high-resolution imaging measurements of the physical structure of supersonic mixing and combustion in turbulent shear flows.

The work consists of two major parts. The first part is an investigation of the outer-scale properties of mixing and combustion in a supersonic shear flow facility. Emphasis is on measuring changes in the large-scale structure and growth rate of a two-dimensional supersonic turbulent shear flow due to compressibility effects, and comparing with previous results from supersonic mixing layers obtained by other investigators. Comparisons with the mixing layers results allow identification of the effects of compressibility that are generic to all supersonic turbulent shear flows. The second major part of this work investigates the highy-resolved multi-dimensional structure of molecular mixing and chemical reaction in subsonic and supersonic turbulent shear flows. These measurements permit new insights to be gained into the fundamental issues that dominate the coupling between turbulent flow, molecular mixing, and nonequilibrium reaction chemistry in turbulent combustion systems.

## Technical Discussion

During the past year we have obtained new experimental results for the outer-scale properties and large-scale structure of supersonic turbulent jets operating in the wake mode in the facility shown in Fig. 1. Typical results are shown in Figs. 2-4. Emphasis in our work is now being placed on the near-field structure and dynamics of the flow, and the experimental facility is being converted to allow detailed investigations in this part of the surpersonic flow field.

A supersonic hydrogen-air flame was stabilized in a Mach 2.5 airstream and images (e.g. Figs. 5-6) were obtained of the OH structure as well as the instantaneous fuel concentration using acetone PLIF imaging measurements. The hydrogen was injected at Mach 1.0 in the direction parallel to the airflow. It was observed that the structure of the supersonic nonpremixed flame is different from that of a typical subsonic nonpremixed flame. The supersonic coflow causes both a lifting of the flame base and intense, small scale fuel-air mixing upstream of the lifted flame, with the supersonic flame observed to have the general nature of a partially-premixed flame. The resulting flame has an early occurrence (8 axial diameters) of centerline OH and an open flame tip similar to a premixed V-shaped flame. The supersonic flames experience more intense mixing than the subsonic flames, as evidenced by the rapid decay of fuel concentration on the centerline and the early upstream occurrence of OH production on the centerline. Several archival publications documenting these new insights have resulted from this work.

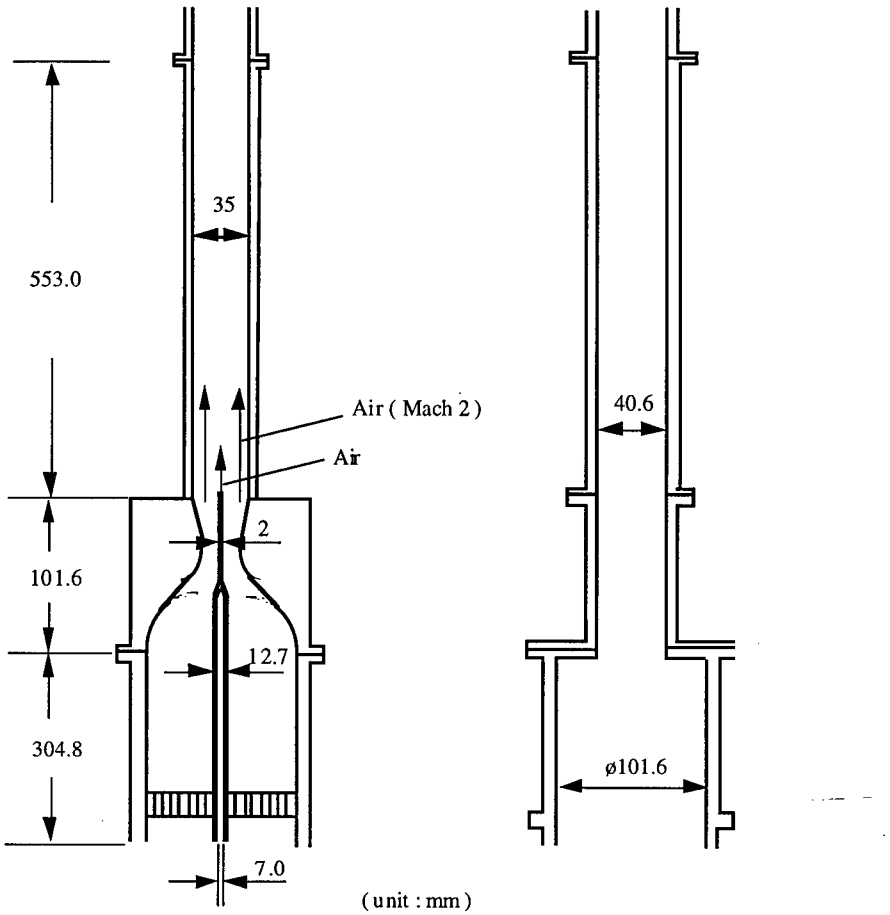


Fig. 1. Schematic of the supersonic combustion facility used for these experiments on two-dimensional supersonic turbulent wake flows, showing front view *(left)* and side view *(right)*. Figures 2 – 4 show wave patterns, wall pressures, large-scale structure, and flow profiles at various downstream locations in the flow.

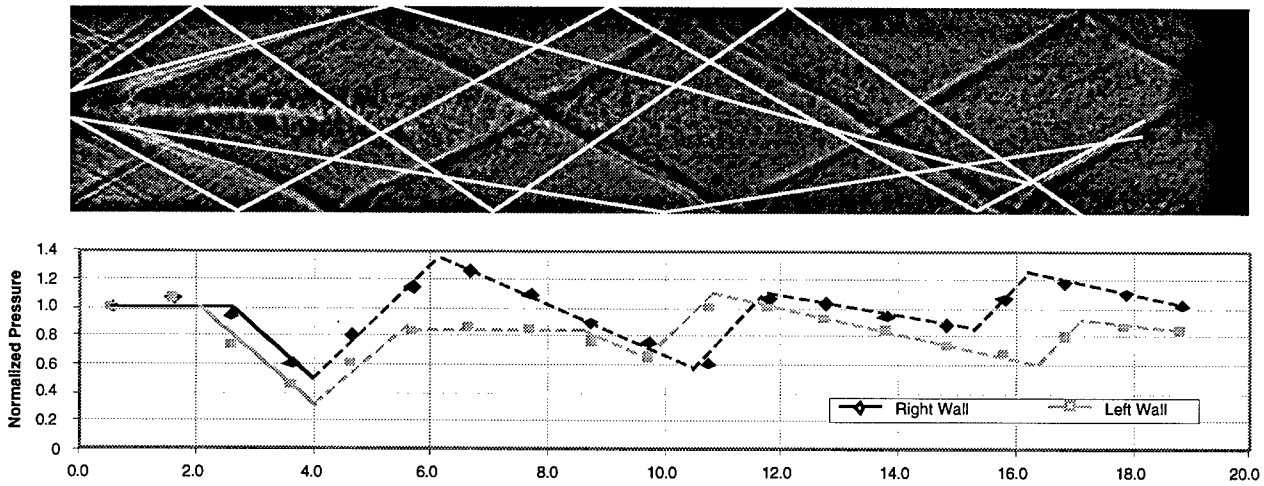


Fig. 2. Reconcilliation of wave patterns in shadowgraph image *(top)* with wall pressure distributions *(bottom)*, indicating leading and trailing waves of expansion fans together with Mach waves and shock patterns in shadowgraph. Lines in lower panel are wall pressure distributions inferred from wave pattern, showing good agreement with measured distributions.

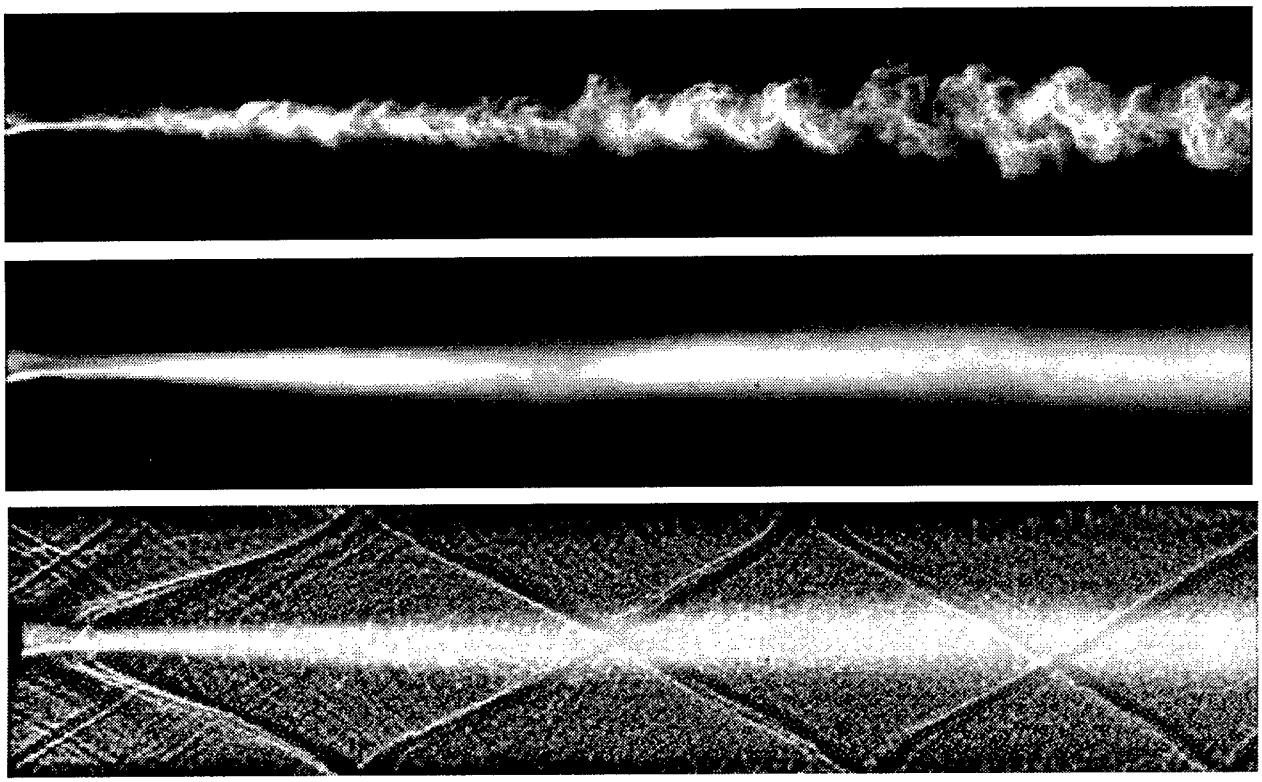

Fig. 3. Typical results for outer-scale properties obtained in the two-dimensional supersonic turbulent shear flow, showing instantaneous mixing regions and large-scale structure as visualized by alcohol fog technique *(top)*, ensemble average *(middle)* showing effects of waves, and shadowgraph *(bottom)* showing wave interactions.

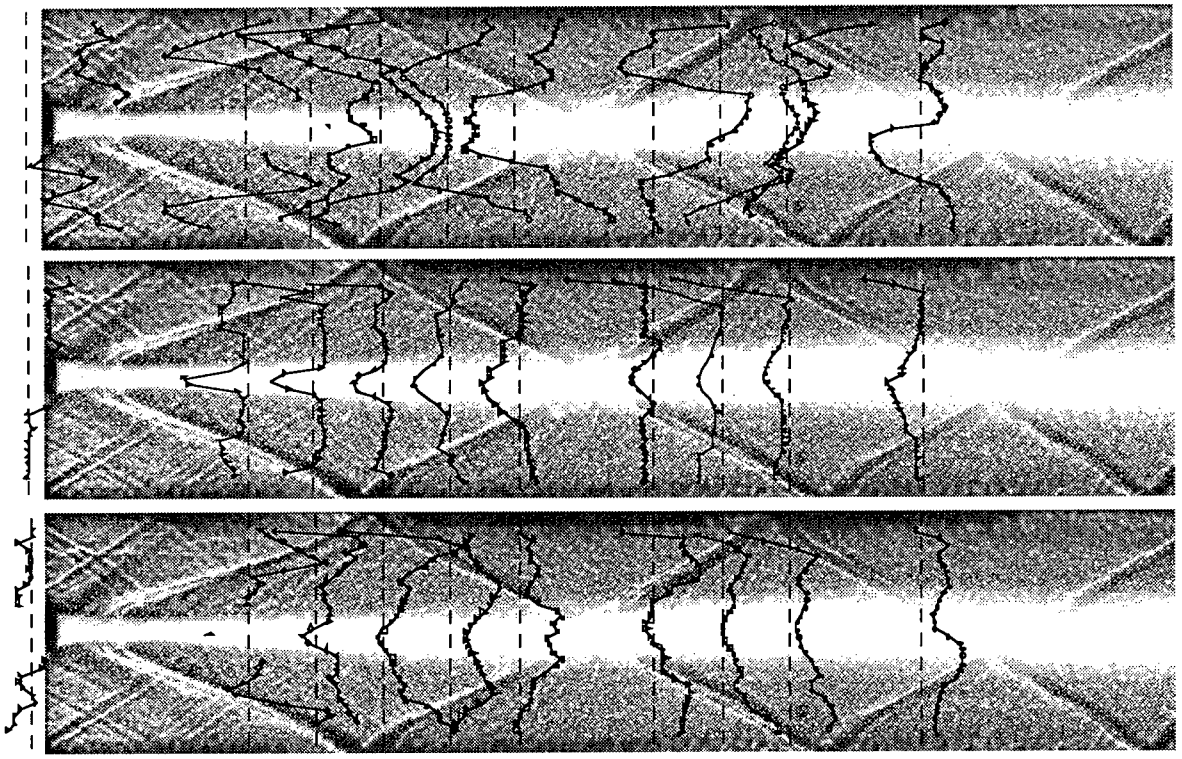

Fig. 4. Flow field surveys in the two-dimensional supersonic turbulent shear flow, showing *(top)* static pressure profiles across the flow, with dashed line giving 70 kPa reference; *(middle)* pitot pressure profiles with dashed line giving 300 kPa reference; *(bottom)* Mach number profiles with dashed line giving M = 1.5 reference.

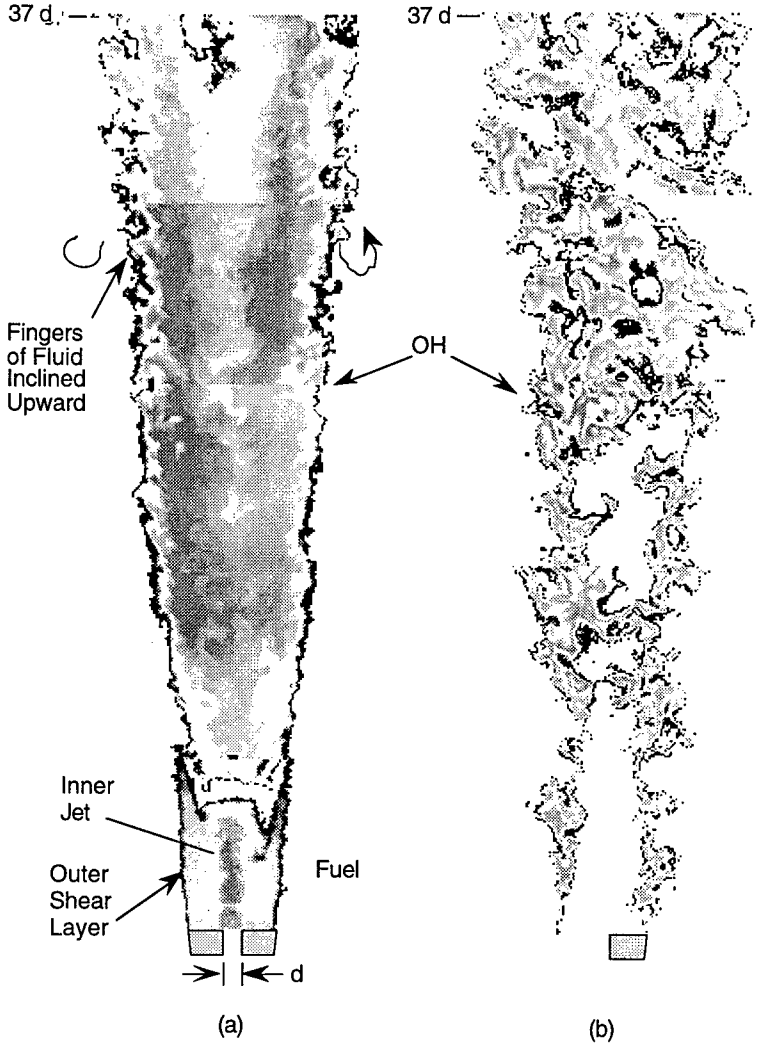


Fig. 5. Instantaneous structure of the OH reaction zone and the fuel concentration field for *(a)* the supersonic flame with coflow air stream at $M_\infty$ = 2.5, and *(b)* the subsonic flame with coflow air stream at $U_\infty$ = 92.7 m/s. Lower region of supersonic flame on left shows fuel concentration. Fuel is hydrogen in both cases. Viewing region is 37 exit diameters in both cases. Flame lengths differ significantly.

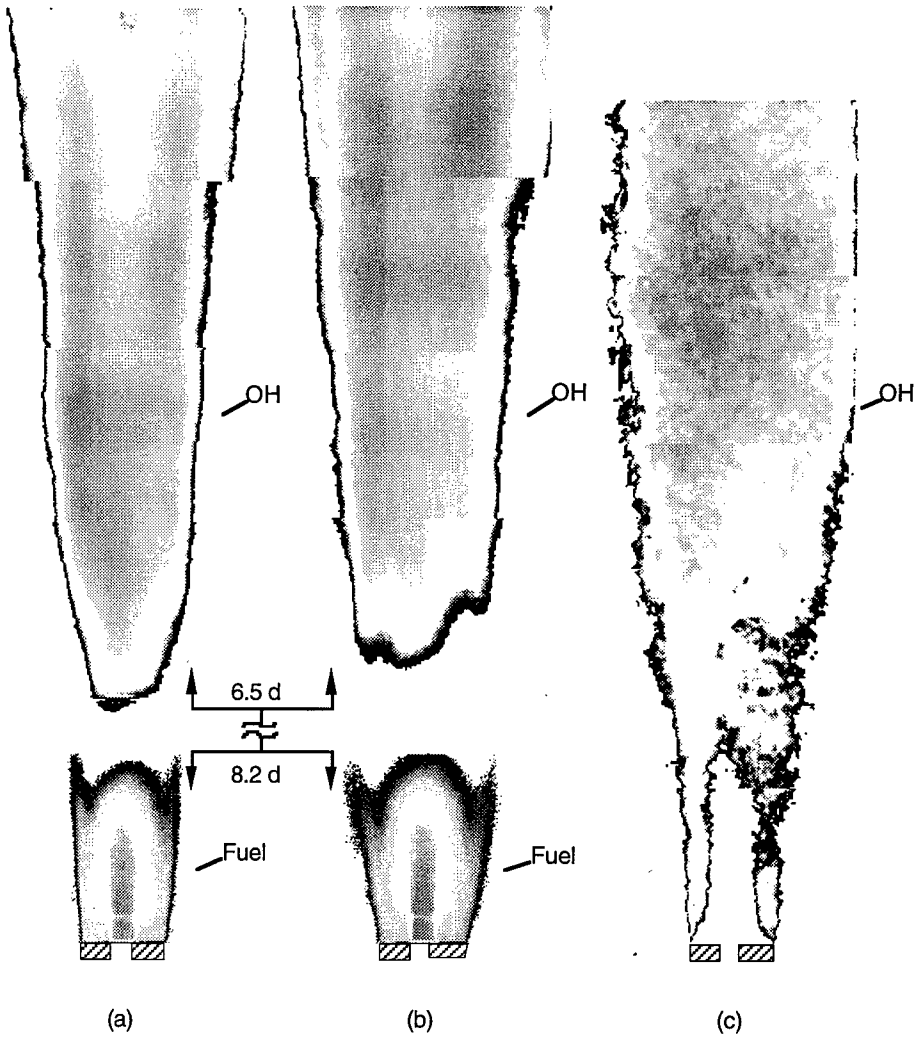


Fig. 6. Averages of 100 images for each of the flames in Fig. 5, showing the supersonic flame with fuel flow rate of *(a)* 0.95 g/s, and *(b)* 1.4 g/s, and *(c)* the subsonic flame with fuel flow rate of 0.83 g/s. For the supersonic flames, the mean OH and fuel conentration fields overlap in the region of 6 - 8 axial diameters. The length of the viewing region is 37 diameters for all three flames.

**Reacting, Compressible Flow Research**
**AFOSR TASK 2308BW**

Principal Investigators: Thomas A. Jackson
Mark R. Gruber

Propulsion Sciences and Advanced Concepts Division
Propulsion Directorate
Air Force Research Laboratory
Wright Patterson AFB OH 45433

## SUMMARY OVERVIEW

This research task addresses relevant technical issues associated with the fuel-air mixing processes in subsonic and supersonic flows, and the role of turbulent transport in mixing and reaction within ramjet and scramjet combustion systems. We have focused our research into three areas: (1) fuel injection and attendant issues of mixing and flame spreading, (2) shock-boundary layer interaction, and (3) non-intrusive measurements in reacting flows. With a large-scale scramjet research facility becoming operational approximately one year ago, we are making a concerted effort to couple our scramjet development effort with this research task. In each of the three research areas we will outline progress and the extent to which the effort has evolved in light of technology shortfalls surfacing in developing a scramjet. In the fuel injection area we have focused considerable attention on liquid/gas co-flow injection into a supersonic cross flow and will describe that work in more detail.

The large-scale scramjet combustion research facility (a.k.a., Room 22) was ready for combustion testing in mid-1998. The facility and test articles are well instrumented and inflow conditions are well documented. [1] The intent of the facility is to incorporate and evaluate technology arising from our research and that of the broader community. Fuel injection and flame piloting are accomplished with minimal intrusion into the flow. Inlet-combustor isolation is accomplished with a long constant area section. Combustor geometry is fixed, but designed for a flight Mach number range of 4 to 7.5. Optical access is extensive.

In the baseline combustor (Figure 1) gaseous ethylene is injected through 4 angled, circular injectors (15° off the combustor floor) positioned upstream of a simple cavity flame holder. The device has been tested with ethylene to an equivalence ratio ($\phi$) of 0.75, and from $\phi = 0.45$ to 0.75 the combustor will light with only a simple spark igniter, establish a strong pre-combustion shock system, and spread flame at approximately twice the injection angle (Figure 2). Initial comparisons of these experimental results with flow modeling [2] indicated that the simulation under-predicted the fuel and flame spreading. However, recent measurements of OH-radical concentration in the region over the cavity and near its

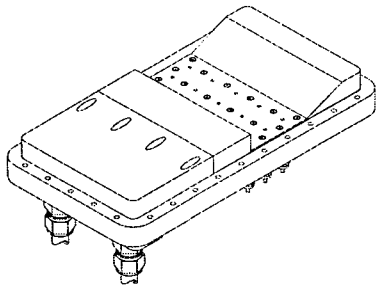

Figure 1. Baseline cavity

closeout surface suggest that initial line-of-sight observations, such as those in Figure 2, did not adequately reveal the spatial variations within the reaction zone. One sequence of OH images is presented in Figure 3. In these images the spanwise origin is the combustor sidewall and the field-of-view is approximately 70% of the flowpath width. Images are recorded at approximately 3 Hz and no attempt has been made to extract any frequency information from the flow measurements. These random shots depict a very unsteady combustion process with substantial spatial variations. Consistently, however, the vertical extent of the flame is higher near the combustor walls than it is in the center. The modeling was performed on a center slice and did not account for wall effects. In a back-pressured, largely subsonic flow, wall effects on flame spreading appear substantial.

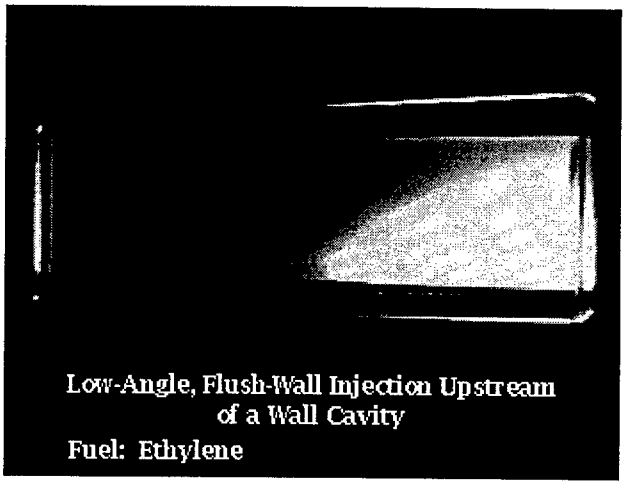


Figure 2. Baseline cavity at Mach 4; $\phi = 0.75$

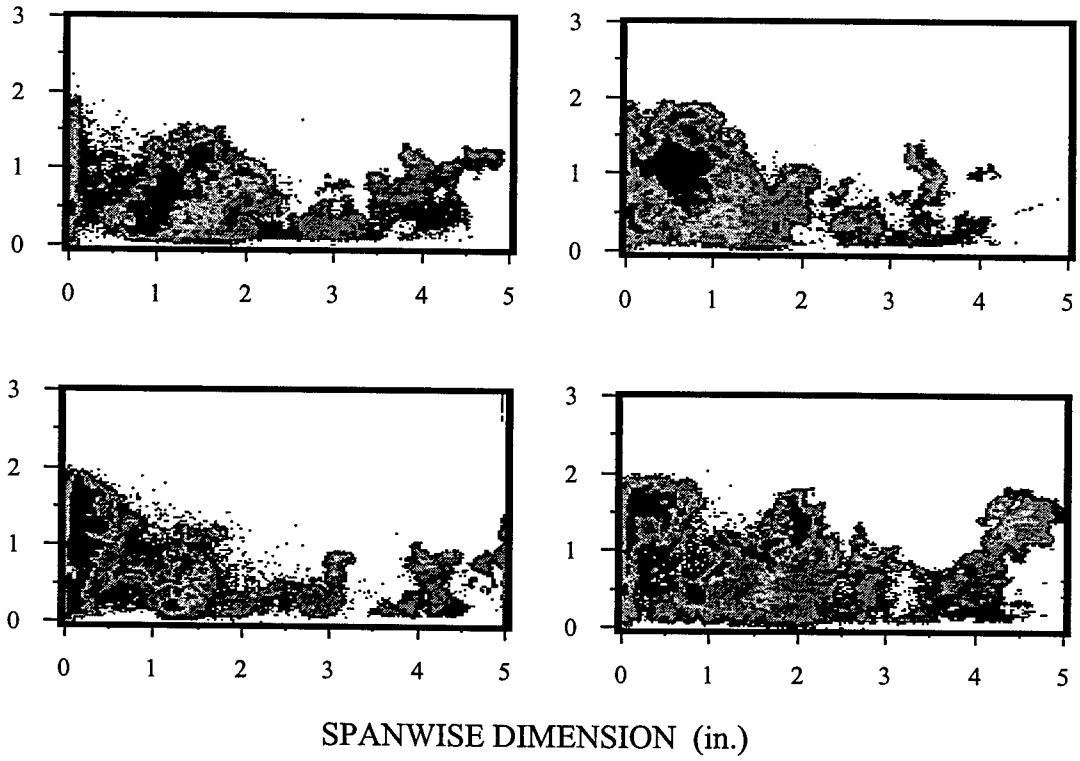


Figure 3. Instantaneous OH images transverse to the combustor flow at cavity closeout, M=4, Q=1000PSF, $T_{in}$=1800R.

The behavior of the ethylene-fueled, baseline combustor and our ability to predict or model it has influenced the direction of this research task. The ignition of the combustor at Mach 4 is reliable, except when we install a low-leakage seal between the combustor and the calorimeter. Modeling ignition has required the artificial addition of heat in the free stream over and above the heat generated by the cavity flame. The leakage of air at the combustor exit, 18 L/H downstream of the pilot, affects ignition in this supersonic flow. The low angled injectors are very effective at spreading fuel. The stability of the cavity pilot, however, is affected by the fuel it entrains from the four main injectors. Variations in fuel flow or inlet Mach number influence the cavity stoichiometry and its effectiveness. The cavity could be fueled separately and removed from the influence of the mains. However, coupling of the pilot with the main fuel flow then becomes the problem. It is our intent to develop a more fundamental understanding of the interactions among the cavity geometry, shock structure, and fuel entrainment. [3-6] Non-intrusive diagnostic tools continue to play a pivotal role in high speed, reacting flow research and we support their development. Development continues on CH imaging as a compliment to OH measurements and filter-based diagnostic techniques for velocity and temperature measurements in complex reacting and non-reacting flows. In the Room 22 evaluations OH imaging has provided valuable insight into a very three-dimensional and unsteady combustion process. It has shown that the large flame-spreading angle can be predicted, at least in the absence of significant wall effects.

## LIQUID/GAS FUEL INJECTION

The effects of gas mass loading on the behavior of a liquid jet injected into a supersonic cross-flow are being studied in an effort to enhance the breakup and atomization of liquid jets for use in scramjet combustors.[7] Preliminary results suggest that for small mass loadings (less than 2% by mass of gas in liquid), the injector utilizes the expansion energy provided by the embedded high-pressure bubbles to shatter the liquid column into small ligaments and, subsequently, generate fine droplets once these bubbles enter the low-pressure environment. For the case with a large amount of gas added to the liquid jet (greater than 2% by mass), the injector uses the co-annular spray structure at the nozzle exit plane to accelerate the breakup processes on the squeezed thin liquid film. Figure 4 illustrates the cross section view of the idealized spray structure with a liquid film thickness of $d_L$ on the nozzle wall. We believe that droplet size is reduced as the ratio of gas added to the liquid mass flow rate is increased. A wide range of parameters, such as liquid properties, nozzle diameters, momentum ratios and gas/liquid mass ratios,

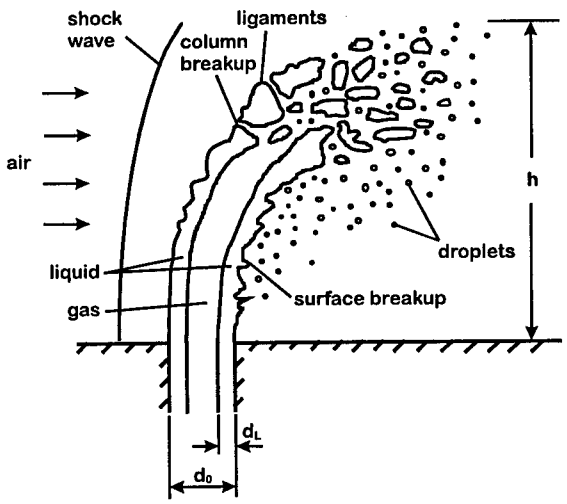


Fig. 4 Sketch of a typical aerated liquid jet breakup process in a supersonic crossflow.

has been investigated. The spray structure and penetration into the cross-stream are of primary interest. Experiments are carried out in a 25.4 mm by 25.4 mm supersonic wind tunnel. A supersonic nozzle, Mach number 1.85, drives the air stream. The mixed flow injector is flush mounted on the bottom plate of the supersonic wind tunnel. The aerated liquid is injected normal to the air stream through the nozzle orifice. Visualization of the global spray structure is performed by conventional color photography using a laser sheet for illumination. Near-field structures, such as penetration heights and liquid column trajectories, are measured from shadowgraphs using a CCD video camera. A frequency-doubled Nd:YAG laser with a wavelength of 532 nm and pulse duration of 10 ns is used as the light source. The shock wave structure inside the supersonic wind tunnel is identified by Schlieren technique. Typical spray structures for a liquid injectant, aerated with nitrogen are illustrated in Fig. 5 for an alcohol/water solution injected through a 500 μm nozzle.

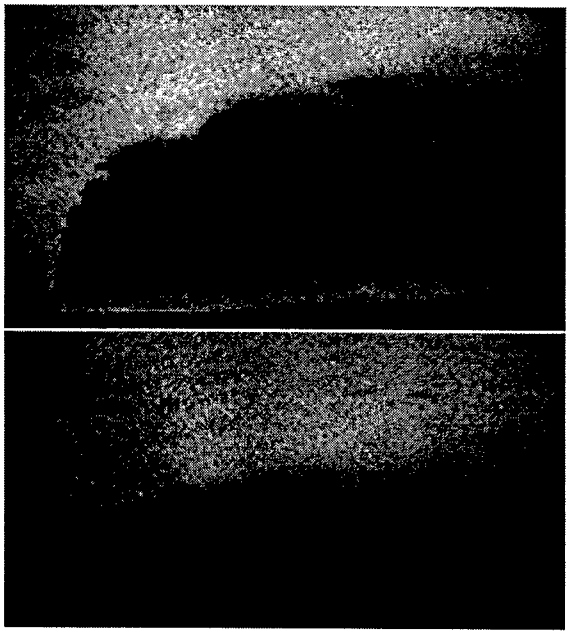

Fig. 5 Shadowgraphs of typical aerated liquid jet in a supersonic crossflow: pure liquid (top) and aerated (bottom).

Based on these cold flow studies, injectors were designed for the Room 22 combustor for operation on room temperature JP7, a liquid middle distillate fuel. Ignition of the combustor was achieved at a Mach 4 simulation and combustion was sustained. Only a portion of the total combsutor fuel flow was aerated. When the gas flow to that portion was halved, the burner could not be lit on liquid fuel. As with the other areas noted above, our research into liquid-gas atomization is encouraged by initial success in a development scramjet combustor and is shaped by what we don't understand about the phenomena.

References:


1. "Calibration of a newly developed direct-connect high-enthalpy supersonic combustion research facility" (1998) Jackson, K. et al, AIAA 98-1510.
2. "A numerical and experimental investigation of a scramjet combustor for hypersonic missile applications," (1998) Baurle, R. et al, AIAA 98-3121.
3. "Supersonic combustion experiments with a cavity-based fuel injector," (1999) Mathur, T. et al, AIAA 99-2102 (to be presented June 1999).
4. "Fundamental studies of cavity-based flameholder concepts for supersonic combustors," (1999) Gruber, M. et al, AIAA 99-2248 (to be presented June 1999).
5. "Experiments with a cavity-based fuel injector for scramjet applications," (1999) Gruber, M. et al, to be presented at XIV ISABE Sep. 1999.
6. "A comparison of isolator pressure rise correlations with new experimental data," (1999) Gustafson, M.D. and Gruber, M.R., to be presented at XIV ISABE, Sep. 1999.
7. "Penetration heights of aerated liquid fuel jets in supersonic crossflows," (1999) Lin, K.C. et al, to be presented at Institute for Liquid Atomization and Spray Systems, May 1999.

# Mixing, chemical reactions, and combustion in subsonic and supersonic turbulent flows

AFOSR Grant F49620–98–1–0052

P. E. Dimotakis and A. Leonard

*Graduate Aeronautical Laboratories*
*California Institute of Technology, Pasadena, CA 91125*

## Summary/Overview

This research is focused on fundamental investigations of mixing, chemical-reaction, and combustion processes, in turbulent, subsonic, and supersonic free-shear flows. The program is comprised of an experimental effort; an analytical, modeling, and computational effort; and a diagnostics and data-acquisition-development effort. The computational studies have been focused on fundamental issues pertaining to hydrocarbon-ignition/-combustion and the numerical simulation of compressible flows with strong fronts, in both chemically-reacting and nonreacting flows.

## Technical discussion

Work on hydrocarbon combustion in high-speed flows has continued focusing on the ignition characteristics of hydrocarbons at high strain rates, examining whether values of the ignition strain rate, $\sigma_{\rm ign}$, comparable to strain rates that would be encountered in a SCRAMJET environment could be achieved. This entails numerical simulations of the ignition characteristics of heated $C_2H_4$, counterflowing against heated air, in the presence of additives such as $F_2$, $H_2$, and NO, with 1-D, full-chemistry/-transport simulations conducted along the counterflow stagnation streamline. $C_2H_4$ is chosen as the fuel as the main constituent of cracked jet-fuel. Previous simulations had focused on ignition-enhancement from $F_2$ and $H_2$ additive blends.[1] In work in progress, the effect of NO on ignition was studied. The finding is that the addition of NO, alone, in amounts of order 10,000 ppm, is responsible for a substantial increase in ignition strain rate, to values as high as 40,000 /s (Fig. 1, left). Additions of small amounts of $F_2$ and $H_2$ also promoted ignition, but to a lesser extent. Premixing $F_2$ with air, however, in amounts greater than 25,000 ppm renders the system hypergolic (Fig. 1, right). Such additives can be utilized to sustain high-strain-rate ignition and flame stability in a SCRAMJET environment. They need only be used at lower-$M_\infty$ flight conditions, where ignition and flame stability are anticipated to be important issues. This part of the work is a collaborative effort between F. Egolfopoulos (USC) and P. Dimotakis.

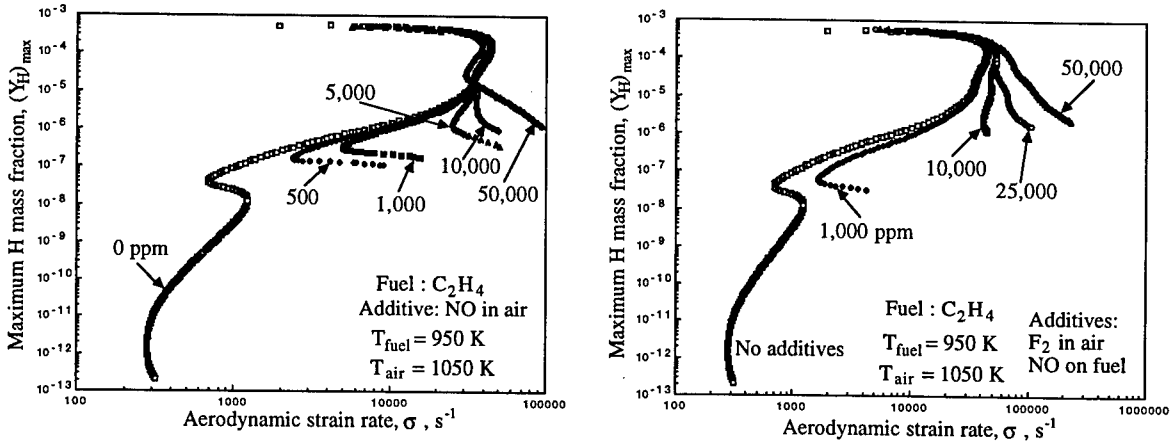


FIG. 1 Promotion of ignition strain rate by additives. Left: NO addition to air stream. Right: $F_2$ addition to air stream, with NO addition to fuel stream.

Recent applications of Image Correlation Velocimetry (ICV),[2,3] which extracts velocity-field information from successive images of Lagrangian markers (particles, dye, *etc.*), include a collaborative effort with R. Pitz (Vanderbilt) on Lagrangian flow-tagging techniques for low- and high-temperature gas-phase flows.[4,5] Briefly, a laser-beam grid is applied using a 193 nm ArF excimer laser to produce lines of ozone in an air stream (OTV: Ozone Tagging Velocimetry), or hydroxyl radicals in a burning hydrocarbon flame (HTV: Hydroxyl Tagging Velocimetry). These species fluoresce and can be used to mark the advection of the grid by laser induced fluorescence (LIF), using a 248 nm KrF laser. ICV is then used to infer the velocity field from two realizations of the advected LIF grid (Fig. 2).

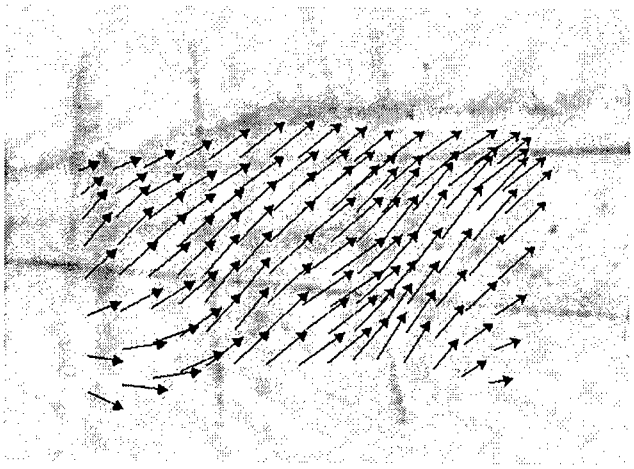

FIG. 2 Image Correlation Velocimetry application to $O_3$-tagged grid. Arrows denote in-plane velocity field vectors of gas-phase flow, $u \simeq 5 - 7\,\mathrm{m/s}$. Underlying grey-scale image depicts the superposition of the initial and advected grid of the fluorescing $O_3$ streaks.

In other related work, we are collaborating with Ö. Savas (Berkeley) in a quantitative assessment of ICV, Lagrangian Particle Tracking (LPT),[6] and other PIV methods. The work on ICV is part of the research effort by S. B. Deusch, in collaboration with P. Dimotakis.

FIG. 3 Rayleigh-Taylor flow: $\rho_1/\rho_2 = 3$. $\rho = 2\,\rho_2$ isosurface at $t = 3.54$. Neighboring-$\rho$ isosurfaces rendered transparent.

Three-dimensional scalar data were analyzed from a direct numerical simulation (DNS) of Rayleigh-Taylor-instability (R-T) flow, with a density ratio, $\rho_1/\rho_2 = 3$. This flow shares many of the characteristics of shear-layer mixing, is important in many variable-density contexts in accelerated flows, such as combustion, transverse jets, and others, as well as inertial-confinement fusion, geophysical/astrophysical flows, *etc.* A first analysis of the DNS data was presented recently.[7] In the present work, 3-D density isosurfaces were derived using the 'marching cubes' algorithm, which guarantees them to be 'hole-free' and the best discrete approximation of the true isosurface. The $\rho = 2\,\rho_2$ isosurface, at (dimensionless) $t = 3.54$, is depicted in Fig. 3. A comparison of runs seeded with different initial disturbances indicates that classical, $\propto g\,t^2$, growth laws of the extent of the turbulent-mixing zone (TMZ) may not be correct and that the initial conditions are not "forgotten", as also recently reported for high-$Re$ shear layers.[8] The work on R-T flows is a collaboration between A. Cook (LLNL) and S. Deusch, P. Dimotakis, S. Lombeyda, and D. Meiron (Caltech). It has been cofunded by the DOE Caltech ASCI/ASAP program.

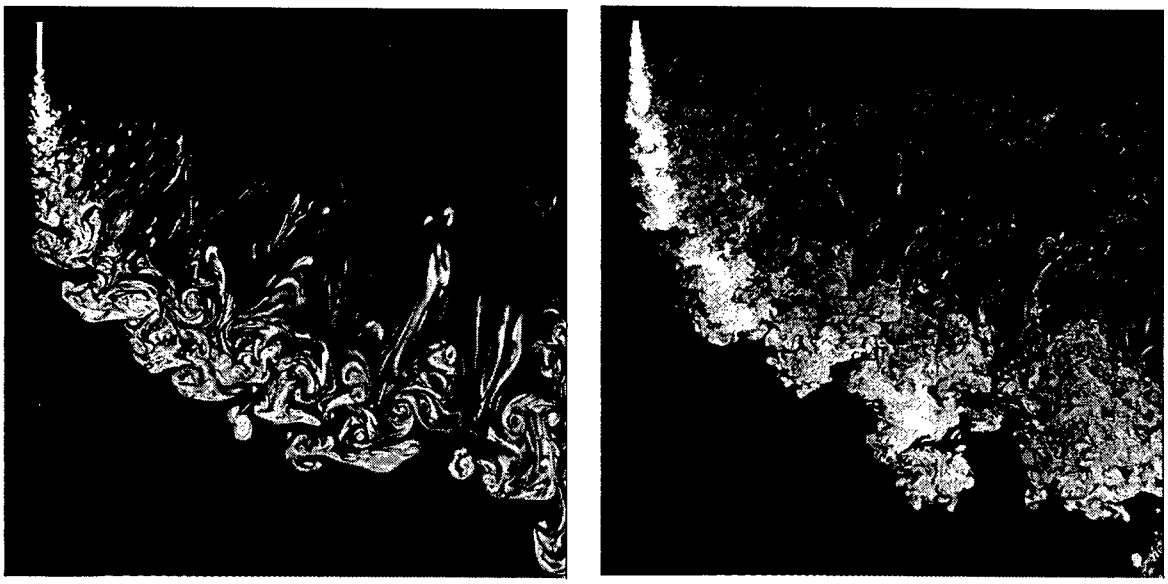

FIG. 4 Transverse jet at $U_j/U_{cf} = 34$. Scalar field compensated for downstream concentration decay. Left: $Re_j \simeq 1.0 \times 10^3$. Right: $Re_j \simeq 1.0 \times 10^4$.

Experiments are in progress on turbulent jets issuing through a wall into a cross-flowing freestream for a velocity ratio of $U_j/U_{cf} = 34$, at jet Reynolds numbers, $Re_j = U_j\, d_j/\nu \simeq 1.0 \times 10^3$, $2.0 \times 10^3$, $5.0 \times 10^3$, and $1.0 \times 10^4$. Typical LIF images in the $(x, y)$-direction are shown in Fig. 4. Jet fluid "fingers" can be seen in the wake extending from the body of the jet toward the wall. These persist for all Reynolds numbers considered, but are not seen at lower velocity ratios.[9] Similar structures, known as "fire devils", are reported in the lee of oil fires.[10]

The structure of the scalar field has been investigated by recording a sequence of transverse-jet images as a three-dimensional space-time dataset. In this space, motion within the image plane is mapped into orientation in $(x, y, t)$-space.[11] For two spatial dimensions, the in-plane components of the Lagrangian velocity of a scalar isosurface are given by,

$$\begin{bmatrix} u_x \\ u_y \end{bmatrix} = \begin{bmatrix} \delta x/\delta t \\ \delta y/\delta t \end{bmatrix} = \begin{bmatrix} \cot \beta_x \\ \cot \beta_y \end{bmatrix} ,$$

where $\beta_x$ and $\beta_y$ are the angles subtended between the space-time (local intersection tangent of the) isosurface and the $x$ and $y$ (spatial) axes, respectively. Figure 5 shows the upper edge of the jet dominated by large, tube-like structures in $(x, y, t)$-space. The underside of the jet (Fig. 6) shows the finger-like wake structures that are much finer in scale and convected at a nearly constant velocity. The work on transverse jets is part of the Ph.D. research of J. Shan, in collaboration with P. Dimotakis and assistance by S. Deusch.

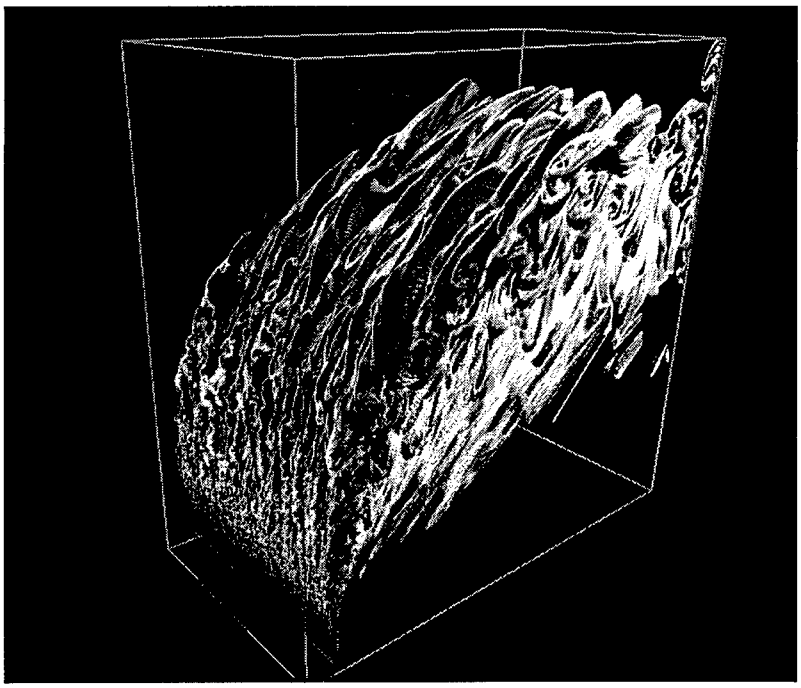

FIG. 5 3-D space-time visualization of $Re_j \simeq 1.0 \times 10^3$ transverse jet: Top view. Time increases into the page.

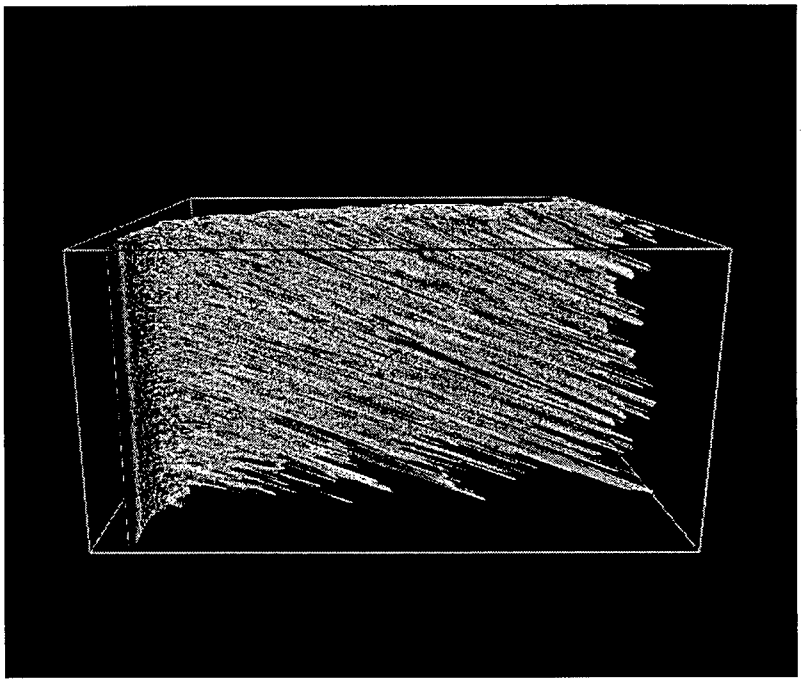

FIG. 6 3-D space-time visualization of $Re_j \simeq 1.0 \times 10^3$ transverse jet: Bottom view (jet "wake"). Time advances down vertical axis.

## References


[1] Egolfopoulos, F. N., and Dimotakis, P. E., "Non-premixed hydrocarbon ignition at high strain rates," *Twenty-Seventh Symposium (International) on Combustion*, 641–648 (1998).

[2] Tokumaru, P. T., and Dimotakis, P. E., "Image Correlation Velocimetry," *Exps. in Fluids* **19**(1), 1–15 (1995).

[3] Gornowicz, G. G., *Continuous-field Image-Correlation Velocimetry and its Application to Unsteady Flow Over an Airfoil*, California Institute of Technology, Aeronautical Engineer's thesis (1997).

[4] Pitz, R. W., Ribarov, L. A., Wehrmeyer, J. A., and Batliwala, F., "Ozone Tagging Velocimetry for Unseeded Velocity Measurements in Air Flows," *AIAA* 20$^{\text{th}}$ *Advanced Measurement and Ground Testing Technology Conference*, Invited Paper 98–2610 (1998).

[5] Wehrmeyer, J. A., Ribarov, L. A., Oguss, D. A., Batliwala, F., and Pitz, R. W., "Flow Tagging Velocimetry for Low and High Temperature Flowfields," 37$^{\text{th}}$ *AIAA Aerospace Sciences Meeting and Exhibit*, Paper 99–0646 (1999).

[6] Sholl, M., and Savas, Ö., "A Fast Lagrangian PIV Method for Study of General High-Gradient Flows," *AIAA* 35$^{\text{th}}$ *Aerospace Sciences Meeting*, Paper 97–0493 (1997).

[7] Dimotakis, P. E., Catrakis, H. J., Cook, A. W., and Patton, J. M., "On the geometry of two-dimensional slices of irregular level sets in turbulent flows," 2$^{\text{nd}}$ *Monte-Verita Colloquium on Fundamental Problematic Issues in Turbulence*, 22–28 March 1998 (Ascona, Switzerland), GALCIT Report FM98–2 (1998).

[8] Slessor, M. D., Bond, C. L., and Dimotakis, P. E., "Turbulent shear-layer mixing at high Reynolds numbers: effects of inflow conditions," GALCIT Report FM98–1 (1998).

[9] Fric, T. F., and Roshko, A., "Vortical structure in the wake of a transverse jet," *J. Fluid Mech.* **279**, 1–47 (1994).

[10] Morton, B., and Ibbetson, A., "Jets deflected in a crossflow," *Exp. Thermal and Fluid Sc.* **12**, 112–133 (1996).

[11] Jähne, B., *Digital Image Processing* (Springer-Verlag, Berlin, 1991).

# SHOCK TUBE STUDIES OF RAM ACCELERATOR PHENOMENA

**ARO DAAH55 - 97 – 1 - 0300**

**Principal Investigator: Ronald K. Hanson**

**High Temperature Gasdynamics Laboratory**
**Department of Mechanical Engineering**
**Stanford University, Stanford, CA**

## SUMMARY/OVERVIEW

This research is aimed at developing an improved understanding of hypersonic exothermic flows through the application of modern experimental methods and finite-rate-chemistry flowfield modeling. Thus far, the emphasis has been on providing fundamental data, of flowfield structure and combustion ignition times, which are relevant to the ongoing development of high-speed propulsion concepts. These data are critically needed to improve the accuracy of computational modeling of these flows.

## TECHNICAL DISCUSSION

Primary activities are highlighted below. Related publications are cited at the end.

### Imaging and Modeling of Shock-Induced Combustion in High-Speed Wedge Flows

Simultaneous OH PLIF and schlieren imaging was applied to study shock-induced combustion and oblique detonation wave formation in 2-D wedge flows. Oblique detonations, which occur in the limit of fast ignition behind an oblique shock wave, are a phenomenon of significant importance to future high-speed propulsion systems, including ram accelerators. Experimental work in the last year has primarily employed a 40° (half-angle) wedge body, with an embedded piezo-electric pressure transducer to record the pressure history at the wedge forebody surface throughout the experiment. The OH PLIF imaging system provides an instantaneous map of the OH distribution (and consequently, the flame front) in the flowfield. Complementary information on the shock wave position in the flow is provided by a schlieren image acquired within 2 μs of the PLIF result. An example result is shown in Figure 1a. Experiments thus far have varied the gas mixture composition, pressure, and velocity to alter the ignition delay and energy release. Analysis is focused on studying the transition to detonation and resultant wave angle through Rankine-Hugoniot shock-polar methods and finite-rate kinetic modeling.

In an effort to develop an in-house numerical modeling capability for comparison with the experimental results, a custom inviscid flow, finite-rate chemistry CFD code for wedge and conical flows has been developed and tested in our laboratory. An example calculation, showing good agreement with the data, is presented in Figure 1b. The successful chemistry mechanism

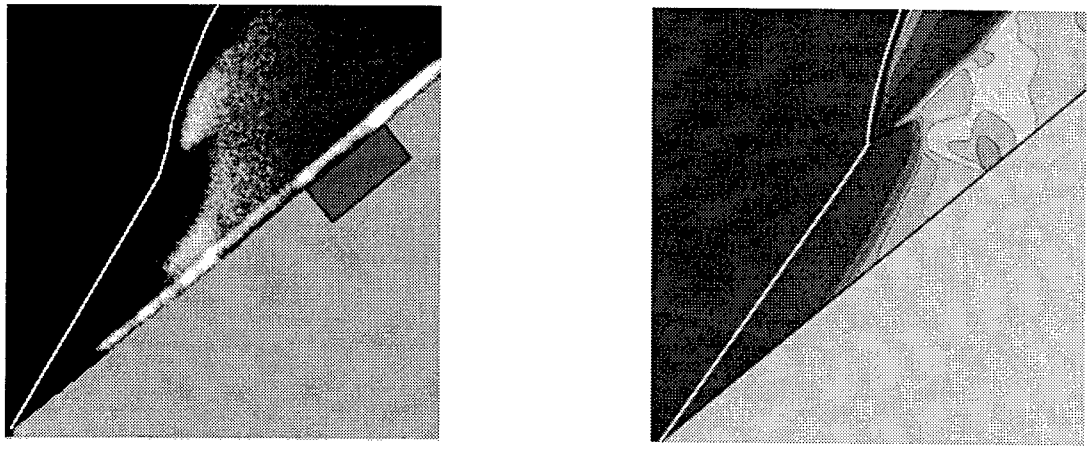

(a) (b)

**Figure 1:** Comparison of experimental and numerical results for supersonic exothermic wedge flow. (a) Experimental OH PLIF image; pressure transducer location shown in blue; shock position (in white) determined from complementary schlieren image. (b) OH contour plot from numerical calculation of flow; shock position shown in white. Mixture: $2H_2 + O_2 + 12N_2$, $V_\infty = 2130$ m/s, $T_\infty = 282$ K, $P_\infty = 0.12$ atm. Total wedge forebody length shown is 30.5 mm.

used in the calculation has been communicated to Dr. M. Nusca at ARL for use in the Army Ram Accelerator CFD codes.

## Experimental Study of Fuel Jets in Supersonic Combustion

Hydrogen transverse jet injection into reacting and non-reacting supersonic flow has also been investigated, with a view toward improving understanding of scramjet mixing and flameholding issues. OH PLIF visualization indicates the autoignition of a hydrogen jet in air cross-flow simulating flight Mach 10 conditions. OH fluorescence appears first in the recirculation region upstream of the jet and extends along the outer edge of the jet plume (Figure 2) demarcating the boundary between the fuel and air.

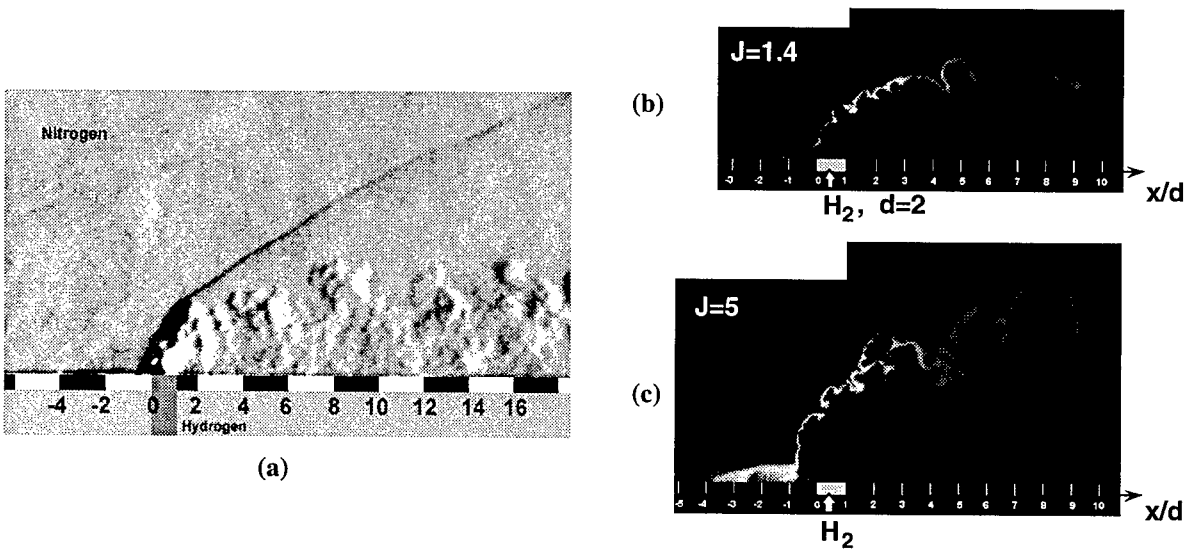


**Figure 2:** Left panel (a) - instantaneous schlieren image of underexpanded hydrogen injection into supersonic cross-flow (non-reacting, nitrogen) obtained by high-speed-framing camera (exposure time of 200ns), imaging 30x50 $mm^2$ of flow field. Right panel - two instantaneous OH-PLIF results for Mach 10 (b) and Mach 13 (c) conditions. Each image is obtained by combination of 2 different instantaneous images: near the exit of the jet ($-5<x/d<1$) and downstream of the jet ($1<x/d<10$).

Schlieren images reveal large scale turbulent structures (which persist at least 20 jet diameters downstream of the injector site) and a complex shock wave structure (a bow shock, an upstream separation wave and a downstream reattachment shock). Eight consecutive schlieren images obtained at 2 μs time intervals, using a new ultra-fast framing camera, were analyzed. The results showed that the coherent structures tend to travel with velocities that are closer to the free-stream velocity in the far-field (x/d > 10). When the images are assembled as a movie, the pulsating nature of the upstream separation region and of the jet causing the bow shock to fluctuate is very apparent, though this unsteady behavior was not anticipated. The unique capabilities of our new high-speed camera will enable further study of these high-frequency flowfield fluctuations and their role in supersonic flameholding.

## Measurement and Modeling of Ignition Kinetics

Our Ram Accelerator Ignition Kinetics studies are a part of a larger program in our laboratory to investigate, through both shock-tube experiments and chemical kinetics modeling, the ignition behavior of a wide variety of relevant military fuels. Earlier work in our laboratory concentrated on high pressure (to 87 atm) $H_2/O_2$ and low pressure $CH_4/O_2$ ignition time measurements and modeling.

We have extended these studies to include investigations of methane-based mixtures of importance to the ARL ram accelerator program with measurements (Figure 3a) made at pressures up to 260 atm, temperatures above 1040 K, equivalence ratios from 0.4 to 6.0 and inert dilution as low as 60%. Modeling of these extreme initial conditions required the development of a low temperature extension to the standard GRI-Mech methane oxidation mechanism. This mechanism (RAMEC) includes more extensive intermediate temperature chemistry, and offers improved predictive ability for high pressure, low temperature, rich mixture conditions when compared to GRI-Mech. A variety of correlations were generated to accurately describe these phenomena. For further details, see the publications by Petersen listed at the end of the abstract.

Recent shock tube studies use a wide variety of diagnostics: infrared and visible emission, narrow-linewidth laser absorption, and side wall pressure. In this work we found that more accurate and precise ignition time data could be obtained by passivating the shock tube walls with the initial test gas mixture and by utilizing CH emission to characterize the ignition time

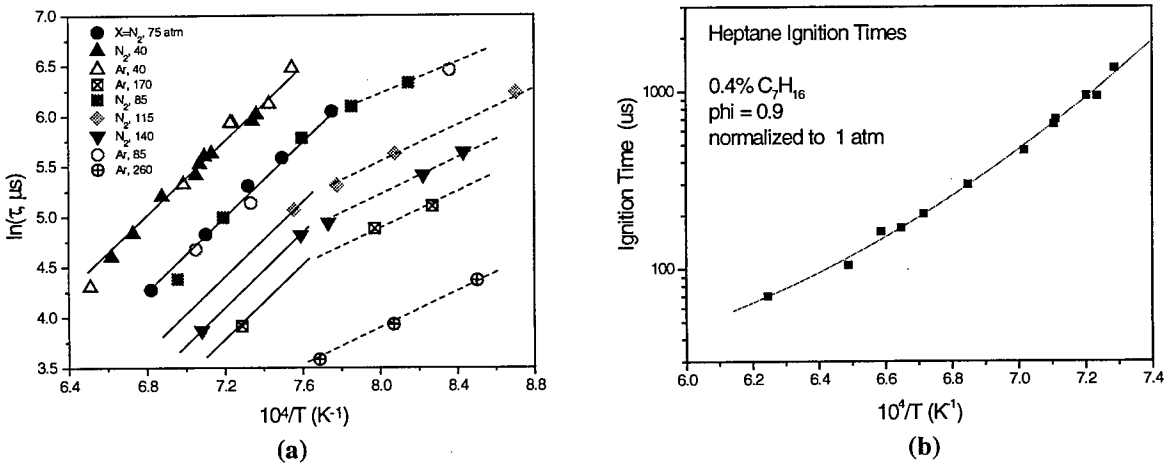


**Figure 3:** Representative ignition delay time data (a) Standard ARL Mixture, $3CH_4 + 2O_2 + 10X$ (X = $N_2$, Ar) (b) n-heptane/$O_2$/Ar

delay. The results of these improvements are apparent in our recent work on heptane (Figure 3b) and JP-10 ignition times, in that the data exhibit unusually low scatter. Measurements with low scatter are advantageous for examining small effects of additives on ignition time.

New work including studies of diesel analogs such as decane, and energetic fuels such as JP-10, is now being initiated.

## PUBLICATIONS/PRESENTATIONS


C. I. Morris, M. R. Kamel, A. Ben-Yakar, and R. K. Hanson, "Combined Schlieren and OH PLIF Imaging Study of Ram Accelerator Flowfields," Paper 98-0244 at the 36th AIAA Aerospace Sciences Meeting and Exhibit, Reno, NV, January 12-15, 1998.

A. Ben-Yakar, M. R. Kamel, C. I. Morris, and R. K. Hanson, "Hypersonic Combustion and Mixing Studies Using Simultaneous OH-PLIF and Schlieren Imaging," Paper 98-00940 at the 36th AIAA Aerospace Sciences Meeting and Exhibit, Reno, NV, January 12-15, 1998.

A. Ben-Yakar and R. K. Hanson, "Cavity Flameholders for Ignition and Flame Stabilization in Scramjets: Review and Experimental Study," Paper 98-3122 at the 34$^{th}$ Joint Propulsion Conference & Exhibit, Cleveland, OH, July 13-15, 1998.

C. I. Morris, M. R. Kamel, and R. K. Hanson, "Shock-Induced Combustion in High-Speed Wedge Flows," 27$^{th}$ *Symposium (International) on Combustion*, The Combustion Institute, pp. 2157-2164.

A. Ben-Yakar and R. K. Hanson, "Experimental Investigation of Flame-Holding Capability of Hydrogen Transverse Jet in Supersonic Cross-Flow," 27$^{th}$ *Symposium (International) on Combustion*, The Combustion Institute, pp. 2173-2180.

Petersen, E. L., Davidson, D. F., and Hanson, R. K., "Ignition Delay Times of Ram Accelerator $CH_4/O_2$/Diluent Mixtures," *Journal of Propulsion and Power*, Vol. 15, No. 1, 1999, pp. 82-91.

Petersen, E. L., Davidson, D. F., and Hanson, R. K., "Kinetics Modeling of Shock-Induced Ignition in Low-Dilution $CH_4/O_2$ Mixtures at High Pressures and Intermediate Temperatures," *Combustion and Flame*, Vol. 117, No. 1-2, 1999, pp. 272-290.

Petersen, E. L. and Hanson, R. K., "Reduced Kinetics Mechanisms for Ram Accelerator Combustion," *Journal of Propulsion and Power*, Vol. 15, No. 2, 1999.

# INTRINSIC BURNING BEHAVIOR AND FLAME STRUCTURE DIAGNOSTICS OF LIQUID PROPELLANTS

ARO Grant/Contract No. DAAH04-96-1-0054

Principle Investigator: Kenneth K. Kuo

Department of Mechanical and Nuclear Engineering
The Pennsylvania State University
University Park, PA 16802

SUMMARY/OVERVIEW:

The combustion behavior and flame structure of XM46 and nitromethane have been studied over a wide range of pressures. Regression rate of XM46 has been characterized up to 207 MPa, displaying a complex curve containing both negative pressure exponent and plateau behavior. Measured intrinsic burning rate was found to be ~4 times higher than those of gelled XM46 propellant. The XM46 flame structure displays 3 different stages: 1) mixture of HAN and TEAN decompose at around 300 °C to form dark species, 2) heavy opaque intermediate molecules break down into transparent species, and 3) transparent species react in the luminous flame. Nitromethane burning rate was measured as a function of both pressure and initial temperature at pressures up to 170 MPa. Three different regimes were observed in the burn rate curve, with slope breaks at approximately 15 and 70 MPa. In the future, the combustion mechanistic study of the two propellants will be undertaken using measured species and temperature profiles with detailed modeling.

AUTHORS: Kenneth K. Kuo, Yi-Ping Chang, and Eric Boyer

TECHNICAL DISCUSSION:

The goal of this research is to study the combustion behavior and flame structure of liquid propellants. There are two liquid propellants under investigation: XM46 and nitromethane. Specific objectives to be accomplished include (1) the measurement of intrinsic burning rates of liquid propellants as a function of chamber pressure over a broad range of pressures up to 207 MPa or 30,000 psia, (2) the investigation of the combustion characteristics of XM46, such as burn-back phenomena, existence of a negative pressure exponent regime, and multi-stage combustion behavior, and (3) the investigation of flame structure of liquid propellants, such as temperature and species profiles, using both intrusive and non-intrusive methods.

A specially designed liquid propellant strand burner (LPSB), which includes an accurate liquid feeding system, was utilized to study intrinsic burning behavior of liquid propellants. In feeding tests, the liquid propellants (LP) were fed up into a tube in order to establish a stable flame at the port of the tube. Once the stable flame was established, one could deduce the burning rate from the preset feeding speed. The traditional static tests of stagnant LP strands were also performed in the LPSB. These experiments were conducted by filling liquid propellant in a quartz tube (7 mm in diameter) or a thin-walled cylindrical straw made from a combustible wax paper to minimize heat loss and confinement effects. The optically accessible windows of the LPSB allowed the visual observation of the whole combustion event and the usage of non-intrusive diagnostic techniques. Also, in some tests, thermocouples were installed in the center of the quartz tube to measure the temperature profile across the burning surface of

the propellant as well as the gaseous flame. Due to the limitations of the optically accessible windows, the tests at pressures higher than 35 MPa were performed in the ultra-high pressure burner.

Conventional vented strand burners generally have pressure limits of less than 70 MPa (~10,000 psi). However, pressures generated inside gun chambers are much higher, possibly exceeding 700 MPa (~100,000 psi). Gaining more knowledge of high-pressure reaction mechanisms can also be useful in understanding detonation initiation and reaction processes for energetic substances. In order to examine the combustion behavior at high pressures, an ultra-high pressure strand burner (UHPSB) was designed, constructed, and tested.

The UHPSB and its remote control system comprise a unique facility established at the High Pressure Combustion Laboratory (HPCL) of Penn State University that allows regression rates of strand propellants to be measured at pressures up to 207 MPa (30,000 psi). Liquid propellant strands can be contained in either a quartz tube (for simplicity) or combustible straws (to minimize heat loss and confinement effects). A total of three thermocouples (TCs), or up to four break wires (BWs) per sample can be monitored using this setup.

Since the test chamber was adapted from a high-pressure compressor storage tank with a length of approximately 2 meters and a 10-cm inside diameter, the internal volume is very large. Therefore, there is negligible pressure change due to the generation of product gases during the combustion event. The high pressure gas environment during combustion was determined by the gas input source from the compressor. The environment was generally nitrogen, but other gases such as air or argon could easily be substituted. The controls and data acquisition system are located in another building apart from the one containing the UHPSB test chamber, for operator safety. Both the compressor and an exhaust solenoid valve can be remotely operated to increase or decrease the chamber pressure to the desired level.

**XM46**

The burning rate vs. pressure curve for XM46 was extended to a much higher pressure level (up to 207 MPa) with recent test results obtained from the UHPSB using combustible straws. The extended results together with all previous data are shown in Fig. 1. The curve displays four different burning rate regimes:

| | |
|---|---|
| $r_b\uparrow$ with P↑ | (for P < 7 MPa) |
| $r_b\downarrow$ with P↑ | (for 7 < P < 28 MPa) |
| $r_b$ nearly constant | (for 28 < P < 100 MPa) |
| $r_b\uparrow$ with P↑ | (for P > 100 MPa) |

It is important to note that the burning rate of XM46 was largely unknown before this investigation. The pressure exponents obtained by previous researchers differed greatly from each other. This study is the first one which covers broad range of pressures without using special additives. For example, the intrinsic burning rates obtained in this investigation are significantly (4 times) higher than the burning rate measured by researchers at ARL for 1 to 2% gelled propellants. This indicates the strong influence of gelling agents on the combustion behavior of LP. In addition, for the low-pressure regimes, the PSU data are higher than those of Vosen. The difference is believed to be caused by the greater heat loss from the reaction zone to his rectangular quartz channel.

The static tests using cylindrical quartz tubes with two thermocouples in the center were performed to observe the combustion phenomena and flame structure. From video images, no luminous flame was present in low-pressure

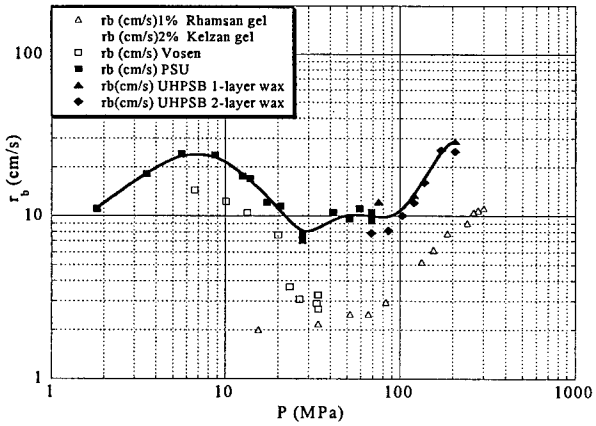

Figure 1. XM46 burning rate curve.

regimes (below 28 MPa). The decomposition of XM46 produced dark smoke with some liquid droplets entrained within the gases; these droplets coated the interior surfaces of the tube and combustion chamber. This smoke formed a dark opaque zone right above the decomposition front. For tests at higher pressures, the dark smoke turned into transparent gases at some axial distance above the decomposition front. The luminous flame did not appear above the transparent zone until the pressure was greater than 28 MPa.

Figure 2 shows typical temperature traces in the reaction zone at two different pressures. For each test, two thermocouples were installed at two axial locations. At a relatively low pressure of 13.8 MPa (2000 psig), the temperature of the dark smoke was around 300 °C. Later in the event, both thermocouples, although at different locations, reached the same maximum temperature (about 600 °C) at the same time. On the video, this corresponded to the sudden clearing of the dark smoke after the regression front passed through the whole column of liquid. Because the whole column of liquid was consumed by the decomposition front, the gas in the tube at this stage became nearly stagnant; however, the reaction processes continued in the gaseous mixture. Near 600 °C, the reaction simultaneously converted all the dark chemical species into transparent ones everywhere inside the tube.

At a higher pressure (33.8 MPa), the temperature jumped up to about 600 °C immediately after the regression front passed the thermocouple and gradually increased to about 700 °C. Then the luminous flame appeared, bringing the temperature up to around 1,700 °C. It is interesting to note that the temperature corresponding to transparent zone (~600 °C) was roughly the same for tests at different pressures.

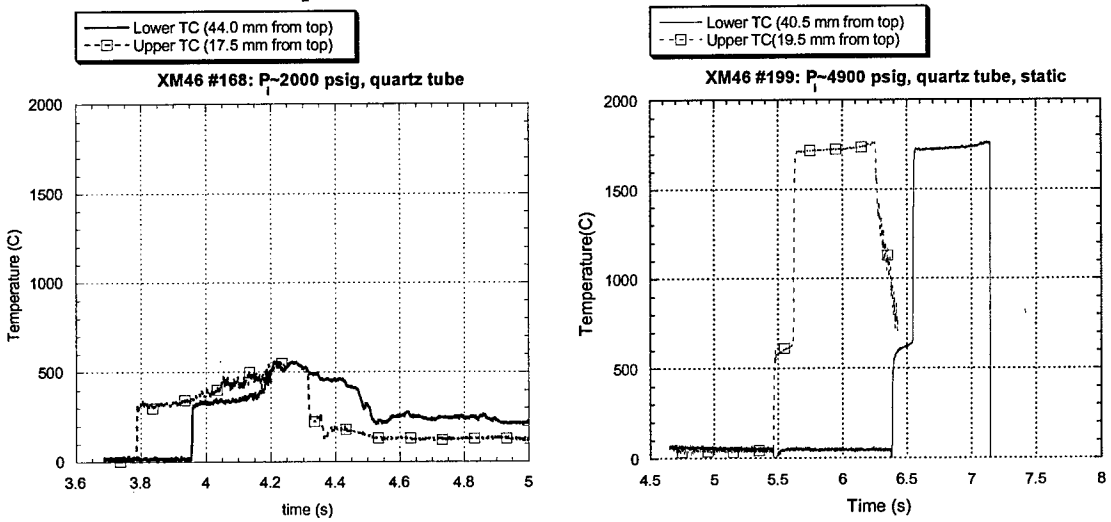


Figure 2. Temperature distribution inside XM46 reaction zone at low and high pressures.

Since both HAN and TEAN decompose at temperatures lower than 300 °C , and the dark smoke above the decomposition front suggests the existence of carbon-containing species, it is proposed that the reaction of XM46 consists of the following steps:

a) Decomposition of HAN and TEAN mixture in XM46 around 300 °C at the pyrolyzing surface of the LP generating brown-colored $NO_2$ and opaque carbon-containing species.
b) Break-down of heavy intermediate species into transparent molecules. This step occurs at around 600 °C.
c) Final reactions between transparent species to produce the luminous flame.

The precise concentration and identities of chemical species in the opaque and transparent zones are currently being studied. The highly undesirable and peculiar burn-back phenomena of XM46 were observed and believed to be caused by the subsurface reactions which cannot be controlled unless the TEAN is replaced by other more HAN-compatible chemical ingredients.

## Nitromethane

Nitromethane combustion behavior was studied over a wide range of pressures. At relatively low pressures (below 15 MPa), the LPSB was used for both feeding and static tests. For high pressures, LP contained in combustible straws was burned in the UHPSB.

Using the LPSB, temperature sensitivity was measured by conducting a series of tests at initial temperatures ranging from –30 to +45 °C. Nitromethane burning rate was found to be most sensitive to initial temperature change at low pressures, with $\sigma_p = 2.9 \times 10^{-3}\ K^{-1}$ at 2.51 MPa (350 psig). The $\sigma_p$ decreased greatly with increasing pressure, dropping to a very low value of $0.6 \times 10^{-3}\ K^{-1}$ at a pressure of 9.96 MPa (1,430 psig). A second-order polynomial fits the deduced points very well over the range examined:

$$\sigma_p = 4.38X10^{-3} - 6.73X10^{-4}\,P + 2.97X10^{-4}\,P^2$$

where P is in MPa and $\sigma_p$ in $K^{-1}$.

A compilation of LPSB, UHPSB, quartz tube (PSU and Naval Ordnance Laboratory--NAVORD) burning rate data is shown in Fig. 3. A relatively high pressure exponent of 1.03 was found using the LPSB. PSU quartz tube tests had a lower burn rate, but a slightly higher exponent, 1.17. Therefore, the burn rates converged as the pressure increased. The close agreement between the measured burning rates from PSU quartz tube tests and NAVORD results can be seen from this figure. This is expected due to the similar test conditions. It is useful to note that the quartz tube burning rate data are significantly affected by the heat loss from the flame zone to the tube walls and confinement effects; therefore, they do not represent the true burning rate of nitromethane. To avoid heat loss to the tube wall, an extremely thin combustible tube was constructed from wax paper for tests conducted in the UHPSB. At higher pressures, a slope break to a much higher exponent (n=2.33) appeared around 15 MPa. An abrupt change in the burning rate slope was also noted by NAVORD in this range as well (although their reported data did not cover this range). They postulated that this was due to formation of liquid surface distortions and subsequent increase in burning surface area. A third pressure regime was indicated by a significant flattening of the slope (n=0.86) at approximately 70 MPa. The slope stayed constant up to the maximum pressure tested, 170 MPa. The three pressure regimes are given in the Fig. 3.

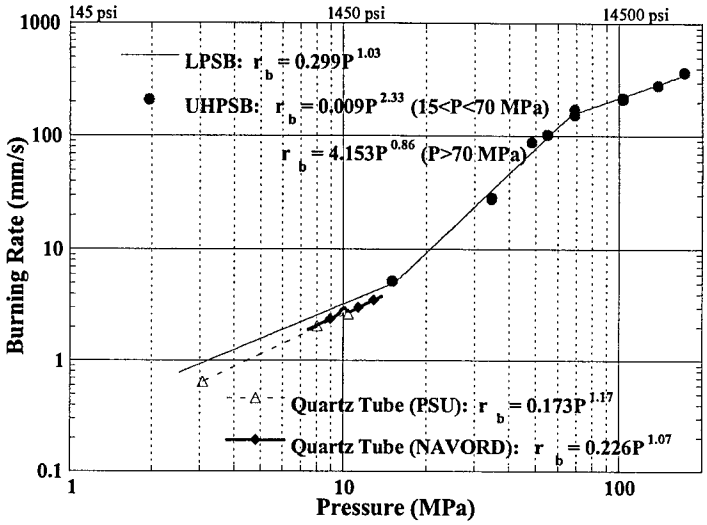

Figure 3. Comparison of measured nitromethane burning rates.

## Future Work

In the near future, research will be conducted in the following areas: 1) temperature sensitivity study for XM46 over a broader range of initial temperatures (-80 to 80 °C), 2) species and temperature profile measurement by non-intrusive diagnostic techniques (e.g., UV/Visible absorption spectroscopy), 3) continuation of combustion mechanism study, including burn-back phenomena, explanation of burning rate trend vs. pressure and initial temperatures, and 4) detailed chemical kinetic study with model simulation.

# EXPERIMENTAL STUDY OF PLASMA/PROPELLANT INTERACTIONS

ARO Grant No. DAAG55-98-1-051
Principal Investigators: Stefan T. Thynell and Thomas A. Litzinger

Department of Mechanical and Nuclear Engineering
The Pennsylvania State University
University Park, PA 16802

**SUMMARY**: The purpose of this experimental investigation is to improve our understanding of the interaction between a normally impinging plasma and a solid propellant. The study is undertaken to explain the burning rate enhancement and reduced role of the propellant's temperature sensitivity that have been observed in gun firings. The experimental facility contains a newly designed and constructed plasma chamber and propellant holder, which allows detailed investigations of pyrolysis products using microprobe mass spectrometry, near surface temperature response from thermocouples, gas-phase pressures using standard transducers, and high-speed filming of the flow field and gas-phase ignition event.

Authors: Stefan T. Thynell and Thomas A. Litzinger

## INTRODUCTION

The potential use of electro-thermal-chemical plasmas as an ignition source, e.g., in large-caliber guns, has revealed several important benefits over conventional ignitor systems. These include, among others, a shorter ignition delay, a reduced temperature sensitivity of the propellant, and a reduced susceptibility to anomalous ignition transients. To effectively design the plasma ignitor system, to optimize the charge configuration and to select a most suitable propellant, it is desirable to increase our understanding at both the practical and fundamental levels of the interaction between the plasma and propellant. It is expected that such an improved understanding will be achieved by systematically and parametrically studying the propellant's response to a single plasma jet using various advanced diagnostic techniques, including among others triple-quadrupole mass spectroscopy, high-speed film camera, and mid-IR emission spectroscopy.

## OVERALL OBJECTIVE

The overall objective of the experimental study is to gain insights from parametric studies that will contribute to the formulation of a more complete understanding of the various chemical and physical processes that occur during ignition by the plasma igniter.

### Specific Experimental Objectives

1. Characterize the stable species distribution in the plasma jet near the propellant's surface.
2. Study the spatial and temporal species evolution behaviors during the exposure of the propellant sample to the plasma jet.

3. Ascertain the surface heat flux variation temporally and spatially using data from local temperature measurements.
4. Perform various parametric studies including:
   - Compare the plasma igniter to other ignition sources, such as a $CO_2$ laser.
   - Investigate the effects of plasma energy on local temperatures and species evolution.
   - Investigate the role of spacing between the igniter exit and the surface of the propellant on local temperatures and species evolution.
   - Determine the role of initial temperature of propellant on the ignition behavior.
   - Perform studies with various propellants including JA2 and TPE-based propellants.
   - If time allows, consider different capillary liner materials and UV/visible radiation as ignition source.

## SUMMARY OF PROGRESS

To meet the objectives of this research program, a new test rig has been designed and constructed. The test rig has several major components: 1) a special chamber which generates the high temperature plasma, 2) a propellant sample holder interfaced to a triple-quadrupole mass spectrometer, 3) an electrical circuit for discharging up to 10 kJ of electrical energy in a few milliseconds, and 4) various diagnostic components such as a mass spectrometer, pressure transducers, thermocouples, IR-detectors and high-speed film camera. A cross-section of the plasma chamber, propellant sample holder, and frame is shown in Fig. 1.

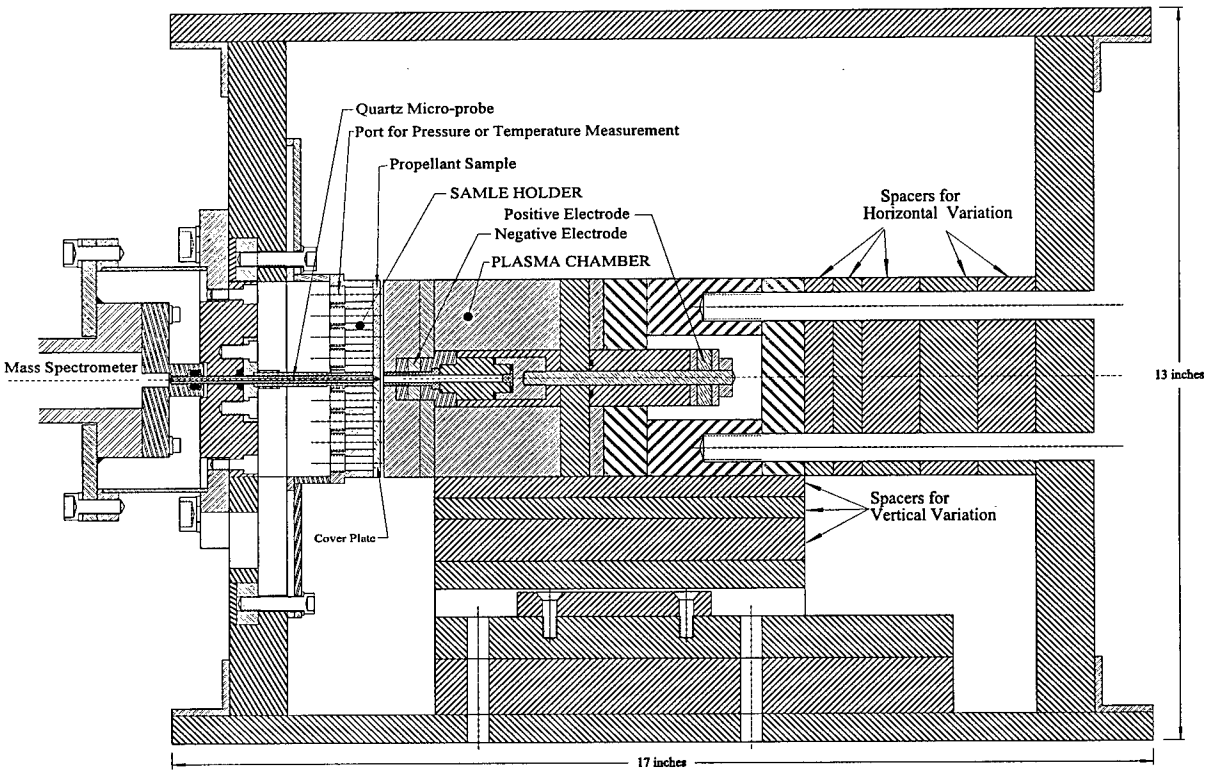


Figure 1. Above is shown the cross-section of the plasma chamber, propellant sample holder, and frame for attachment to triple-quadrupole mass spectrometer. The plasma chamber can be moved horizontally (to the right) by four inches and vertically (down) by 1.5 inches. The quartz micro-probe is attached to several large pumps and thus fixed in space.

Figure 2 shows that the propellant sample covers a portion of the square plate. Overall, the sample holder has nine access ports to the gases flowing from the plasma chamber and impinging normally on the propellant surface. In a given experiment, these ports allow simultaneous measurement of pressure at four positions, temperature at four positions, and gases at a single location. The plasma chamber can also be moved vertically (1.5 inches) and horizontally (4 inches) (see Fig. 1) in order to acquire temporal species profiles at different distances from the plasma exit port.

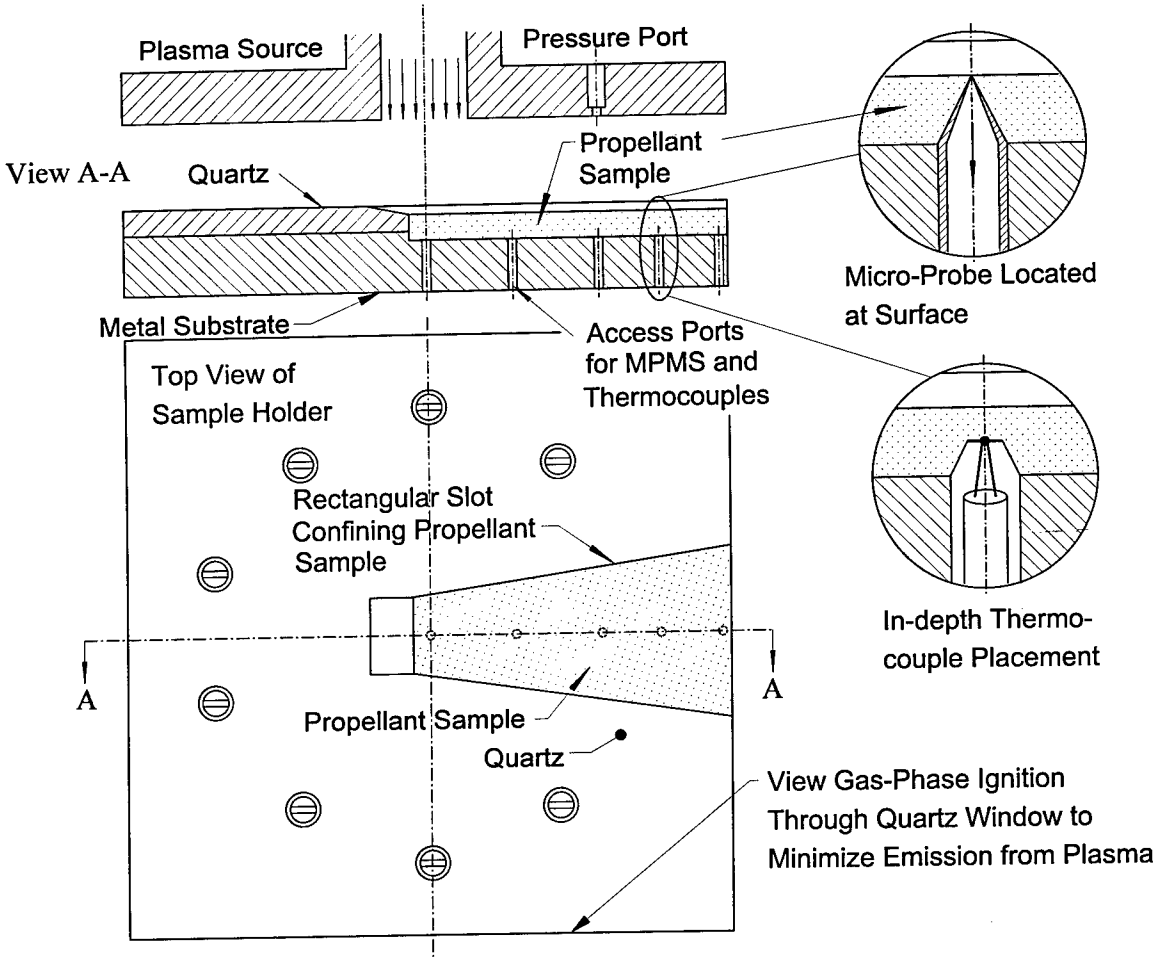


Figure 2. Schematic diagram of sample holder for allowing an optical access to the near-surface region of the propellant. By placing the propellant sample slightly below the surface of the quartz, a side view would give direct view of light emission from propellant gases due to ignition, in which emission from plasma is reduced. Sampling from microprobe mass spectrometry (MPMS) occurs from below, by placing the tip of the microprobe parallel to the virgin propellant.

The basic *RLC* electrical circuit utilizes two 96μF capacitors connected in parallel, one 30μH inductor, a floating mercury switch, a crowbar diode for minimizing the destructive effects of oscillating current flows, and Rogowski and Pearson coils for instantaneous current and voltage measurements. These components were received recently. Since the experiment involves high voltages (10kV) and currents (10 to 15 kA), checkout tests of indiviual componets of the electrical circuit are currently under way. These include the performances of the mercury switch,

dump resistor, capacitors, crowbar diode, and capacitors. Safety is addressed as the experimental procedures are being developed. Subsequently, system checkout tests will be performed. In addition, purchase of a high-speed camera as of DURIP funding has been initiated with the Purchasing Department at Penn State.

# ROCKET FLOWS & ROCKET FLAMES

AFOSR Grant/Contract No F49620-96-1-0031
Principal Investigator: John Buckmaster

University of Illinois, Department of Aeronautical & Astronautical Engineering
104 S.Wright St., Urbana IL 61801. limey@uiuc.edu

## Summary/Overview

We are concerned with the nature of the flow field in solid propellant rocket motors, the nature of the flames, the manner in which these interact, and the processes that control the regression rate of the propellant surface. We have examined, via a combination of perturbation and numerical strategies, the effects of deviation from axial symmetry on the flow field, and we have explained the swirling flows observed in cold-flow experiments. We are engaged in a systematic study of the flame geometry using a scientific computation strategy, and have shown how the stoichiometry and the Peclet number control the location of those parts of the flame that supply the heat that is conducted to the surface. Earlier speculations on the nature of the flame geometry have been shown to be flawed.

## The generation of axial vorticity in solid-propellant rocket-motor flows

collaborators: S.Balachandar & M.Short, Department of Theoretical & Applied Mechanics, University of Illinois at Urbana-Champaign.

We have examined small deviations from axial symmetry in a solid-propellant rocket motor, and have described a 'bath-tub-vortex' effect, in which substantial axial vorticity is generated in a neighborhood of the chamber center-line [1]. The unperturbed flow field is essentially inviscid at modest Reynolds numbers, even at the chamber walls, as has long been known, but the inviscid perturbed flow is singular at the center-line, and viscous terms are required to regularize it. We examine perturbations so small that a linear analysis is valid everywhere ( $\varepsilon Re$ small, where $\varepsilon$ is a measure of the perturbation amplitude and $Re$ is a Reynolds number); and larger perturbations in which a nonlinear patch is created near the center-line of radius $O(\sqrt{\varepsilon})$. Our results provide an explanation of swirl experimentally observed by Dunlap *et al.* [2], and a cautionary note for those concerned with numerical simulations of these flows, whether laminar or turbulent.

Figure 1 shows the axial vorticity in the nonlinear patch for a disturbance in the linear region (outside the patch) $\propto e^{i\theta}$ where $\theta$ is the cylindrical angle coordinate. For $\varepsilon Re = 50$, the maximum vorticity $\approx \pm 23$. We believe that it grows indefinitely with $\varepsilon Re$. Pure swirl disturbances ($n = 0$) have been described, as well as modes of greater degree ($n \geq 2$).

# The geometry of binder flames supported by heterogeneous propellants

collaborators: T.L.Jackson, Center for the Simulation of Advanced Rockets, University of Illinois at Urbana-Champaign.

We have continued our elementary flame studies designed to provide an understanding of the complex field that is generated by burning a heterogeneous solid propellant of the kind used in high-performance rockets. The most complete report of our progress is presented in [3]. One component of this is published in [4], an early and preliminary version of which was presented in [5].

We have considered a propellant whose surface is one-dimensional periodic, generating a two-dimensional combustion field [6]. Two important parameters are the Peclet number $Pe$ and the solid-phase stoichiometric coefficient $\beta$. We show that for $\beta = 7$, a representative value, there are essentially two flame configurations: For small Peclet numbers, mixing between the surface and the flame is sufficient to generate a continuous and near-uniform deflagration; on the other hand, for Peclet numbers of order 10 or so, each period contains a pair of button-like premixed flames centered over the fuel so that there are significant 'holes' in the combustion field over the oxidizer. Diffusion-flame structures that are part of the combustion field play no role in generating the heat that is conducted back to the propellant surface. Most of our calculations assume that both Lewis numbers are equal to 1 and the solutions are steady, but time-periodic oscillating solutions are obtained for sufficiently large values of Lewis number.

Figure 2 shows level surfaces of what is essentially the mixture fraction, and the stoichiometric level surface (SLS) is labelled 0. Here $y$ is measured parallel to the propellant surface, with fuel-binder located in $|y| < \alpha$, oxidizer (AP) in the remainder of the interval. Nominally we expect the diffusion flame supported by the binder products and the AP decomposition flame products to lie on the SLS, but there are significant leading edge structures (edge-flames) characterized by substantial mixing. It is noteworthy that the SLS does not intersect the propellant surface at the AP/binder interface $|y| = \alpha = 0.2$, but on the AP surface. This is a consequence of the stoichiometry (much more oxidizer is required than fuel) and the correct use of flux conditions at the propellant surface.

Finite chemistry calculations reveal the reaction rate contours shown in Figure 3, and the diffusion flame corresponding to the SLS of Figure 2 is quite clear. But most of the heat conducted back to the surface is generated in two intense reaction zones centered at $|y| \approx 0.4, x \approx 0.25$. The nonuniformity of the surface heat flux arising in this way is apparent from Figure 4 ($\delta$ is a Damköhler number). Clearly there is little heat carried to the main body of the AP, and presumably this would not regress in a satisfactory fashion were it not for the AP decomposition flame. We are currently making similar calculations for 2D-periodic propellants that support 3D flames.

In another study [7], we have examined a single diffusion flame anchored to 1/4-spaces of solid fuel and oxidizer. A time-periodic shear flow is applied, to model the shear that can be generated by the interaction of acoustic waves and the rotational base flow in a rocket chamber, e.g. [8]. The response of the flame to this shear, the heat flux to the surface etc., are calculated numerically. Significant enhancement of the maximum temperature and the time averaged total heat flux to the surface are found. These enhancements are essentially maximized at zero frequency (quasi-steady combustion zone), and in this limit the response depends critically on the instantaneous direction of the shear.

Figue 5 shows variations of the total heat flux to the surface for different frequencies. The horizontal broken lines are the steady-state fluxes. Clearly the shear enhances the heat flux averaged over a period.

All of the calculations sketched above have been carried out in the context of the simplest of models. One of its characteristics is an uncoupling of the fluid mechanics and the combustion processes, just as in Burke and Schumann's seminal paper on diffusion flames. However, we have recently developed a suitable fluid-mechanics code accurate at arbitrarily small Mach numbers, and we are currrently testing it. Our ultimate goal is to be able to carry out 3D flame calculations with full fluid-mechanics coupling, coupling with the heat-conduction process in the solid, and non-planar regression of the solid surface. We expect to do this for simple chemistry models that account for the AP decomposition flame and the binder flame.

## References


[1] S.Balachandar, J.Buckmaster, M.Short. in review *Journal of Fluid Mechanics.*

[2] R.Dunlap, A.M.Blackner, R.C.Waugh, R.S.Brown. *Journal of Propulsion* **6** 690-704 (1990).

[3] J.Buckmaster, T.L.Jackson. *AIAA paper 99-0323* January 1999.

[4] J.Buckmaster, T.L.Jackson, J.Yao. *Combustion & Flame* **117** 541-552 (1999).

[5] J.Buckmaster, J.Yao. *Proceedings of the Fourth Asian-Pacific International Symposium on Combustion and Energy Utilization*, Chulalongkorn University, Bangkok, Thailand, December 8-11, 1997. Volume 1 (of 2), ISBN 974-637-363-3, pp 112-115.

[6] T.L.Jackson, J.Buckmaster. paper to appear in *Journal of Propulsion and Power.*

[7] J.Buckmaster, T.L.Jackson. in review *Combustion & Flame.*

[8] T-S.Roh, S.Apte, V.Yang. *27th Symposium (International) on Combustion*, the Combustion Institute, pp 2335-2341 (1998).


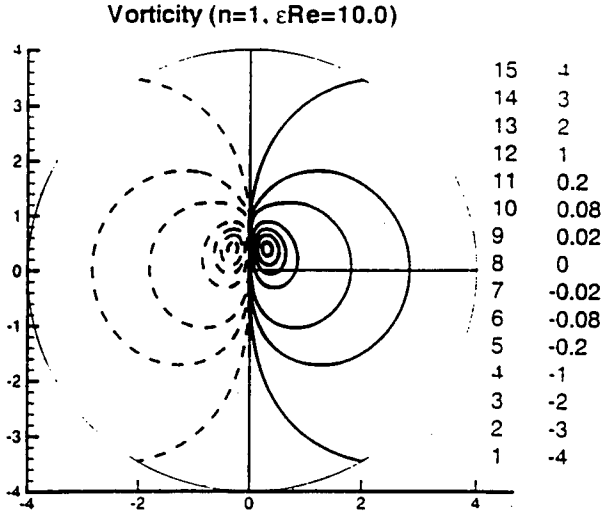


Fig.1. Vorticity in the non-linear patch.

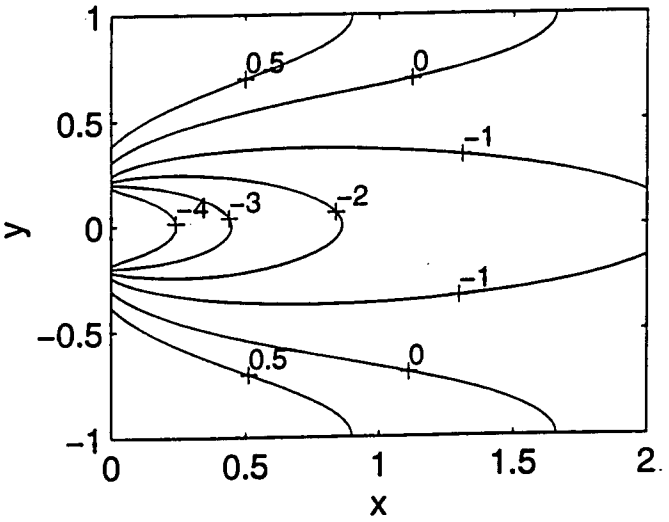


Fig.2. Mixture fraction level surfaces, $\alpha = 0.2, Pe = 10$.

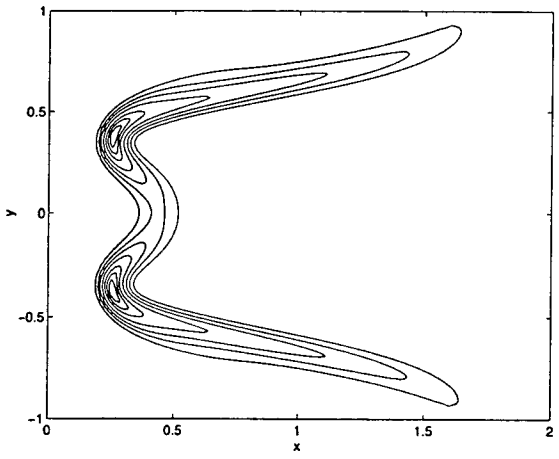


Fig.3. Reaction rate contours,
$\delta = 0.2, Pe = 10, \alpha = 0.2$;
contours 8,6,4,2,1,0.5,0.2.

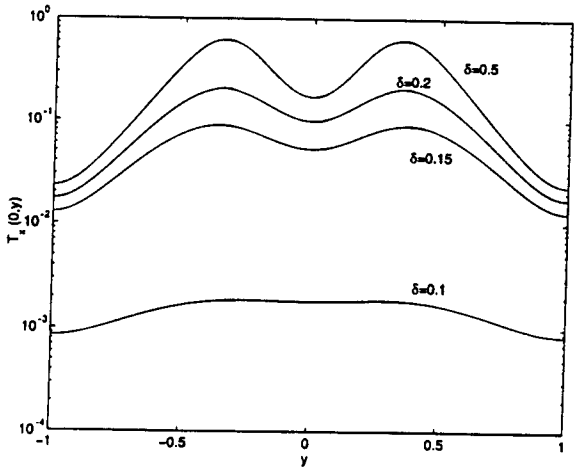


Fig.4. Surface heat flux, $Pe = 10, \alpha = 0.2$.

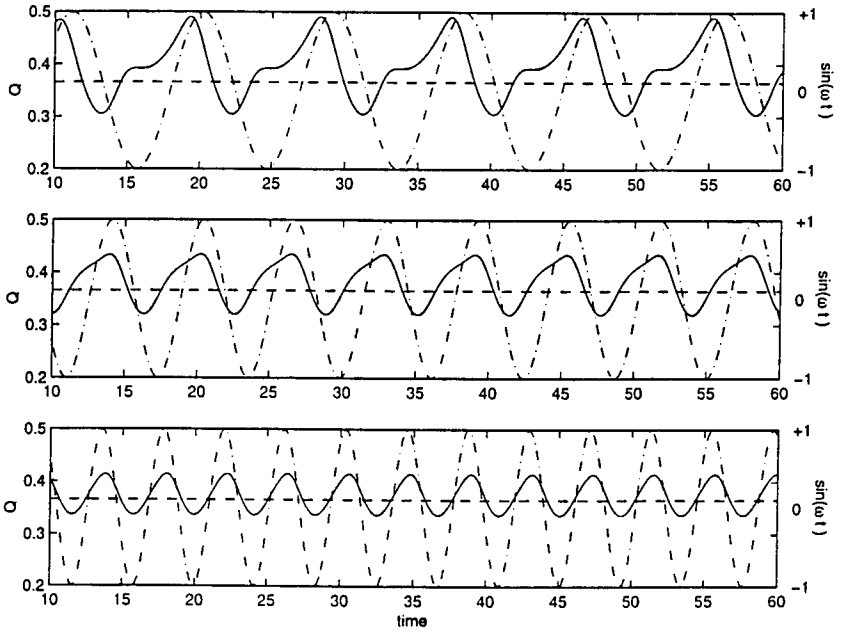


Fig.5. Total surface heat flux.

# COMBUSTION RESEARCH

## AFOSR TASK NO. 93WL036/92WL031

James R. Gord and W. M. Roquemore
Air Force Research Laboratory
Propulsion Directorate
Wright-Patterson Air Force Base OH

**Abstract**

Global Engagement—the Air Force Strategic Vision for the 21st Century—demands enabling propulsion and power solutions such as those currently under development in the Propulsion Directorate of the Air Force Research Laboratory. This strategic vision requires high-performance systems designed to ensure continued air and space superiority; however, signature-reduction concerns and sensitivity to global environmental issues demand low-emissions performance of these propulsion systems as well. Often the very conditions that yield high performance (such as high-heat-release combustion) also contribute to the formation of undesirable engine emissions (such as $NO_x$). Such challenges define the mission of the Propulsion Directorate.

Within the context of this larger mission, the Combustion Branch of the Propulsion Directorate's Propulsion Sciences and Advanced Concepts Division pursues basic research and exploratory development projects to achieve and exceed Air Force propulsion and power goals. Combustion Branch personnel have evolved and refined the work breakdown structure (WBS) depicted in Figure 1 to pursue these ends. This WBS is designed to permit seamless integration of 6.1 and 6.2 efforts and provide customers with the technologies required to achieve the Directorate's mission. At the top of the WBS lie basic-research efforts that have traditionally been supported by AFOSR 6.1 funds. These efforts involve the development and application of advanced optical diagnostics and computer-based simulation and modeling techniques. Together these tools are applied to the study of simple laboratory flames in which fundamental combustion chemistry and physics can be isolated and explored in detail. These three elements of the WBS permit painstaking cross-validation of both the optical diagnostics and the computer codes. These validated experimental and computational tools and the lessons learned during these fundamental combustion studies are applied to exploratory development of advanced combustor concepts during 6.2 efforts. The products of this WBS element are subsequently transitioned to customers that include 6.2 and 6.3 programs in the Turbine Engine Division and the Integrated High-Performance Turbine Engine Technology (IHPTET) Program, for example.

With across-the-board budget cuts affecting all aspects of the Combustion-Branch effort, steps have been taken to maintain each of these WBS elements through increased leveraging of available resources. For example, much of the organization's continued development and application of advanced laser-based diagnostics is now achieved via

collaboration with small businesses through the Small Business Innovation Research (SBIR) Program. Increasingly close teaming with Fuels-Branch researchers has permitted the conservation of precious resources. Finally, cross-directorate teaming has been established in a number of cases to exploit developments across diverse research areas for mutual gains. Some of the products of these collaborative arrangements are highlighted in the material that follows.

This presentation summarizes recent developments in a number of basic-research efforts, including continuing studies of vortex-flame interactions, high-speed visualization of gas turbine spark ignition, and asynchronous optical sampling for ultrasfast pump-probe measurements. Illustrative figures and references to selected recent publications and presentations are included.

**Vortex-Flame Interactions**

A thorough understanding of turbulent reacting flows is essential to the continued development of practical combustion systems. Unfortunately, these studies represent a tremendous research challenge due to the inherent complexity of such flows. In an effort to reduce the complexity of these systems while capturing the essential features that define their physics and chemistry, Combustion-Branch personnel have been studying the interaction of an isolated vortex with a well-controlled flame. These studies have been conducted as part of an international collaboration that includes scientists and engineers from The Central School of Paris and The University of Bielefeld, Germany.

The experimental apparatus (Figure 2) includes a piston-cylinder device configured to provide a precisely controlled toroidal vortex. The generated vortex interacts with a nonpremixed hydrogen-air flame supported in a counterflow burner. The counterflow configuration permits precise control of the flame and the associated strain field. Two-color particle-image velocimetry (PIV) and acetone-vapor planar laser-induced fluorescence (PLIF) have been employed to characterize the vortex and to describe the underlying counterflow velocity field. Flame extinction during these interactions has been studied through the use of OH PLIF (Figure 3), and temperature fields have been imaged through the use of planar Rayleigh scattering.

UNICORN (UNsteady Ignition and COmbustion with ReactioNs), a time-dependent direct-numerical-simulation code with full chemistry for hydrogen-air flames, has been applied to the study of these vortex-flame interactions. This code was developed over the course of the past several years through AFOSR 6.1 funding and validated through a host of 6.1-funded combustion studies. Recent experiments confirm the "Katta-type" annular extinction mechanism predicted by the UNICORN code.

**Spark Ignition**

Spark-ignition systems play a critical role in the performance of essentially all gas turbine engines. These devices are responsible for initiating the combustion process that sustains engine operation. Demanding applications such as cold start and high-altitude relight require continued enhancement of ignition systems. To characterize advanced ignition systems, the Combustion Branch has developed imaging techniques based on high-

repetition-rate laser sources and an ultrafast-framing charge-coupled-device (CCD) camera. Spontaneous-emission measurements as well as laser-based schlieren (Figure 4) and interferometry have been accomplished with this instrumentation and applied to the study of a novel Unison spark igniter. This particular igniter features a multiple-spark "plume" mode of operation that shows great promise for improved cold-start and high-altitude-relight capability over igniters currently in use throughout military and commercial fleets.

While phase-locked imaging was employed to capture the time dynamics of vortex-flame interactions, the Unison spark igniter precludes this approach. Each spark of the igniter is a unique transient event; therefore, a time sequence can not be constructed by adjusting the phase over the course of many spark events; rather, an entire time sequence is acquired for each spark event utilizing the high repetition rates available with modelocked Ti:sapphire laser sources and this unique camera.

**Asynchronous Optical Sampling (ASOPS)**

Time-resolved studies achieved through pump-probe experiments based on state-of-the-art picosecond- and femtosecond-pulsed lasers sources can reveal detailed chemical kinetics and dynamics on ultrashort time scales. While the pump-probe configuration delivers exceptional temporal and spatial resolution, it suffers from some significant limitations when practiced in a traditional delay-line-based geometry. Time-resolved data acquired with a slow-scanning delay line are subject to baseband noise, and any deviation from perfect delay-line alignment and beam collimation produces erroneous pump-probe signals arising from walk off and blooming effects. Asynchronous Optical Sampling (ASOPS), an alternative pump-probe configuration pioneered by Lytle and Laurendeau through 6.1 funding from AFOSR, offers solutions to these limitations. The pump-probe delay is realized in the form of a repetitive phase walk out between two modelocked lasers operating at slightly different pulse-repetition rates. While Lytle and Laurendeau accomplished ASOPS with modelocked Nd:YAG lasers and synchronously pumped dye lasers, Combustion-Branch personnel have recently constructed an all-solid-state asynchronous optical sampler based on diode-pumped Nd:$YVO_4$ lasers and femtosecond modelocked Ti:sapphire lasers (Figure 5). This system has been characterized and applied to the study of supercritical aviation fuels. Combustion applications lie on the horizon.

**Acknowledgment/Disclaimer**

This work was sponsored (in part) by the Air Force Office of Scientific Research, USAF, under task number 93WL036/92WL031. The views and conclusions contained herein are those of the authors and should not be interpreted as necessarily representing the official policies or endorsements, either expressed or implied, of the Air Force Office of Scientific Research or the U.S. Government.

**Selected References**

1. G. J. Fiechtner, P.-H. Renard, C. D. Carter, J. R. Gord, and J. C. Rolon, "Vortex-Flame Interactions: Experimental Verification of the Annular Extinction Predicted by Katta," submitted to Combustion and Flame, May, 1999.

2. G. J. Fiechtner and J. R. Gord, "Absorption and the Dimensionless Overlap Integral for Two-Photon Excitation," submitted to Journal of Quantitative Spectroscopy and Radiative Transfer, April, 1999.

3. M. Linne, T. Settersten, J. Gord, and G. Fiechtner, "Comparison of Density Matrix and Rate Equation Analyses for Picosecond Pump/Probe Combustion Diagnostics," accepted for publication, AIAA Journal, August, 1998.

4. I. Vihinen, J. R. Gord, J. M. Donbar, R. D. Hancock, W. M. Roquemore, G. J. Fiechtner, C. D. Carter, K. D. Grinstead, Jr., V. R. Katta, and J. C. Rolon, "Flame-Vortex Interactions in a Counterflow Burner," Journal of Heat Transfer **120**, 540 (1998).

5. V. R. Katta, C. D. Carter, G. J. Fiechtner, W. M. Roquemore, J. R. Gord, and J. C. Rolon, "Interaction of a Vortex with a Flat Flame Formed Between Opposing Jets of Hydrogen and Air," Twenty-Seventh Symposium (International) on Combustion, The Combustion Institute, Pittsburgh, Pennsylvania, 587 (1998).

6. "Experimental Studies of Vortex-Flame Interactions in an Opposed-Jet Burner," G. J. Fiechtner, P.-H. Renard, C. D. Carter, J. R. Gord, J. M. Donbar, and J. C. Rolon, Joint Technical Meeting of the United States Sections/The Combustion Institute, The George Washington University, Washington, DC, March, 1999.

7. "Regimes of Interaction Between a Nonpremixed Hydrogen-Air Flame and an Isolated Vortex," G. J. Fiechtner, C. D. Carter, V. R. Katta, J. R. Gord, J. M. Donbar, and J. C. Rolon, AIAA 37$^{th}$ Aerospace Sciences Meeting & Exhibit, Reno, Nevada, January, 1999.

8. "Phase Sensitive Imaging in Flows," C. W. Fisher, M. A. Linne, N. T. Middleton, G. J. Fiechtner, and J. R. Gord, AIAA 37$^{th}$ Aerospace Sciences Meeting & Exhibit, Reno, Nevada, January, 1999.

9. "Experimental and Computational Visualization of Vortex-Flame Interactions in an Opposed-Jet Burner," J. R. Gord, J. M. Donbar, G. J. Fiechtner, C. D. Carter, V. R. Katta, and J. C. Rolon, International Conference on Optical Technology and Image Processing in Fluid, Thermal, and Combustion Flow, Yokohama, Japan, December, 1998. Paper No. VS1015.

10. "Dynamic Interactions between a Flame and an Isolated Vortex," G. J. Fiechtner, C. D. Carter, K. D. Grinstead, Jr., J. R. Gord, J. M. Donbar, and J. C. Rolon, Fall Meeting of the Western States Section of the Combustion Institute, University of Washington, Seattle, Washington, October, 1998. Paper No. 98F-10.

11. "A Modelocked-Ti:Sapphire-Based Asynchronous Optical Sampler for Ultrafast Pump-Probe Experiments," J. R. Gord, K. D. Grinstead, Jr., G. J. Fiechtner, and C. E. Bunker, 25$^{th}$ Annual Conference of the Federation of Analytical Chemistry and Spectroscopy Societies (FACSS), Austin, Texas, October 11-16, 1998.

12. "Visualization of Vortex-Flame Interactions in a Counterflow Diffusion Flame," I. Vihinen, J. R. Gord, J. M. Donbar, G. J. Fiechtner, C. D. Carter, and J.-C. Rolon, 8$^{th}$ International Symposium on Flow Visualization, Sorrento (NA), Italy, September 1, 1998.

13. "PIV and OH LIF Imaging of Flame-Vortex Interactions in an Opposed-Jet Burner," J. R. Gord, J. M. Donbar, G. J. Fiechtner, C. D. Carter, and J.-C. Rolon, 9$^{th}$ International Symposium on Applications of Laser Techniques to Fluid Mechanics, Lisbon, Portugal, July 16, 1998.

14. "Flame-Vortex Interactions in a Nonpremixed $H_2/N_2$/Air Counterflow Burner," G. J. Fiechtner, C. D. Carter, J. R. Gord, K. D. Grinstead, W. M. Roquemore, and J. C. Rolon, 34$^{th}$ AIAA/ASME/SAE/ASEE Joint Propulsion Conference and Exhibit, Cleveland, OH, July 13, 1998. Paper No. 98-3770.

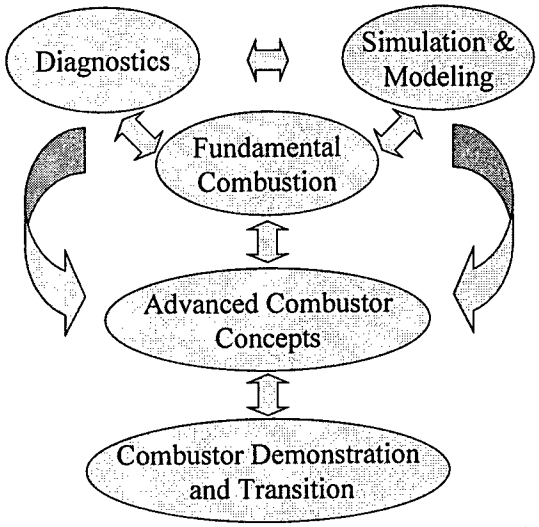


Figure 1: Combustion Branch work breakdown structure (WBS).

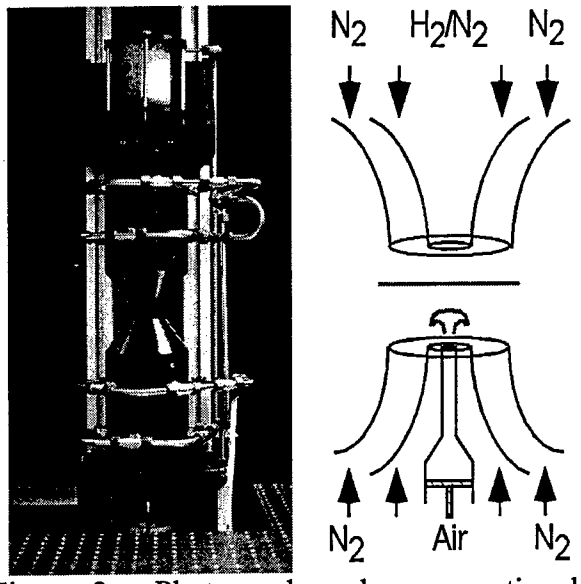


Figure 2: Photograph and cross-sectional diagram of the counterflow burner.

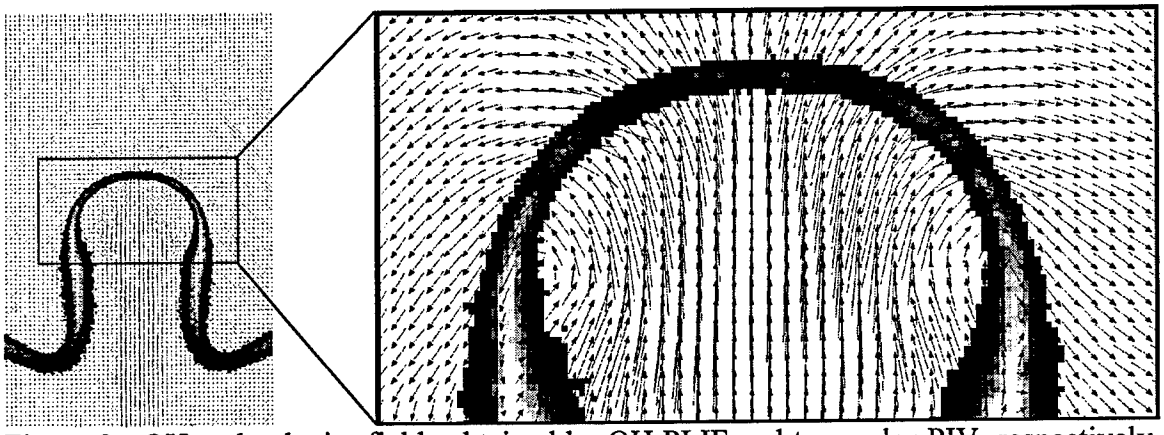

Figure 3: OH and velocity fields obtained by OH PLIF and two-color PIV, respectively, during a vortex-flame interaction.

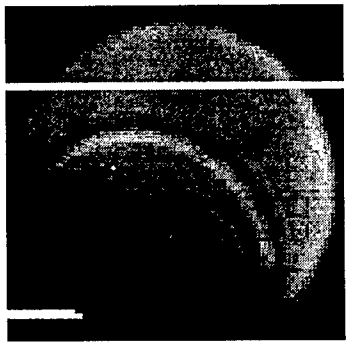

Figure 4: Laser schlieren image of a gas turbine spark igniter.

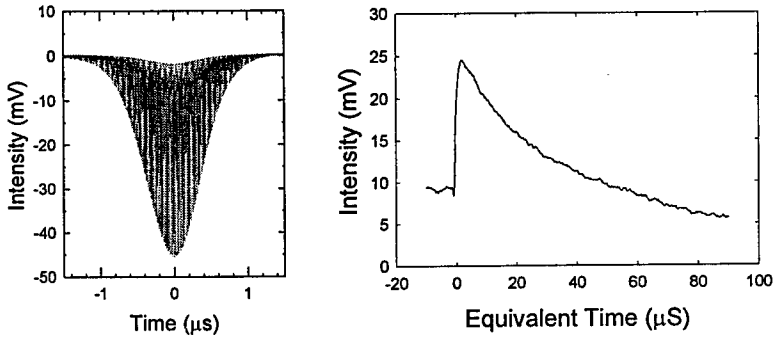


Figure 5: Equivalent-time representations of the ASOPS cross-correlation function and the stimulated-emission decay obtained for IR-125 in methanol. Conversion to real time yields a cross-correlation width (FWHM) of ~200 fs and an IR-125 stimulated-emission lifetime of ~470 ps.

# INTELLIGENT TURBINE ENGINES
# EXPERIMENTAL COMBUSTOR INVESTIGATIONS

**ARO Contract Number DAAH04-96-1-0008**

**Principal Investigators:** **B.T. Zinn, M. Allen, M. Brooke, A. Glezer, W. Haddad, J. Jagoda, S. Menon, Y. Neumeier, J.V.R. Prasad, L. Sankar and J. Seitzman**

**Georgia Institute of Technology**
**Schools of Aerospace, Mechanical and Electrical & Computer Engineering**
**Atlanta, Georgia 30332-0150**

## SUMMARY/OVERVIEW

This program focuses on fundamental and practical issues that will facilitate the development of intelligent control systems for improving the performance of gas turbine engines. This report outlines last year's progress on the work related to the experimental investigation of combustor related issues. These include the control of fuel-air mixing, the manipulation of pattern factors, the development of smart fuel injectors, the use of neural networks to control the combustion process and the development of sensors for monitoring water mole fractions and temperature uniformities.

## TECHNICAL DISCUSSION

This extended abstract is focused on some of our recent accomplishments aimed at improving the performance of combustors in gas turbine engines. These include applications of synthetic jets to the control of fuel-air mixing as well as to manipulating pattern factors, development of smart fuel injectors for controlling fuel spray characteristics, and work on non-intrusive, optical sensors for real time monitoring of water content and temperature profile uniformity at the turbine inlet. Progress on the modeling of the reacting, two phase flow field in the combustor are reported elsewhere in this volume. Progress on our studies dealing with compressors, their actuators, sensors and control strategies, will not be presented this year.

**Fuel-air mixing** using synthetic, zero-mass-flux jet technology continued to be investigated during the current year. These synthetic jet actuators consist of cavities with a small orifice on one side and a flexible diaphragm on the other. Flow is periodically drawn into the cavity from the surrounding near field and re-injected as a well directed jet into the far field. Last year it had been demonstrated that the action of a series of small synthetic jet actuators fitted azimuthally around the exit of a pair of concentric pipes carrying two flows significantly enhances mixing between these flows. This year we concentrated our efforts on identifying the detailed mechanisms responsible for the mixing enhancements. To this end, tests were carried out using a single jet issuing from a one inch nozzle into still air. The nozzle exit was fitted with an azimuthal array of nine small synthetic jet actuators. Hot wire anemometry was used to measure mean velocity and turbulence intensity distributions in the flow field, while planar laser induced fluorescence (PLIF) of acetone seeded into the main jet allowed us to quantify the mixing between that flow and the surroundings. The nine actuators were run in phase, either continuously or spatially and/or temporally amplitude modulated. Where applicable, the modulation signal took the shape of a near square wave. While the synthetic jets increased small scale mixing, the modulation created large scale vortical structures, which modified the global entrainment process. Two dimensional $(r,\phi)$ distributions of phase averaged stream wise velocity components during three cycles of modulation ( see Fig. 1) showed a decrease in stream wise

velocity of the primary jet when the actuators were turned on. This was accompanied by a change in direction of the radial velocity, reminiscent of the passage of a vortex ring through the measurement location. At the same time, two velocity peaks (A & B in Fig. 1)were triggered by the transients associated with the modulations. PLIF measurements showed that while the effect of the actuator on small scale mixing is reduced during the 'down time' that forms part of each modulating cycle, the large structures generated by the modulations cause a net increase in mixing, at least in the near field of the one inch jet. Both velocity and concentration measurements indicated that the large structures created by the modulations moved downstream with the local convective velocities.

Synthetic jets were also used to **control pattern factors**. In these tests the actuator was larger and the diaphragm was replaced by a moveable piston. A single piston could be used to generate multiple synthetic jets if the cylinder was closed off using a cover plate with a number of orifices. The actuator was mounted to the wall of a duct that carried an off-axis, hot stream of combustion products from a propane torch, surrounded by a flow of cold air. It was shown that the actuators could be used to significantly manipulate the non-uniform temperature profile at the duct exit. Typical results obtained in these tests are shown in Fig. 2. The action of the synthetic jets clearly reduced the temperature gradients resulting in an almost uniform temperature field. A variety of orifice shapes, sizes and orientations have been tested and their effectiveness compared using an entropy based mixing parameter. Mean velocity distributions in the flow field were also measured. Results are being compared to steady and pulse jets in cross flow data found in the literature in order to understand the mechanisms responsible for the observed enhanced large scale mixing.

We continued development of an **internally mixed air-assist fuel injector** that provides a controlled spray of desired mass flow rates, droplet diameters and trajectories over a range of operating conditions. A performance map of this injector is shown in Fig. 3. Sauter mean diameters (SMD) are plotted against liquid flow rates over a range of liquid supply pressures. For a given pressure, SMD increases with liquid flow rates. However, the liquid (fuel) supply pressure can be used to vary the SMD for a given flow rate (vertical line in Fig. 3) or change the flow rate for a fixed SMD (horizontal line in Fig. 3). To further optimize the operation of the injector a model of the two phase flow in the injector was developed. This simulation solves the conservation equations subject to the boundary conditions that the pressures at the exit plane of the nozzle be matched and that the air expands continuously inside the injector. The interaction between liquid and air at their interface inside the injector is described as a shear force in the model. Preliminary comparison with experimental data has shown good agreement.

Fast hardware **neural networks** have been used during this reporting period to control simulated combustion instabilities. An eight input neural network chip was designed, built and connected to a computer running a combustor model simulation. Inputs form the model to the chip are used to adjust the network's weights randomly until the difference between desired and actual outputs are minimized. In the example shown in Fig. 4, the variable to be minimized is the fluctuation of the engine pressure. For a cold start (all neural net weights equal to zero), the engine could be stabilized in 5 seconds. A chip with 7 times more weights and 3 times as many inputs currently under development should significantly reduce this time.

An infra-red, line-of-sight, absorption **sensor for monitoring water mole fractions and temperature uniformity** in the exit plane of a high pressure combustor was developed. During the current reporting period, the water absorption band near 2.0 _m was studied and three regions were identified. At 10 atmospheres ambient pressure they are: (i) a low wave number region where absorption by water vapor increases with temperature, (ii) a high wave number regions where such absorption decreases with temperature, and (iii) an intermediate region with weak temperature dependence. The combination of these three allows the effect of temperature to be separated from that of water vapor concentration. A facility has been built in which the sensor can be tested on a 2 _m broad spectrum light source that has been passed

through gas mixtures of different, elevated pressures, temperatures and water vapor concentrations.

A **MEMS fabricated pressure sensor** capable of operating in the high temperature, high pressure environment of a gas turbine engine is being developed. The transducer must be able to withstand temperatures in the 400 to 500 °C range and pressures up to 50 atmospheres and its frequency response must be at least 2 kHz. Previously, we have shown that the mechanical structure of the transducer could be fabricated using alumina-based ceramic tape, which can operate at higher temperatures than silicon-based materials. It was also demonstrated that passive circuit elements could be integrated into the mechanical structure. During the past reporting period we modified the sensor to include a wireless as well as passive method for retrieving pressure data from the sensor. A wireless scheme omits the need for high temperature wiring, bonding and interconnects to the sensor, while a passive scheme eliminates the need for a power supply and an active circuit on the sensor. Passive, wireless telemetry can be achieved using a single multi-loop antenna coil connected to an impedance analyzer, where the phase of the impedance of the antenna is monitored as a function of frequency. If any element of a resonant circuit placed near the coil varies with pressure the circuit's resonance frequency varies with pressure. This variation can be detected by monitoring the phase shift of the signal detected by the antenna coil.

Such a resonance circuit with the MEMS pressure sensor as a pressure sensitive capacitor was designed and built. Tests carried out in a pressure chamber showed that as the ambient pressure was increased, capacitance of the sensor increased causing the resonance frequency of the circuit to decrease measurably. Tests carried out in the 0-1 bar and 0-100 bar ranges showed the sensor to be quite linear with little temperature sensitivity.

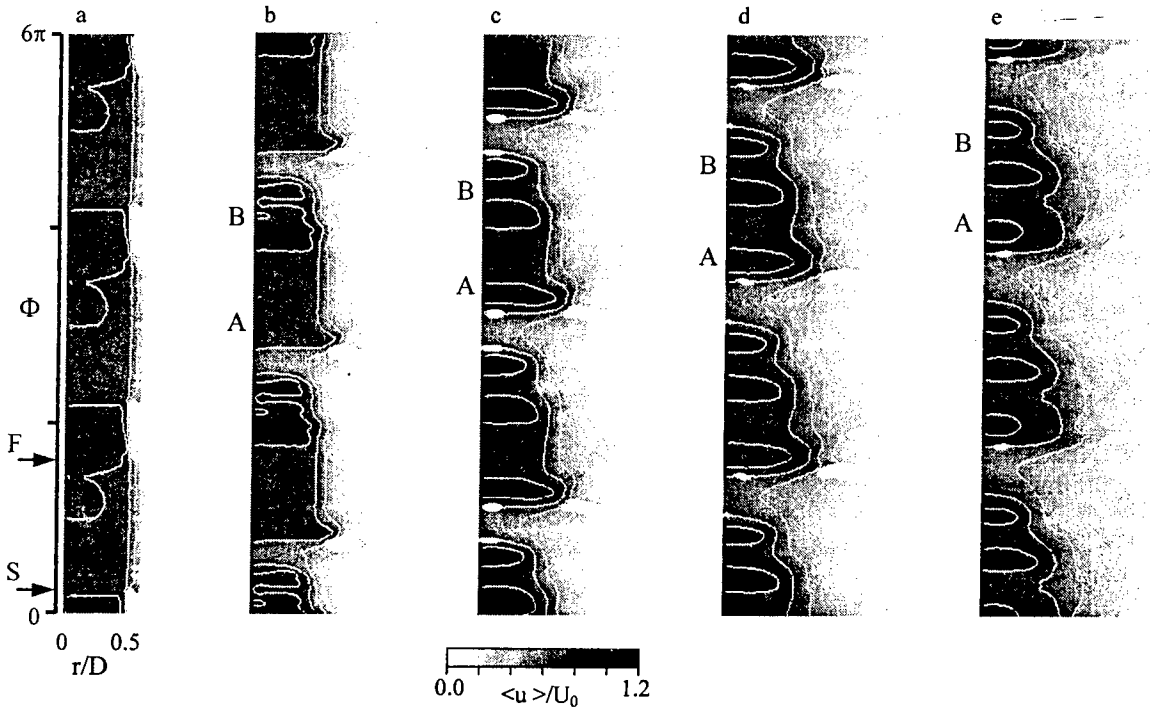


**Fig.1. Raster plots of normalized phase average streamwise velocity as a function of phase and radial location for forcing with all 9 actuators modulated at 40 Hz, x/D = 0.04 (a), 1 (b), 2 (c), 3 (d), 4 (e). S and F mark the phases where the control jets start and finish the active portion of their cycle. Contour lines $\langle u \rangle / U_0 = 0.2$ increments.**

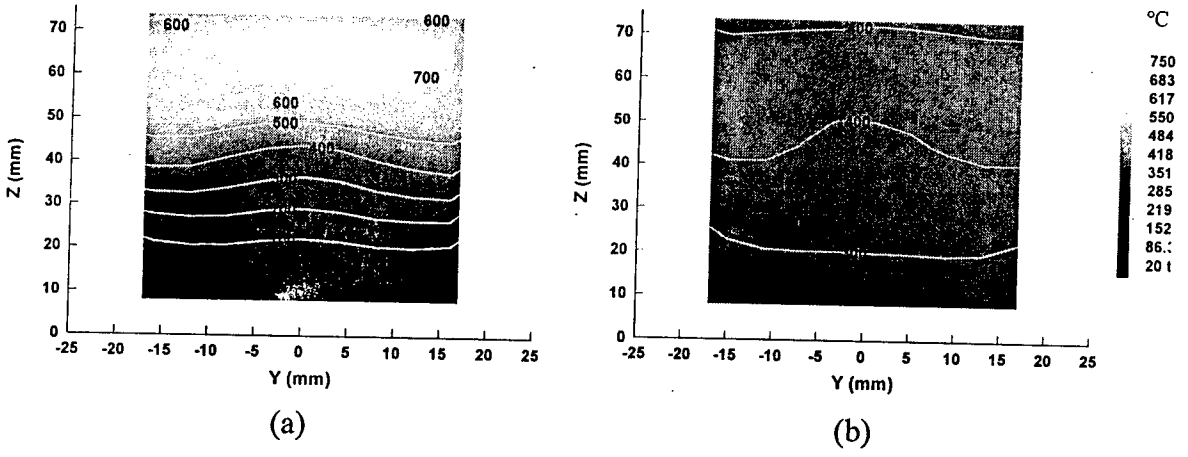


**Fig. 2. Increased temperature uniformity produced by four synthetic jets, placed 80 jet diameters upstream of the measurement location, operating at 10 Hz, and with an average velocity approximately 2.3 times the velocity of the cross-stream (main) flow. The jets blow vertically (Z direction) and their locations across the rectangular duct are indicated by the arrows on the lower (Y) axis.**

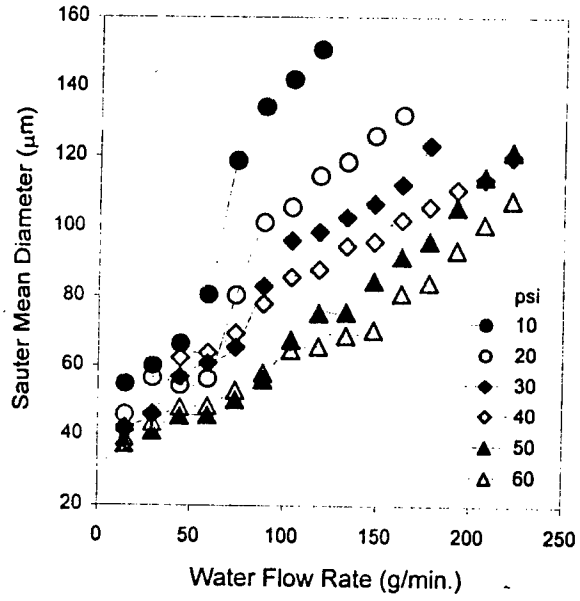


**Fig. 3. Performance map for the internally mixed air-assisted injector. The traces indicate constant liquid supply pressures.**

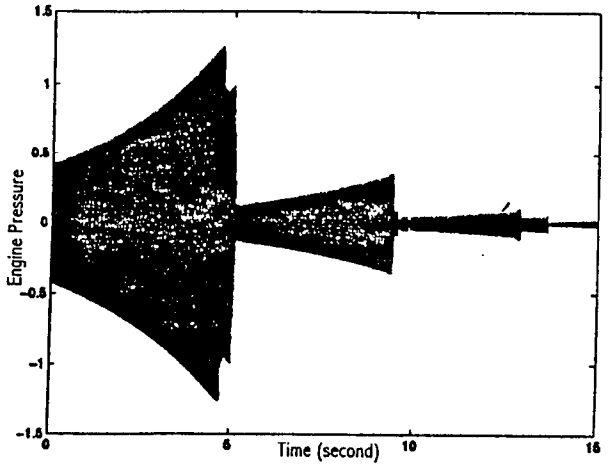


**Fig. 4. Typical results for a simulated combustion instability being controlled by a neural net chip.**

# ENGINE RESEARCH CENTER: ADVANCED DIESEL ENGINE RESEARCH CHEMICALLY REACTING SHEAR LAYER-I: AN EXPERIMENTAL STUDY USING HYDROCARBON FUELS

(ARO Grant/Contract No. DAAH04-94-G-0328)

Principal Investigators: M. Corradini, P. Farrell, D. Foster, J. Ghandhi, J. Martin, R. Reitz, C. Rutland

Engine Research Center
University of Wisconsin-Madison
1500 W. Engineering Dr.
Madison, WI 53711

SUMMARY/OVERVIEW:

Results from a reacting shear layer experiment using a hydrocarbon fuel with full heat release are discussed. Under reacting conditions the layers is still seen to be dominated by large-scale structures, although they appear to be smaller, indicating a smaller growth rate, and more widely spaced than observed for similar non-reacting conditions. Planar images show a thin reaction sheet which can extinguish at low Damkohler numbers. The objective of this work, and a parallel computational effort, is to provide a better fundamental understanding of mixing-controlled combustion; the process which limits the power output of Diesel engines.

AUTHORS: Lyle M. Pickett and Jaal B. Ghandhi

TECHNICAL DISCUSSION:

The latter stage of the combustion in a Diesel engine is mixing-limited. The insufficient mixing rate ultimately limits the amount of fuel which can be burned before excessive soot is produced, and hence, the power output of the engine. It has been demonstrated that augmenting the mixing rate can extend the equivalence ratio at which the soot limit is achieved [1]. The Diesel engine environment is, however, a challenging environment in which to make detailed measurements since it is difficult to isolate individual effects due to the strong coupling of the flowfield. The objective of this study is to investigate the interaction of fluid mechanical and chemical rates in a simplified flow which will allow independent control of the mixing and chemical rates. A parallel computational effort is also underway. The findings from these investigations will contribute to the understanding of turbulent reacting flows, and will enhance the modeling of the mixing-controlled phase of Diesel combustion in the multi-dimensional CFD codes.

**Experimental Apparatus:** To investigate the fundamental interaction between turbulent mixing and hydrocarbon chemistry, a reacting planar shear layer facility has been constructed at the University of Wisconsin Engine Research Center as shown in Figure 1. The facility can be operated at a maximum high speed air velocity of 10 m/s, and the entire system is installed within a pressure vessel capable of operation up to 6 atm. In these experiments the mixing rate is

controlled by the velocity and density ratios of the two streams, while the chemical kinetic rate is controlled by the concentration and temperature of the reactants. Practical chemistry from higher hydrocarbon fuels (e.g. propane) with full heat release is emphasized.

The air and fuel/diluent streams enter separately at the bottom of the vertically mounted pressure vessel. After undergoing a circular to rectangular transition, the two streams pass through a tube bundle followed by a relaxation section, and progressively finer screens before entering the nozzle. A symmetric nozzle with a 2:1 contraction ratio is used in conjunction with a 3.8° tapered splitter plate with a tip thickness of approximately 0.1 mm. The exit dimensions of the nozzle are 5 cm × 20 cm. The test section is designed with movable walls to eliminate the axial pressure gradient, and optical access is gained through two large windows normal to the shear interface as seen in Figure 1. Thin windows capable of passing a laser sheet are installed in the movable walls. Two small thermocouples are mounted at the nozzle exit to monitor the inlet temperatures of the two streams.

Due to the high velocities and high ignition energy requirements of hydrocarbon fuels, a

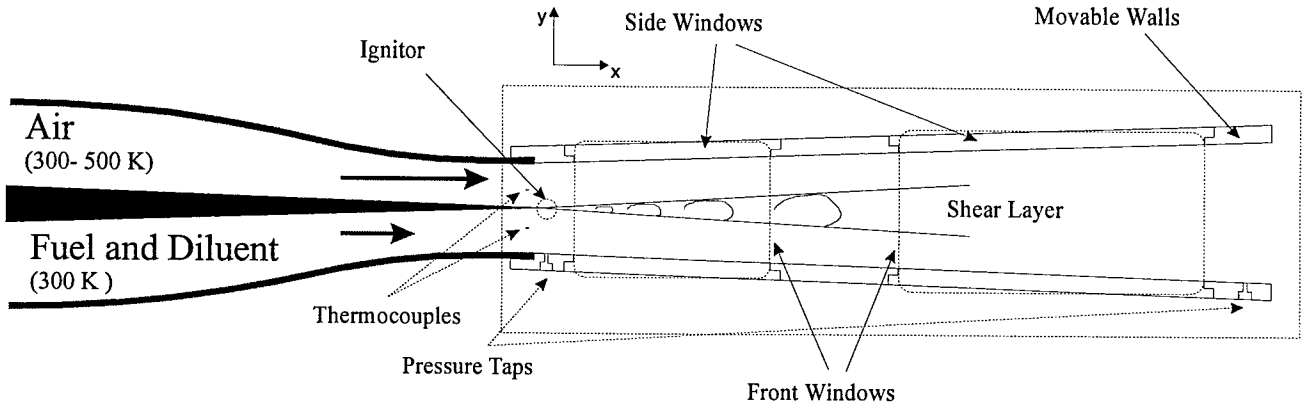


**Figure 1** Shear layer test section.

swirl burner is employed as the ignition source. The burner is installed at the tip of the splitter plate, and is directed across the shear layer, normal to the flow direction. The exit of the pressure vessel has a throttling valve to avoid acoustic disturbances, and the exhaust stream is sent through a quench tower before going into the building exhaust. Acoustic baffles were also required in the delivery system to avoid acoustic coupling with the chemical reaction.

**Non-Reacting Flow:** Initial tests were performed under non-reacting conditions to verify the facility. Velocity data were obtained using hot-wire anemometry and indicated that the inlet conditions were uniform within 1.3% and that the free stream turbulence level was less than 0.8%. Further, the velocity profile was measured at several downstream locations under atmospheric pressure. The velocity profiles were found to be were self-similar for distances beyond 200× the momentum thickness at the splitter plate tip. The growth rate of the shear layer obtained from velocity data was found to fall within the range reported in the literature [2]. Flow visualization indicated the presence of large scale structures which persist throughout the layer with a size, spacing and convective velocity consistent with the literature values.

**Reacting Flow:** Under reacting conditions the combustion in the mixing layer has been found to produce a significant amount of soot when operating with propane. The presence of the soot has allowed the characterization of the combustion process through high speed movies of the flame (soot) luminosity. These images provide a line of sight projection of the flame zone. A more

detailed investigation of the flame zone is acquired by imaging the light scattered from a sheet of laser light passed normal to the shear layer. A pulsed Nd:YAG laser formed into a 300 μm thick sheet with a pulse duration of 10 ns was used in conjunction with a narrow bandpass filter on the camera. The sheet passed through the midpoint of the transverse direction.

Figure 2 shows a comparison of a non-reacting shadowgraph image (a), and reacting images acquired using the soot luminosity, (b), and the elastic scattering from the soot, (c). The images are all obtained with a high speed velocity, $U_1$, of 3 m/s and a velocity ratio, $r$, of 0.4 at a system pressure of 2 atm. The oxidizer stream is air and the fuel stream is 40% by volume propane with a balance of argon. The presence of the combustion does not affect the presence of the large scale structures which are observed under non-reacting conditions. The spacing of the vortex cores does, however, appear to increase with the presence of the heat release. In addition, the visual thickness of the layer appears to decrease slightly due to the combustion. These phenomena are thought to be due to the a combination of the decrease of entrainment due to the expansion of the burned gases, the increase in viscosity at the elevated temperatures and the effect of buoyancy which acts in the vertical direction in Figure 2.

The soot luminosity, Figure 2 b), shows the presence of brighter vortex core regions, where more mixing has taken place, and thin, high-strain braid regions that connect the cores. It should be noted that the soot is expected to present only on the fuel side of the flame. The high luminosity from the vortex cores would indicate the high concentration of fuel in the core

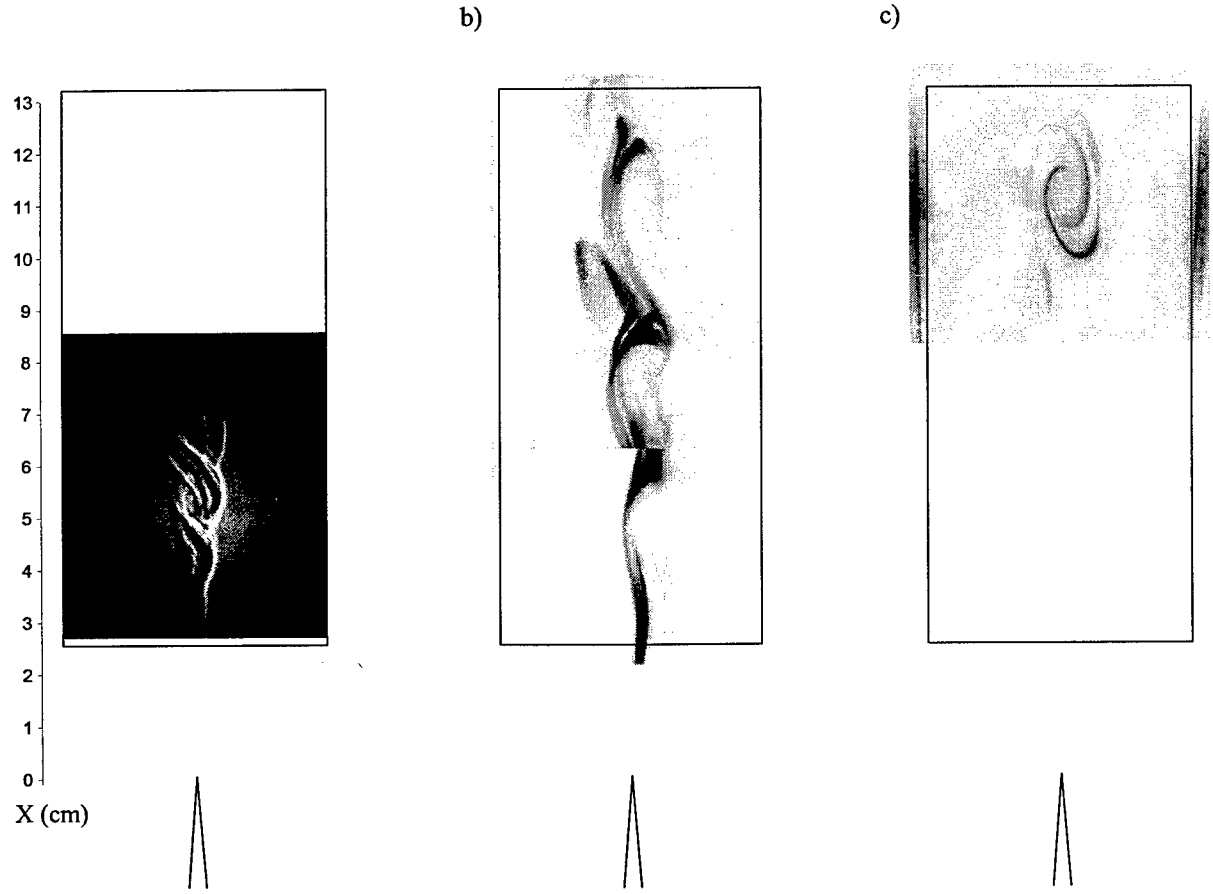


**Figure 2** Comparison of reacting and non-reacting shear layer; a) non-reacting shadowgraph, b) flame luminosity, c) elastic scatter from laser sheet illumination. Conditions for all tests: $U_1 = 3$ m/s; $T_1 = 400$ K; $r = 0.4$; $T_2$=300 K; $P = 2$ atm; $X_{fuel} = 0.4$.

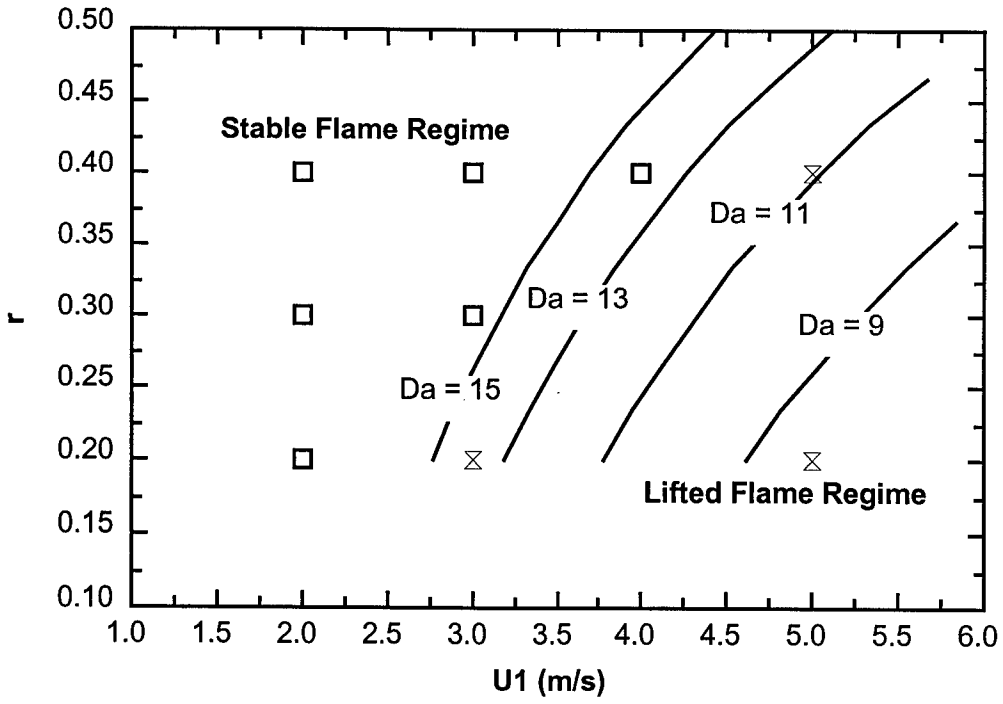


**Figure 3** Reacting mixing-layer regimes at various operating conditions. Mixing layer Damkohler number calculated at x = 10 cm. P = 2 atm, $T_{air}$ = 300 K, $T_{fuel}$ = 300 K, $X_{C3H8}$=0.4, $X_{Ar}$ = 0.6. Da =$\tau_d / \tau_{chem}$ , $\tau_d = \delta/\Delta U$, $\tau_{chem} = \delta_L/S_L$.

regions. However, the elastic scatter soot image, Figure 2 c), indicates that the soot zone is thin and largely two-dimensional at this location.

As the fuel concentration is decreased, the flame position is observed to shift towards the fuel side. With a larger velocity difference (a lower value of *r*) the flame penetrates more of the vortex core and the braid region appears thinner. At even higher velocity ratios and convective speeds the flame is strained and extinguished near the splitter plate tip. In some situations a lifted flame can stabilize downstream from the splitter plate, or complete extinction can occur. The flame behavior at various operating conditions is indicated in Figure 3. These results can be related to lines of constant Damkohler number, showing the relationship between characteristic mixing time and chemical time of the shear layer. The trend for flame liftoff is predicted at lower Damkohler number which agrees with what has been observed qualitatively in the layer. A lower velocity ratio increases the strain in the layer and reduces the characteristic mixing time. Changes in fuel concentration and temperature also result in corresponding changes in the chemical time.

## References

1] Kurtz, E.M. and Foster, D.E., "Exploring the Limits of Improving DI Diesel Emissions by Increasing In-Cylinder Mixing, SAE Paper 982678, 1998.

2] Brown, G. L., and Roshko, A. (1974), "On Density Effects and Large Structures in Turbulent Mixing Layers," *J. Fluid Mech.*, vol. 64, part 4, pp. 775-816.

# MULTI-SCALAR IMAGING IN TURBULENT NONPREMIXED FLAMES

AFOSR Grant No. 97-1-0096

Principle Investigator: Marshall B. Long

Yale University
Department of Mechanical Engineering and Center for Laser Diagnostics
New Haven, Connecticut 06520-8284

## SUMMARY/OVERVIEW

Our current research examines issues relating to measurement of scalars and velocity in turbulent flows. Preliminary results of simultaneous particle-imaging velocimetry and optical flow are discussed. The latter technique shows promise for the extraction of velocity vectors from the brightness variations present in turbulent flow images and offers the capability of simultaneous velocity and scalar measurements with a single dual-frame CCD camera.

## TECHNICAL DISCUSSION

An ongoing focus in our laboratory has been the development and application of laser imaging techniques that can provide two- and three-dimensional measurements in turbulent flames. One parameter of significant interest is the mixture fraction, $\xi$, defined as the mass fraction of all atoms originating from the fuel stream. Images of $\xi$ allow calculation of axial and radial gradient information, and in particular the scalar dissipation $\chi$, which controls the rate of molecular mixing in the flow. Experimental determination of these parameters is important for developing and testing turbulent flame models. The method we most often use for mixture fraction determination is a two-scalar approach, involving assumptions of unity Lewis number and simplified one-step reaction between fuel and oxidizer streams. It has been shown that the measurement of fuel concentration and Rayleigh scattering is sufficient to determine mixture fraction by this approach, and has been successfully applied in turbulent flames.[1-7] During the current funding period, multiple scalar measurements have been explored to investigate the confidence in the mixture fraction calculation around the stoichiometric contour. At this location, the fuel concentration approaches zero and the Rayleigh signal varies slowly with mixture fraction. In one set of experiments, nitrogen Raman imaging allowed an independent calculation of mixture fraction from a passive conserved scalar formulation leading to improved performance of the two-scalar approach.[8]

Data sets generated from measurement of scalar quantities such as mixture fraction would be more useful to the modeling community with the addition of simultaneous velocity information. Experiments of this type have been performed in the past using simultaneous biacetyl/particle seeding.[9] In those experiments, two separate lasers and cameras were used for PIV and biacetyl fluorescence. The second harmonic of a double-pulsed Nd:YAG laser was used for the PIV measurements. Biacetyl fluorescence was excited at 440 nm with a flashlamp-pumped dye laser. Both laser beams were overlapped with a dichroic beam splitter and then formed into a single sheet to illuminate a planar region of the flow. The timing of the lasers was arranged so that the dye laser pulse occurred during the period between the two pulses from the Nd:YAG laser. The flame selected for study was an unsteady premixed propane/biacetyl/air flame, stabilized on a piloted burner. The air was seeded with both biacetyl vapor and submicron alumina particles and then mixed with propane. An example of the simultaneous scalar/velocity data is shown in Fig. 1.

While we demonstrated that PIV can be combined with scalar measurements using PLIF, these techniques complicate simultaneous laser-based measurements of certain scalar quantities due to interference from the seed particles. In particular, simultaneous imaging of Rayleigh scattering is

impossible, making temperature and mixture fraction measurements difficult. A number of "non-particle" velocimetry approaches have been applied in turbulent flows, though few have found broad applicability under reacting conditions. For instance, the Scalar Imaging Velocimetry approach of Dahm *et al.*[10] produces a velocity field by inverting the scalar transport equation, but has been applied primarily to large Schmidt numbers flows for which four-dimensional data are available. The Image Correlation Velocimetry (ICV) technique of Tokumaru and Dimotakis[11] provides a basis for measuring the displacement fields of gas-phase fluid motions. Extension of this approach to reacting flows appears feasible[12,13] provided appropriate scalars are selected for imaging and validation experiments are carried out. Recent work on dynamic programming algorithms for optical flow have been reported to achieve results which in some cases are superior to conventional PIV.[14] These techniques are based on concepts known to the computer vision community as optical flow.

Optical flow is concerned with the apparent motion of an image (or brightness) pattern between two frames.[15] Under well-posed conditions, the optical flow will faithfully characterize the actual motion field giving rise to the sequential images. Several optical flow methodologies exist, and the more common approaches are based on either differential techniques or region-based matching.[16] In recent work, we have examined region-based approaches[17] because these do not suffer from the difficulties associated with numerical differentiation or the requirement of small displacements (~1 pixel/frame) as is the case with differential techniques.[10,14] These and other approaches can at best provide an approximation to the instantaneous two-dimensional fluid velocity given a planar scalar measurement. The approximation is valid when the velocity in the third, unmeasured direction is small, or the scalar gradient in that dimension is small.[10] However, this requirement is no less restrictive than with two-dimensional PIV.

Although the various approaches are sometimes calibrated using synthetic images[15,18], direct comparisons between velocities obtained from optical flow and PIV are not available. In an attempt to fill this gap, we have performed preliminary experiments in an isothermal turbulent jet of air seeded with both acetone and alumina particles. The nozzle used in these experiments consists of simple tube with a squared-off end (6.35 mm OD; 4.57 mm ID). The turbulent jet issues into an unconfined low velocity coflow of air (~1 m/s). The illumination source consists of the fourth harmonic (266 nm) of an Nd:YAG laser (Continuum, Powerlite 8000) which is formed into a sheet approximately 5 mm high with a beam energy of ~6 mJ per pulse. The laser is operated in dual-pulse mode with a pulse separation of 50 μs. The camera employed for the acetone fluorescence is a dual-frame Cooke Corp./PCO SensiCam with an interline progressive-scan CCD (1280 x 1024 pixels). This camera allows the acquisition of two exposures separated by as little as 200 ns. The primary collection lens is a large-format camera objective (Canon, 85 mm, *f*/1.2) with a corresponding magnification of 31 pixels/mm. A glass filter (Schott, WG305) is used to minimize residual Mie scattering. The acetone fluorescence is broadband, peaking around 430 nm. This setup allows the acquisition of two acetone fluorescence images for use in optical flow velocimetry. A Photometrics CH350 camera with a UV sensitive CCD coating (QE=10%) and a Nikon Nikkor UV lens (*f*/4.5) allows direct imaging of the Mie scattering from the seed particles. This camera is exposed during both pulses of the laser, and velocities are extracted from this single image using an autocorrelation technique. The submicron alumina particles are introduced into the air using a cyclone seeding unit. Acetone seeding is accomplished by passing air through a fritted tube submerged in a 500 mL flask filled with acetone. This bubbler is placed in a water bath at room temperature to maintain the temperature of the liquid. For this experiment, the air flow rates were split uniformly between particle and acetone seeder to provide a $Re$=2540 jet of air. Fig. 2 shows representative scalar images for this flow which could be used as input to an optical flow algorithm for extraction of velocity vectors.

In future work, the relative performance of different optical flow implementations will be evaluated to identify approaches most suitable for application to turbulent reacting flows. As this technique matures, extension to three dimensions for simultaneous 3D scalar/velocity measurements could become feasible in complex gas-phase reacting environments.

The dual-frame camera used in this experiment offers additional capability beyond velocimetry applications (both PIV and optical flow techniques). The fast electronic shuttering (down to 100 ns) offers the possibility of eliminating additional optical components necessary in intensified systems where gateability is the only requirement. This improves the spatial resolution of the imaging system. To demonstrate this, an air-diluted methane flame (54% CH4, 46% air by volume) stabilized on the same nozzle was examined with the non-intensified imaging system. This blue, moderately sooty flame was selected in order to assess the ability to discriminate against flame interferences using the camera's fast shutter capability. For this experiment, a flashlamp-pumped dye laser (Candela, LFDL-20, 1.2 J/pulse) was employed for Rayleigh scattering measurements. The luminosity was integrated single-shot for 4 $\mu$s (to bracket the duration of the 2 $\mu$s dye laser pulse) and 1000 $\mu$s, where the latter value was intended to be representative of a CCD camera operating with a conventional mechanical shutter and minimum 1 ms exposure time. In the fast shutter case, luminosity accounts for less than 5% of the signal relative to a standard helium background image, and about 3% of the signal in the hot zone of the flame. This contrasts with the long exposure case where these values increase to 48% and 25%, respectively.

REFERENCES


1. Long, M.B., Frank, J.H., Lyons, K.M., Marran, D.F., and Stårner, S.H., "A Technique for Mixture Fraction Imaging in Turbulent Nonpremixed Flames," *Ber. Bunsenges. Phys. Chem.*, **97**:1555-1559 (1993).
2. Frank, J.H., Lyons, K.M., Marran, D.F., Long, M.B., Stårner, S.H., and Bilger, R.W., "Mixture Fraction Imaging in Turbulent Nonpremixed Hydrocarbon Flames," *Twenty-Fifth Symposium (International) on Combustion*, The Combustion Institute, Pittsburgh, PA, 1994, pp. 1159-1166.
3. Stårner, S.H., Bilger, R.W., Lyons, K.M., Frank, J.H., and Long, M.B., "Conserved Scalar Measurements in Turbulent Diffusion Flames by a Raman and Rayleigh Ribbon Imaging Method," Combust. Flame, **99**:347-354 (1994).
4. Marran, D.F., Frank, J.H., Long, M.B., Stårner, S.H., and Bilger, R.W., "An Intracavity Technique for Improved Raman/Rayleigh Imaging in Flames," *Opt. Lett.*, **20**: 791-3 (1995).
5. Stårner, S.H., Bilger, R.W., and Long, M.B., "A Method for Contour-Aligned Smoothing of Joint 2D Scalar Images in Turbulent Flames," *Combust. Sci. and Tech.*, **107**:195-203 (1995).
6. Stårner, S.H., Bilger, R.W., Frank, J.H., Marran, D.F., Long, M.B., "Mixture Fraction Imaging in a Lifted Methane Jet Flame," *Combust. Flame*. **107**:307-313 (1996).
7. Stårner, S.H., Bilger, R.W., Frank, J.H., Marran, D.F., Long, M.B., "Measurements of Mixture Fraction and Scalar Dissipation in a Turbulent Hydrogen Diffusion Flame," paper presented at the *15th International Colloquium on the Dynamics of Explosions and Reactive Systems*, University of Colorado, Boulder, CO, July 30 - August 4 (1995).
8. Fielding, J., Schaffer, A.M., Long, M.B., "Three-Scalar Imaging in Turbulent Nonpremixed Flames of Methane," *Twenty-Seventh Symposium (International) on Combustion*, (in press) The Combustion Institute, Pittsburgh, PA (1998).
9. J.H. Frank, K.M. Lyons, and M.B. Long, "Simultaneous Scalar/Velocity Field Measurements in Turbulent Gas-Phase Flows," *Combust. Flame*, **107**:1-12 (1996).
10. Dahm, W.J.A., Su, L.K., Southerland, K.B., "A Scalar Imaging Velocimetry Technique for Fully Resolved Four-Dimensional Vector Velocity Field Measurements in Turbulent Flows," *Phys. Fluids A*, **4**:2191-2206 (1992).
11. Tokumaru, P.T., Dimotakis, P.E., "Image Correlation Velocimetry," *Exp. In Fluids*, **19**:1-15 (1995).
12. Komiyama, M., Miyafuji, A., Takagi, T., "Flamelet Behavior in a Turbulent Diffusion Flame Measured by Rayeligh Scattering Image Velocimetry," *Twenty-Sixth Symposium (International) on Combustion*, The Combustion Institute, Pittsburgh, PA, pp. 339-346 (1996).

13. Grunefeld, G., Graber, A., Diekmann, A., Kruger, S., Andresen, P., "Measurement System for Simultaneous Species Densities, Temperature, and Velocity Double-pulse Measurements in Turbulent Hydrogen Flames," *Combust. Sci. and Tech.*, **135**:135-152 (1998).
14. Levy, Y., Golovanevsky, B., Kowalewski, T.A., "Fluid Image Velocimetry for Unseeded Flow," *9th International Symposium on Applications of Laser Techniques to Fluid Mechanics*, Lisbon, Portugal, July 13-16 (1998).
15. Horn, B.K.P. and Schunk, B.G., *MIT Artificial Intelligence Laboratory* , Memo No. 572 (1980).
16. Barron, J.L., Fleet, D.J., and Beauchemin, S.S., "Performance of Optical Flow Techniques," *Int. J. Comp. Vision,* **12**:43-77 (1994).
17. Anandan, P., "A Computational Framework and an Algorithm for the Measurement of Visual Motion," *Int. J. Comp. Vision,* **2**:283-310 (1989).
18. Quénot, G.M., Pakleza, J., and Kowalewski, T.A., "Particle Image Velocimetry with Optical Flow," *Exp. In Fluids*, **25**:177-189 (1998).

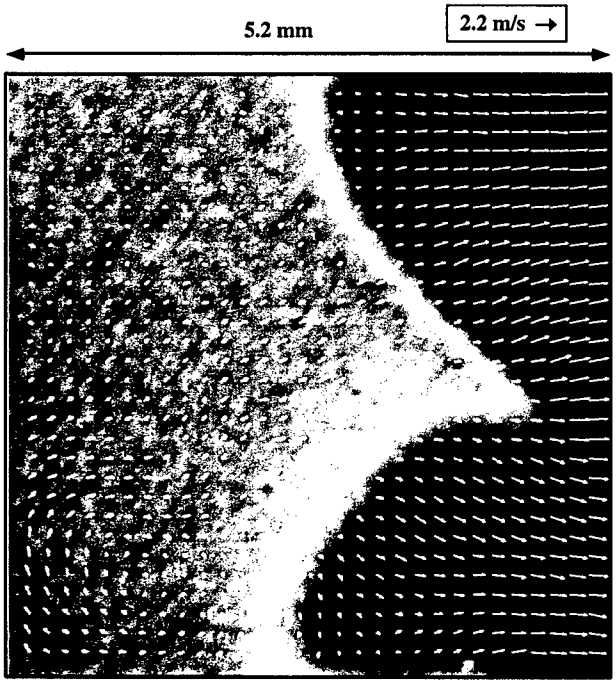


Figure 1. A measurement of the reactant concentration and velocity field in a premixed propane/biacetyl/air flame. The velocity field is plotted from a frame of reference convected downstream at 4.8 m/s.

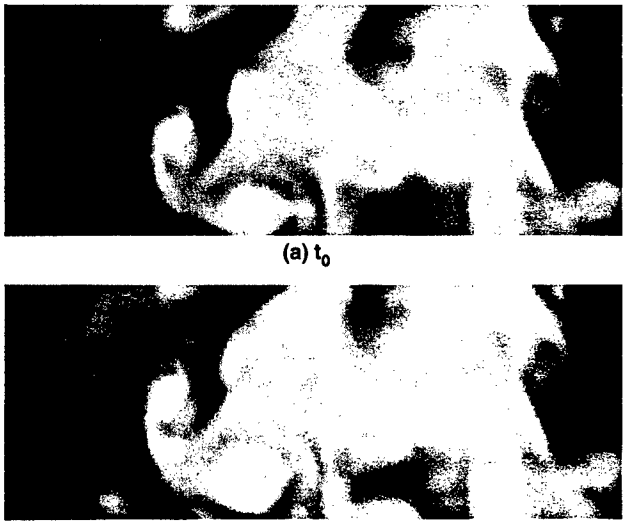


Figure 2. Acetone fluorescence in a jet of seeded air obtained with double-pulsed 266 nm excitation, imaged at two times with a dual-frame camera. Images such as this may be able to provide simulataneous concentration and velocity information.

# PHYSICAL AND CHEMICAL PROCESSES IN FLAMES

(AFOSR Grant No. F49620-98-1-0075)

Principal Investigator: Chung K. Law

Princeton University
Princeton, NJ 08544

## SUMMARY/OVERVIEW

The objectives of the present program are two-fold, namely to study the structure and dynamics of laminar premixed and nonpremixed flames, and to develop detailed and simplified chemical kinetic mechanisms for the oxidation of hydrocarbon fuels. During the reporting period progress has been made in the following projects: (1) a computational study on the pulsating propagation and extinction of hydrogen/air flames; (2) development of comprehensive chemical kinetic mechanisms for hydrocarbon oxidation; (3) experimental determination of laminar flame speeds of $C_1$ to $C_8$ hydrocarbons; (4) an experimental and modeling study of propene pyrolysis and oxidation kinetics; (5) an experimental, RRKM, and modeling study of propyne pyrolysis and oxidation in flow reactor and in laminar flames; (6) a quantum mechanical and kinetic modeling study of acetylene oxidation in shock tubes; and (7) an experimental and modeling study of the structure and sooting limits in counterflow methane/air and propane/air diffusion flames from one to five atmospheres.

## TECHNICAL DISCUSSION

1. Steady and Pulsating Propagation of Rich Hydrogen/Air Flames at Atmospheric and Elevated Pressures

Previous computational simulation of atmospheric one-dimensional planar hydrogen/air flames with detailed chemistry and transport has shown that pulsating instability develops as the rich flammability limit is approached. Figure 1 shows the transition in the flame response as the burning becomes progressively weaker with increasing fuel equivalence ratio, $\phi$, at one atmosphere and allowing for radiative loss. Specifically, for $\phi$=7.3, the maximum flame temperature and hence flame propagation remain steady. However, the propagation becomes oscillatory at $\phi$=7.4, changes to period doubling at $\phi$=7.6, and extinguishes at $\phi$=7.8. Since the steady-state extinction turning point occurs at $\phi$=10.22, the result shows that oscillation reduces the flammability limit defined for the steady flame.

The present study extends the previous investigation to include effects of elevated ambient pressure, for pressures ranging from 1 to 20 atmospheres, with emphasis on the influence of chain-mechanisms in $H_2/O_2$ oxidation. For steady burning, Fig. 2 shows that, with increasing pressure, the burning rate first increases (Regime I), then decreases (Regime II), and then increases again (Regime III), thereby resulting in the occurrence of a maximum burning rate and a minimum burning rate. In Fig. 3 the states of these maximum and minimum burning rates are plotted for the system pressure and the temperature at the maximum heat release rate of the flame. In the same figure the crossover temperature for the second and extended second explosion limits for the hydrogen/oxygen system is also plotted, showing that the states of maximum and minimum burning rates largely correspond to those of the crossover temperature. Sensitivity analysis then demonstrated that Regime I is dominated by the $H+O_2$, $O+H_2$, and $OH+H_2$ fast-branching sequence, Regime II is significantly influenced by the $H+O_2+M$ terminating reaction, and Regime III is dominated by the slow-branching $HO_2$ and $H_2O_2$ chemistry. It is significant to recognize that the response of the burning rate, which is expected

to be fundamentally affected by diffusion, follows that of the explosion chemistry of the homogeneous system.

Further calculations were performed for the states of steady extinction, the onset of pulsation, and the extinction of the pulsating flame, as shown in Fig. 4. It is again observed that pulsating extinction occurs at lower concentrations than those of the steady flames, indicating a narrowing of the flammability limit when considering flame unsteadiness. Furthermore, the states for the onset of pulsation are very close to those of the maximum burning rate, which implies that the onset of pulsation is also controlled by the crossover temperature, as shown in Fig. 3. The cause for this very close coincidence has yet to be identified, although it must be somehow related to the slowing down of the reaction rate by the $H+O_2+M$ reaction, beyond the maximum burning state, and thereby the increase in the effective activation energy. This in turn favors the Sivashinsky criterion $Ze(Le-1)\gtrsim 11$ for the onset of pulsating instability, where Ze is the Zel'dovich number and Le the Lewis number.

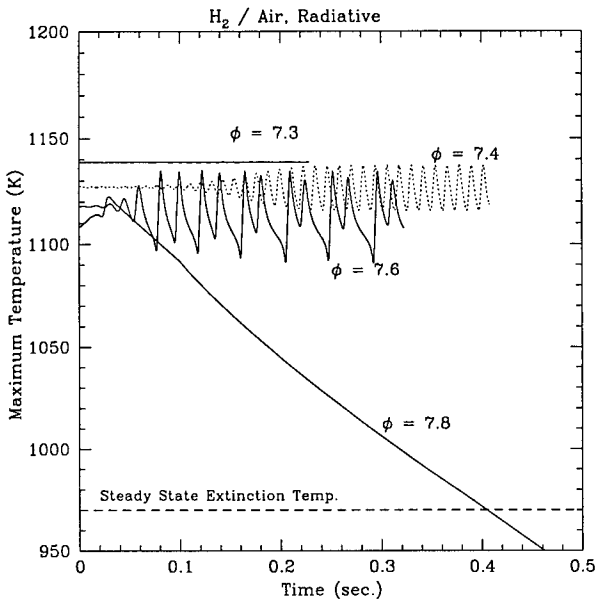


Figure 1

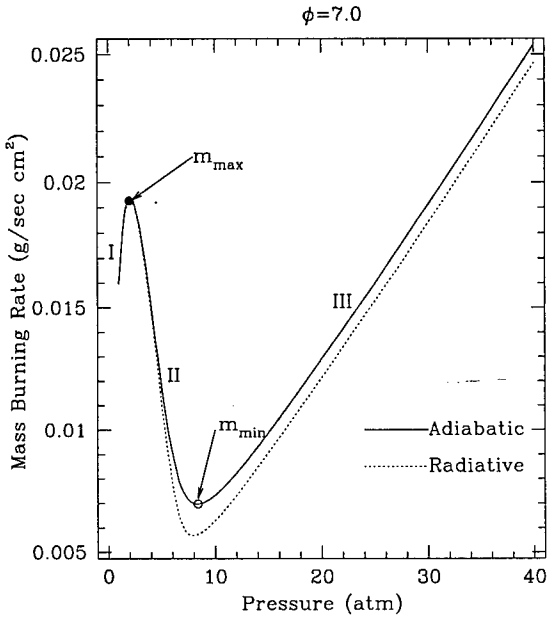


Figure 2

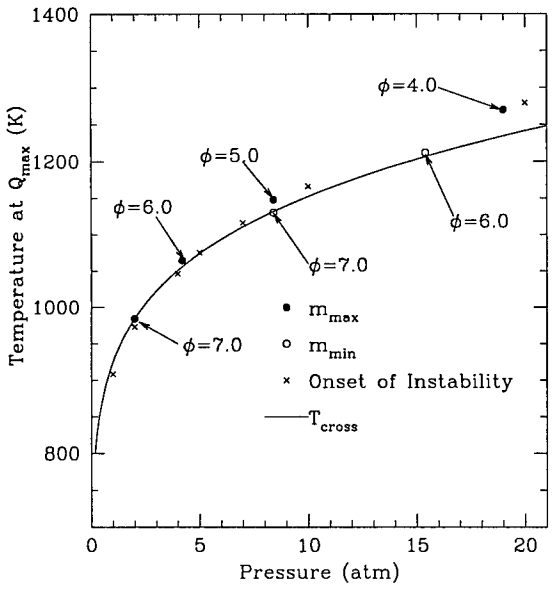


Figure 3

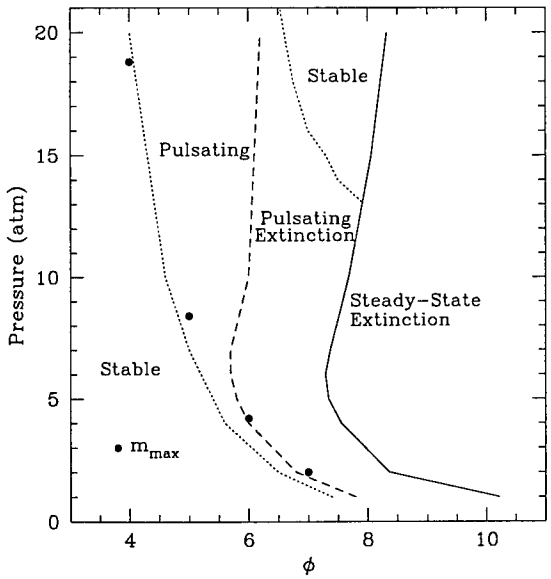


Figure 4

The study also found that a mixture that is pulsatingly extinguishable, and hence nonflammable, can assume a steady burning mode at higher pressures (Fig. 4). This is caused by the reduction in the effective activation energy for the weakly-branching reactions which are dominant under high pressures.

The above results are reported in Publication Nos. 1 and 2.

2. Development of Comprehensive Kinetic Mechanisms for Hydrocarbon Oxidation

Recognizing the lack of a comprehensive chemical kinetic mechanism for aeropropulsion fuels in general, and the significantly reduced residence time and hence heightened performance sensitivity to chemical kinetics in supersonic combustion in particular, an experimental-computational effort is undertaken for the development of such a mechanism for hydrocarbon fuels up to $C_8$. The basic requirements for this mechanism include: (a) fundamental input of thermochemistry and elementary reaction kinetics; and (b) predictive capability of the wide spectrum of combustion phenomena, from the response of homogeneous systems such as shock tube and auto-ignition delays, to the ignition, steady burning, and extinction of premixed and diffusion flames for which diffusive transport is present, and ultimately to the characteristics of pollutant formation. The reaction mechanism should also be applicable to a wide variety of hydrocarbon fuels and should incorporate any pressure effects on the combustion responses. To achieve this goal, experiments will be conducted to acquire fundamental combustion data such as the laminar flame speeds and the extinction of stretched premixed and diffusion flames, while *ab initio* quantum mechanical calculations will also be performed to determine the rate coefficients. To bring the fundamental understanding of reaction kinetics to a predictive model, systematic optimization of the reaction rate parameters within their uncertainties will be performed, and the optimized model validated against an even wider range of combustion data. Lastly, the detailed reaction mechanism will be reduced to smaller mechanisms that are still quantitatively predictive but are sufficiently simple for implementation in large-scale modeling.

During the reporting period, progress was on the combustion kinetics of low molecular-weight fuels, including acetylene, ethylene, propyne, allene, propene, and propane. The reaction kinetics of these fuels constitutes a critical subset of a comprehensive mechanism of aeropropulsion fuels. In addition to the study of small hydrocarbons and recognizing the lack of reliable, fundamental combustion data for alkane and alkene fuels in general, a comprehensive experimental study on the laminar flame speeds of $C_1$ to $C_8$ hydrocarbons was also conducted. These data are critical for the present and future tasks of mechanism development.

Theoretically, high-level *ab initio* calculations were performed for a number of reaction systems pertinent to $C_2$ and $C_3$ combustion. The reaction rate constants were determined by the Rice-Ramsperger-Kassel-Marcus (RRKM) theory. Numerically, computation and sensitivity analysis were conducted using detailed reaction mechanisms, which were validated against a variety of experimental data, including fuel pyrolysis and oxidation in shock tubes, laminar flame speeds, detailed species time and spatial profiles in static reactors or in combusting flows.

Progress made in this endeavor is reported in the following.

3. Determination of and Fuel Structure Effects on Laminar Flame Speeds of $C_1$ to $C_8$ Hydrocarbons

Laminar flame speeds determined by using the counterflow twin flame configuration were compared for various $C_1$ to $C_8$ hydrocarbons, including alkanes, alkenes, alkynes, aromatics, and alcohols. The data were compared over an extensive range of equivalence ratios at room temperature and atmospheric pressure. The comparison shows that the laminar flame speeds of normal alkanes are close throughout the entire range of equivalence ratios studied, except for methane whose flame speeds are consistently lower. The more unsaturated the molecule the higher the flame speed for fuels having the same carbon number in the order of alkanes < alkenes < alkynes. Methyl substitution for hydrogen or branching reduces the flame speeds for both

alkanes and alkenes. The flame speeds of large saturated cyclic species (cyclohexane and cyclopentane) are close to those of their normal alkane analogs.

This work is reported in Publication No. 4.

4. Propene Pyrolysis and Oxidation Kinetics in Flow Reactor and Laminar Flames

The pyrolysis and oxidation of propene were studied experimentally in an atmospheric flow reactor. Species profiles were obtained in the intermediate to high temperature range (~1200 K) for lean, stoichiometric, rich, and pyrolytic conditions. Laminar flame speeds of propene/air mixtures were also determined over an extensive range of equivalence ratios, at room temperature and atmospheric pressure, using the counterflow twin flame configuration. A detailed chemical kinetic model consisting of 465 reactions and 71 species was used to describe the high temperature kinetics of propene, propyne, allene, and propane. It was shown that the kinetic model could accurately predict a wide range of combustion data for these fuels, including laminar premixed flame speeds, speciation in flow reactors, and ignition in shock tubes. Notable uncertainties in the reaction kinetics of these fuels are identified and discussed.

This work is reported in Publication No. 5.

5. RRKM, Flow Reactor, and Detailed Kinetic Modeling Study of Propyne Pyrolysis and Oxidation

The oxidation of propyne was studied experimentally in an atmospheric flow reactor and in laminar premixed flames. Species profiles were obtained for propyne oxidation experiments conducted in the Princeton Turbulent Flow Reactor in the intermediate to high temperature range (~1170 K) for lean, stoichiometric, and rich conditions. A detailed chemical kinetic model of high-temperature propyne oxidation, consisting of 437 reactions and 69 species, was developed. It is shown that this kinetic model predicts reasonably well the flow-reactor and flame-speed data determined in the present study, and the shock-tube ignition data available in the literature. The remaining uncertainties in the reaction kinetics of propyne oxidation are discussed and an important part of the reaction kinetics is examined and described below.

The pressure-dependent rate coefficients for several reactions relevant to propyne pyrolysis were determined with *ab initio* quantum mechanical calculations and Rice-Ramsperger-Kassel-Marcus (RRKM) analyses. These include the mutual isomerization of propyne and allene, the chemically activated reactions of propyne and allene with the H atom and of acetylene with methyl on the $C_3H_5$ potential energy surfaces. Propyne pyrolysis was also experimentally studied in a flow reactor at 1210 K and 1 atm. A detailed reaction mechanism, employing the current RRKM rate coefficients, is shown to accurately predict the experimental acetylene and methane profiles determined in the flow reactor and literature shock-tube data of propyne and allene pyrolysis up to 1500 K.

The pyrolysis work is reported in Publication No. 7.

6. Quantum Mechanical and Kinetic Modeling Studies of the Initiation Reactions in Acetylene Oxidation in Shock Tube

The reaction kinetics of acetylene underlies all hydrocarbon combustion kinetics. Acetylene oxidation has been extensively studied in shock tubes. A large amount of data exist, which can be used to verify the acetylene subset of the detailed reaction mechanism for aeropropulsion fuels. However, validation of this mechanism subset has been hampered by a long-standing and unresolved issue in acetylene oxidation, namely the nature of the oxidation initiation processes. For this reason, the reaction between acetylene and molecular oxygen was analyzed using quantum mechanical calculations and kinetic modeling of acetylene oxidation in shock tubes. Calculations at the G2(B3LYP) level of theory show that the direct attack of molecular oxygen on the $\pi$ bond in acetylene has a larger energy barrier than acetylene $\leftrightarrow$ vinylidene isomerization, such that this isomerization followed by the reaction of vinylidene with molecular oxygen is the energetically favorable initiation reaction of acetylene oxidation. It is further shown that detailed

kinetic models of acetylene oxidation including this initiation process predict well the experimental shock tube ignition delay data. Through this study, it is the first time that a carbene species is proposed as the major player in the initiation process of unsaturated hydrocarbon oxidation. It remains to be seen whether such a mechanism is generally applicable to the oxidation of other unsaturated hydrocarbons as well.

This work is reported in Publication 8.

7. Structure and Sooting Limits of Diffusion Flames from 1 to 5 Atmospheres

Previous studies on the structure and soot formation of atmospheric, non-sooting and near-sooting counterflow ethylene diffusion flames have shown that the experimental soot volume fractions and laser scattering signals can be satisfactorily predicted by a detailed kinetic model of soot formation. By further extending the study to include the influence of pressure and fuel dilution on the critical sooting strain rates, it was identified that, when the flame temperature is held constant, the density-weighted strain rate at the sooting limit can be correlated with the system pressure, p, and fuel mole fraction, $X_F$, according to $\rho_o K_p \sim p X_F^{0.5}$, where $\rho_o$ is the mass density of the cold oxidizer gas mixture, and $K_p$ the local strain rate at the sooting limit. Hence, a plot of $\rho_o K_p$ versus $p X_F^{0.5}$ defines the sooting boundary in that the region above the straight line is non-sooting, and that below it is sooting (Fig. 5). It was further shown that such a correlation can be understood by plotting $p X_F^{0.5}$ versus the peak acetylene partial pressure, which again exhibits a linear dependence. Hence a linear relationship exists between the sooting limit, $\rho_o K_p$, and the partial pressure of acetylene (Fig. 6), implying that a larger acetylene partial pressure requires stronger straining to prevent soot formation.

The sooting limit correlation identified highlights the practical significance of such a correlation, in that it provides an unambiguous means to predict whether a flame environment with given strain rate, pressure, and fuel mole fraction would result in a local sooting condition in a complex flame environment such as the turbulent diffusion flame. In addition, the simplicity of the correlation indicates its fundamental importance, which is yet to be fully understood through kinetic modeling studies.

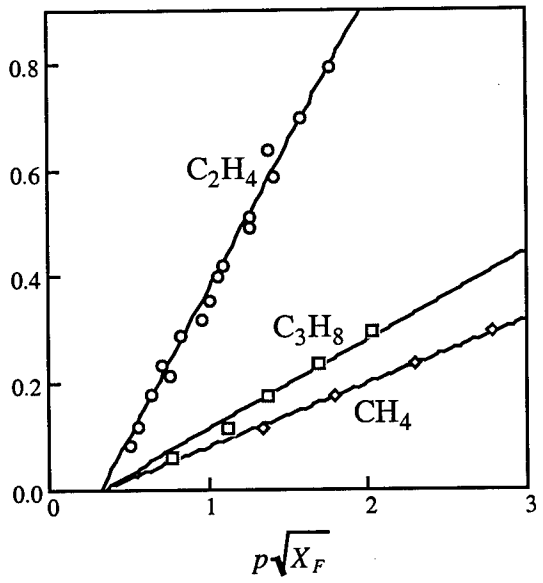


Figure 5

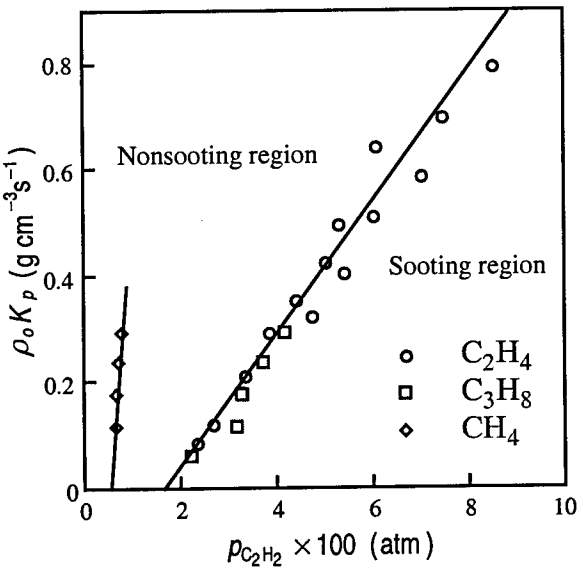


Figure 6

The present work extends the study to methane and propane flames. The temperature and major species concentration profiles were measured with spontaneous Raman scattering, and computationally simulated with detailed kinetics and transport. Good agreement was found between the experimental data and the computational simulation, hence providing benchmark data for further studies. It was also shown that the previously developed global and local sooting

limit correlations are again applicable (Fig. 5), respectively relating the density-weighted strain rate at the sooting limit with the global parameters of the system pressure and fuel mole fraction in the fuel stream, and with the local flame parameter of the peak acetylene partial pressure. This again demonstrates the importance of acetylene as a crucial intermediate in soot formation in flames. In addition, the local correlations for the propane and ethylene flames collapse into a single relation (Fig. 6). The fact that the correlation for the methane flames is different from those of propane and ethylene is not unexpected considering the significantly different kinetic features of methane from those of other fuels, particularly in terms of the detailed reaction kinetics of PAH and soot formation from methane, which is yet to be fully understood.

This work is reported in Publication No. 10.

MAJOR PUBLICATIONS (May, 1998 – April, 1999)


1. "Pulsating instability in near-limit propagation of rich hydrogen/air flames," by E.W. Christiansen, C.J. Sung, and C.K. Law, *Twenty-seventh Symposium (International) on Combustion*, The Combustion Institute, Pittsburgh, PA, pp. 555-562 (1998).
2. "Steady and pulsating propagation and extinction of rich hydrogen/air flames at elevated pressures," by E.W. Christiansen, C.J. Sung, and C.K. Law, to be submitted.
3. "Laminar flame speeds and oxidation kinetics of iso-octane/air and n-heptane/air flames," *Twenty-seventh Symposium (International) on Combustion*, The Combustion Institute, Pittsburgh, PA, pp. 521-528 (1998).
4. "Determination and fuel structure effects on laminar flame speeds of $C_1$ to $C_8$ hydrocarbons," by S.G. Davis and C.K. Law, *Combustion Science and Technology* vol. 140, pp. 427-450 (1999).
5. "Propene pyrolysis and oxidation kinetics in flow reactor and laminar flames," by S.G. Davis, C.K. Law, and H. Wang, submitted.
6. "An experimental and kinetic modeling study of propyne oxidation," by S.G. Davis, C.K. Law, and H. Wang," Twenty-*seventh Symposium (International) on Combustion*, The Combustion Institute, Pittsburgh, PA, pp. 305-312 (1998).
7. "Propyne pyrolysis in a flow reactor: an experimental, RRKM, and detailed kinetic modeling study," by S.G. Davis, C.K. Law, and H. Wang, submitted.
8. "On initiation reactions of acetylene oxidation in shock tubes. A quantum mechanical and detailed kinetic modeling study," A. Laskin, and H. Wang, *Chemical Physics Letters* vol. 303, pp. 43-49 (1999).
9. "An augmented reduced mechanism for methane oxidation with comprehensive global parametric validation," by C.J. Sung, C.K. Law, and J.-Y. Chen, *Twenty-sseventh Symposium (International) on Combustion*, The Combustion Institute, Pittsburgh, PA, pp. 295-304 (1998).
10. "Structure and sooting limits in counterflow methane/air and propane/air diffusion flames from 1 to 5 atmospheres," by C.J. Sung, B. Li, H. Wang, and C.K. Law, *Twenty-seventh Symposium (International) on Combustion*, The Combustion Institute, Pittsburgh, PA, pp. 1523-1530 (1998).

# ENGINE RESEARCH CENTER: ADVANCED DIESEL ENGINE RESEARCH

Particle Image Velocity Measurements/CFD Predictions of In-Cylinder Flows and Correlation with Engine Combustion

(ARO Grant/Contract No. DAAH04-94-G-0328)

Principal Investigators: M. Corradini, P. Farrell, D. Foster, J. Ghandhi, J. Martin, R. Reitz, C. Rutland

Engine Research Center
University of Wisconsin-Madison
1500 Engineering Dr.
Madison, WI 53706

SUMMARY/OVERVIEW:

There are competing requirements to the design of an inlet port for use in an engine. First, the inlet port must be designed to minimize loss associated with gas flow through the port and valve system. Second, the in-cylinder gas phase fluid mechanics, established as a result of gas flow through the port and the interaction of the flow with the in-cylinder geometry, needs to result in flow that is appropriate for the combustion process. There are three requirements for this flow to be "appropriate:" 1) The flow should result in a turbulent flow field at the time of combustion that produces acceptable combustion rates. 2) The flow should not result in difficulties with combustion, for example, as a result of ignitability problems or other sources of cyclic variation. 3) The in-cylinder flow will have a significant effect on the equivalence ratio distribution found in the engine at the time of ignition and subsequent combustion. Thus, the in-cylinder flow should assist in the production of an appropriate mixture.

The objective of this project is to determine the effect of the intake port geometry on combustion and in-cylinder flows, and ultimately on engine performance and emissions. This paper compares particle image velocity measurements coupled with CFD predictions of in-cylinder flows with the performance of an engine, defined by emissions measurements, heat release analysis, and measurements of flame position. These comparisons were performed for each of three different intake port geometries.

AUTHORS: Mitchell Patrie, Brandon Rubenstein, and Jay K. Martin

TECHNICAL DISCUSSION:

**Experimental Apparatus:**

Two different engines were used in this set of studies. One engine was configured specifically for the application of PIV to determine the in-cylinder fluid mechanics. This engine included such features as an extended see-through piston, sapphire windows in the cylinder power, and balance shafts allowing operation at high engine speeds. The second engine was configured for

combustion measurements, including the use of ionization sensors for the measurement of flame position. Table 1 lists the engine specifications for both test engines.

| | |
|---|---|
| Bore | 87 mm |
| Stroke | 67 mm |
| Displacement | 398 cc |
| Compression Ratio | 8.5:1 |
| Speed | 1200-3600 RPM |
| Power | 10.4 kW (14 HP) |
| Valve Configuration | Twin overhead valves |
| Combustion Chamber | Flat-roof, shallow-bowl piston |

Table 1: Engine Specifications.

INTAKE PORT GEOMETRIES - Three different intake port geometries were used for testing (Fig. 1). The directed and helical port geometries were designed as alternatives to the production intake port. These ports were fabricated within blocks of aluminum, which were then secured in a production engine head in lieu of the production intake port. There was some flexibility in this

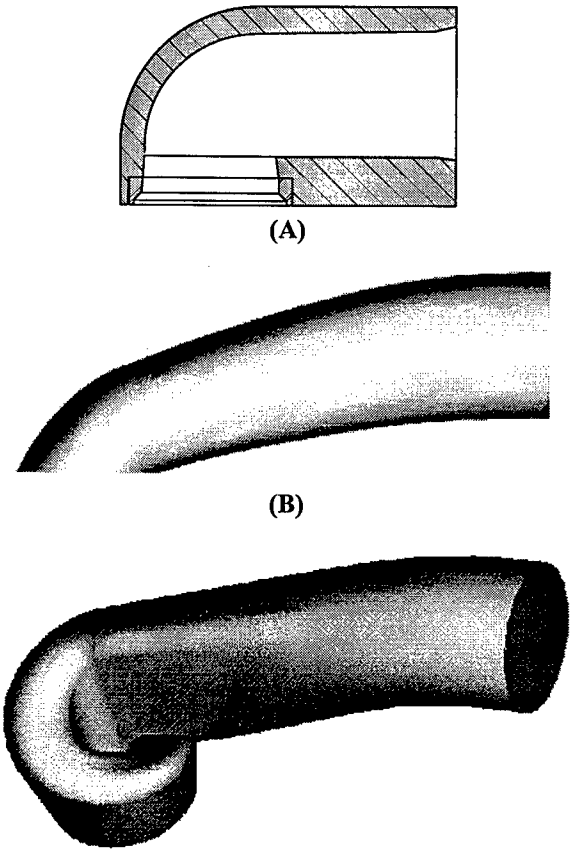


Figure 1: The three intake port geometries used in testing. All are shown approximately 60% of full size; flow is from right to left. (A) Cross-section of production port geometry, including valve seat. (B) Side view of the directed intake port. (C) Perspective view of the helical intake port.

arrangement, in that the port could be rotated to various angles of approach before being fastened in place. The directed intake port geometry (Fig. 1B) was positioned to approach the intake valve on a tangent to the bore axis; the helical intake port geometry was also configured for a tangential approach. In designing these ports, the intent was not to optimize engine performance, but rather to create a quantifiable *difference* in performance that could then be correlated with observable flow fields. Concurrent with engine performance evaluation, the in-cylinder flow fields associated with each of the intake port geometries have been mapped via particle image velocimetry, so that a useful relationship between intake port geometry, in-cylinder flows and engine performance can be identified [Patrie, 1997].

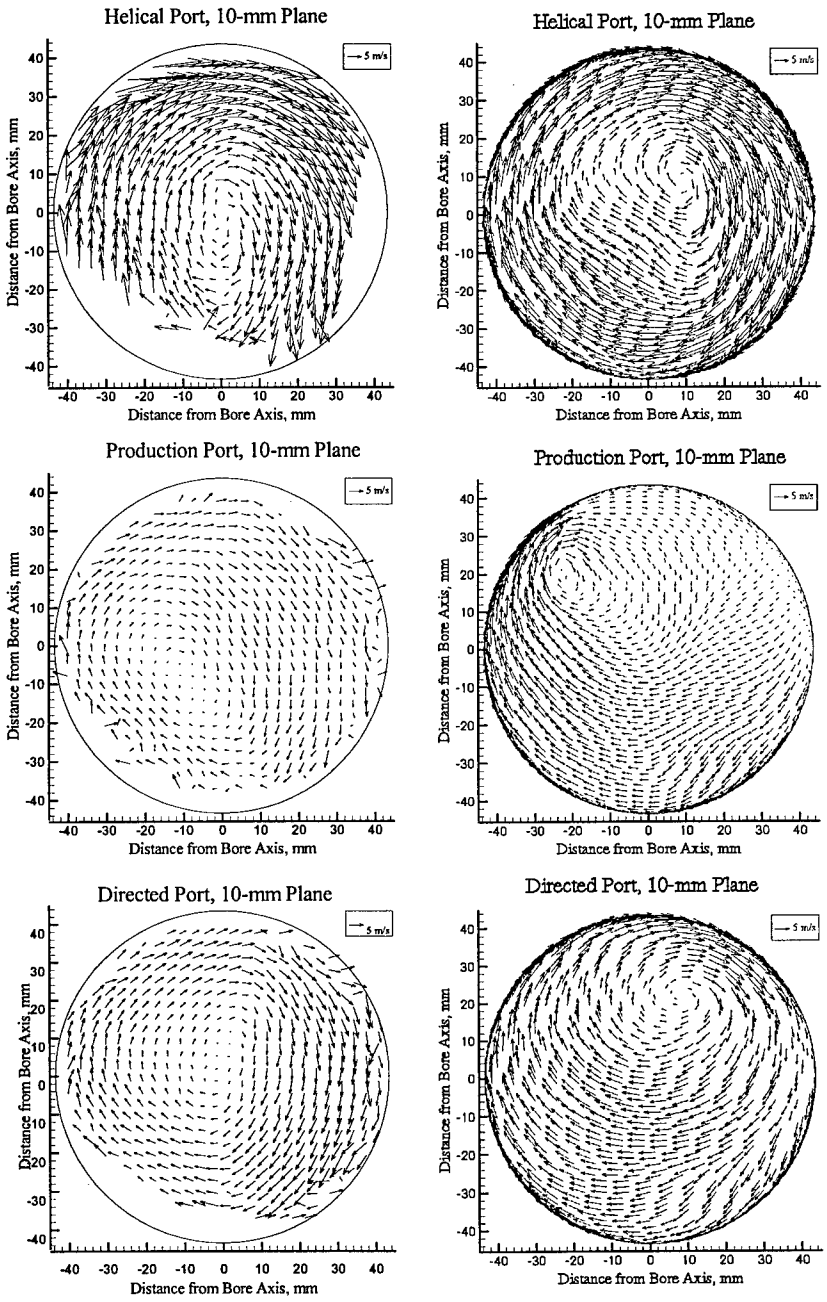


Fig. 2 Comparison of the measured flows (left-hand column) and the computed flows (right-hand column) for the three intake port geometries.

**Results:**

Shown in Fig. 2 are the PIV results of the ensemble-averaged mean flow field, and comparison with CFD predictions of the mean flow field. As illustrated, there is a high degree of correspondence between the flow field measurements and predictions. All three flows at this position in the cylinder show a single swirl structure, with the primary different being the location of the swirl center, and the magnitude of the swirl velocity.

Figure 3 provides examples of the measured flame position and variability in flame propagation. Again the data compares the results that were produced for each of the three different intake ports. As shown, the flame position and flame variability are both strongly influenced by the in-cylinder flow.

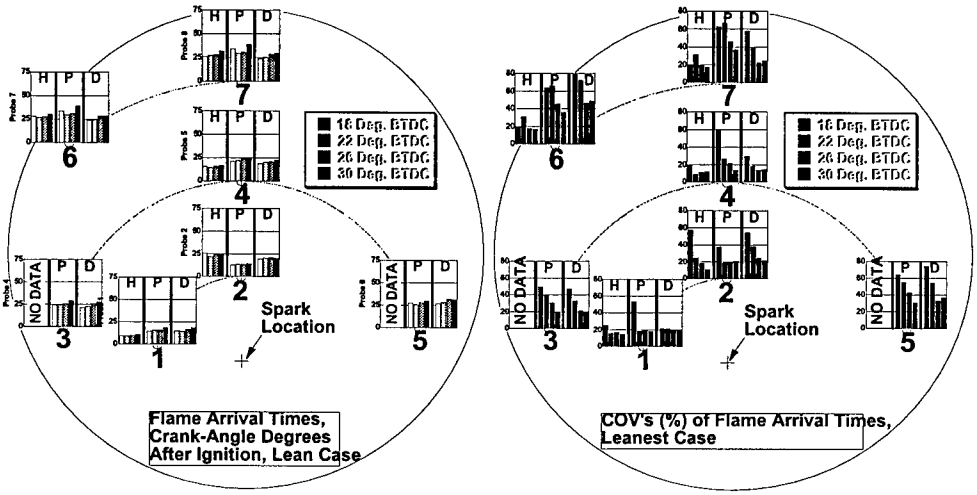


Fig. 3 Comparison of the measured flame arrival times and the coefficient of variation in the flame arrival times resulting from the changes in flow generated by the three different intake ports.

**References**


1] Patrie, M.P., Particle Image Velocimetry Measurements of In-Cylinder Flows and Correlation with Engine Performance, Ph.D. Thesis, University of Wisconsin-Madison, 1998.

2] Rubenstein, B., Personal Communication, 1999.

# MODELLING MIXING AND REACTION IN TURBULENT COMBUSTION

AFOSR Grant F-49620-97-1-0126
Principal Investigator: S. B. Pope

Mechanical & Aerospace Engineering
Cornell University
Ithaca, NY 14853

## SUMMARY

In both space and aircraft applications, the design of combustors in propulsion systems remains a significant technical challenge. Given the cost, difficulty and time consumed in experimental testing, it is well recognized that computer modeling is essential to exploring different design concepts, and to reducing the cost and time of the design cycle. Computer models are currently used in the design of combustors, but substantial improvements are needed in their accuracy, reliability, and computational efficiency. At the heart of the problem is the modelling of turbulent combustion.

Increasingly, this modelling is based on PDF methods, in which the turbulent fluctuations are fully represented in terms of the joint probability density function (PDF) of the flow and thermochemical properties. The objectives of this research are to obtain numerically-accurate solutions to the PDF model equations, and to assess the physical accuracy of different sub-models by comparing PDF calculations with reliable experimental data.

## RECENT ADVANCES

As described in the following three sections (and more completely in the cited references) the principal advances made recently under this program are:

1. Joint PDF calculations of nonpremixed piloted jet flames using the ISAT algorithm to implement a 16-species augmented reduced mechanism.
2. The development and implementation of PDF methodology as a subgrid-scale combustion model for large-eddy simulations.
3. The development of more accurate and efficient numerical algorithms for the solution of the PDF transport equations.

## NONPREMIXED PILOTED JET FLAMES

A continuing focus of our work is the use of PDF methods to make calculations of nonpremixed piloted jet flames. In the earlier work of Saxena & Pope (1998, 1999), a $C_1$-skeletal mechanism was used in the computation of flame L measured by Masri, Dibble & Barlow (1996). Currently we are using the 16-species augmented reduced mechanism (ARM) developed by Sung, Law & Chen (1998) to study the series of flames (primarily flames D and F) measured by Barlow & Frank (1998). The ARM contains $C_2$ species, and as a consequence it remedies discrepancies observed with the $C_1$-skeletal mechanism. As an example, Fig. 1 shows the mean of $CO$ conditional on the mixture fraction for flame D. Excellent agreement is observed whereas, with the skeletal mechanisms, the calculated $CO$ is too large for rich mixtures by a factor of up to 2.

In these calculations, a modelled transport equation is solved for the joint PDF of velocity, turbulence frequency, and thermochemical composition (Van Slooten, Jayesh & Pope 1998, Van Slooten & Pope 1999). Mixing is modelled by the EMST model (Subramaniam & Pope 1998, 1999). The modelled transport equation (which involves 21 independent variables) is solved by a particle-mesh method (Pope 1994). Very importantly, on each of the $10^9$ particle steps, the chemistry is implemented via the ISAT algorithm (Pope 1997), which reduces the computer time requirements by a factor of 50.

## LARGE-EDDY SIMULATION OF TURBULENT COMBUSTION

In collaboration with the group at SUNY Buffalo, we have implemented the PDF methodology as a subgrid scale combustion model in LES (Colucci et al. 1998, Jaberi et al. 1999, Giequel et al. 1998).

For turbulent combustion, LES has several attractions: large-scale unsteady motions and the effects of heat release are directly represented; and RANS turbulence modelling is avoided. It is important to appreciate, however, that, for the turbulence-chemistry interactions, LES faces the same formidable closure problem as statistical approaches. The challenge of simultaneously accounting for turbulent (subgrid scale) fluctuations and realistic finite-rate combustion chemistry is the same in LES as in statistical approaches—but in a much more costly computational setting.

As an illustration of this work, Fig. 2 shows DNS and LES calculations of a reactive mixing layer. With the neglect of subgrid-scale fluctuations, the calculated temperature is 40% too high; whereas the LES/PDF calculations are in good agreement with the DNS.

## PDF SOLUTION ALGORITHMS

In both research and applications, there is great benefit of having accurate and efficient numerical solution algorithms. In turbulent combustion modelling, more often than not, numerical algorithms strongly influence the rate of progress.

For the last 5 years, our PDF calculations have been performed using the particle-mesh method implemented in the code PDF2DV (Pope 1994). Comprehensive testing (Xu & Pope 1999) has shown the method to be convergent, and second-order accurate. That is, as the number of particles $N$ tends to infinity, and the grid spacing $h$ tends to zero, the numerical errors tends to zero, the statistical error as $N^{-\frac{1}{2}}$, the bias as $N^{-1}$ and the spatial discretization error as $h^2$.

While PDF2DV can be used to obtain accurate solutions to the modelled PDF transport equation, there are two motivations to develop alternative algorithms. The first is the fact that the bias in PDF2DV is unexpectedly large, and hence a large number of particles is required in order to make this numerical error acceptably small. An alternative algorithm, with smaller bias, would achieve the same accuracy at lower computational cost. The second motivation is to develop a PDF algorithm that can be combined with existing finite-volume codes, to facilitate technology transfer and the incorporation of the PDF methodology within existing LES codes.

The alternative numerical approach being developed is a completely consistent hybrid algorithm (Muradoglu et al. 1999, Jenny et al. 1999), consisting of a finite-volume (FV) code and particle code. The FV code solves the standard mean equations for the conservation of mass, momentum and energy, along with the mean equation of state. The particle method solves the modelled transport equation for the fluctuating velocity and thermochemical composition. The information exchanged between the codes is as follows: the mean velocity from the FV code is used in the particle code (to convect the particles); the various turbulent fluxes, the source of sensible energy and the mean molecular weight determined from the particles are used in the FV code. In contrast to previous hybrid algorithms (e.g., PDF2DS, Pope & Correa 1988), this method is completely consistent: there is no inconsistency between the fields represented in the two codes.

The early results obtained with the hybrid algorithm (Muradoglu et al. 1999) demonstrate its convergence, and, importantly, reveal that the bias is negligibly small. As an illustration, Fig. 3 shows the convergence of the method. In most particle methods, complete convergence is not obtained. Instead the statistical errors never decrease below a level determined by the number of particles. In contrast, Fig. 3 shows the continuous convergence of the hybrid method.

## REFERENCES


Colucci, P. J., F. A. Jaberi, P. Givi, and S. B. Pope (1998). Filtered density function for large eddy simulation of turbulent reacting flows. *Phys. Fluids 10*, 499–515.

Gicquel, L. Y. M., F. A. Jaberi, P. Givi, and S. B. Pope (1998). Filtered density function of velocity for large eddy simulation of turbulent flows. *Bull. Amer. Phys. Soc. 43*, 2120.

Jaberi, F. A., P. J. Colucci, S. James, P. Givi, and S. B. Pope (1998). Filtered mass density function for large eddy simulation of turbulent reacting flows. *J. Fluid Mech.*, (to be published).

Jenny, P., S. B. Pope, M. Muradoglu, and D. A. Caughey (1999). A hybrid algorithm for the joint PDF equation of turbulent reactive flows. *J. Comp. Phys (submitted).*

Masri, A. R., R. W. Dibble, and R. S. Barlow (1996). The structure of turbulent nonpremixed flames revealed by Raman-Rayleigh-LIF measurements. *Prog. Energy Combust. Sci. 22*, 307–362.

Muradoglu, M., P. Jenny, S. B. Pope, and D. A. Caughey (1999). A consistent hybrid finite-volume/particle method for the PDF equations of turbulent reactive flows. *J. Comp. Phys* (to be published).

Pope, S. B. (1994). PDF2DV: A Fortran code to solve the modelled joint PDF equations for two-dimensional recirculating flows. Unpublished, Cornell University.

Pope, S. B. (1997) Computationally efficient implementation of combustion chemistry using *in situ* adaptive tabulation. *Combust. Theory Modelling 1*, 41–63.

Pope, S. B. and S. M. Correa (1988). Joint PDF calculations of a non-equilibrium turbulent diffusion flame. In *Twenty-First Symp. (Int'l) on Combust.*, Pittsburgh, pp. 1341–1348. Combustion Institute.

Saxena, V. and S. B. Pope (1998). PDF calculations of major and minor species in a turbulent piloted jet flame. In *Twenty-Seventh Symp. (Int'l) on Combust.*, Pittsburgh, pp. 1081–1086. Combustion Institute.

Saxena, V. and S. B. Pope (1999). PDF simulations of turbulent combustion incorporating detailed chemistry. *Combust. Flame 117*, 340–350.

Subramaniam, S. and S. B. Pope (1998). A mixing model for turbulent reactive flows based on Euclidean minimum spanning trees. *Combust. Flame 115*, 487–514.

Subramaniam, S. and S. B. Pope (1999). Comparison of mixing model performance for nonpremixed turbulent reactive flow. *Combust. Flame 117*, 732–754.

Sung, C. J., C. K. Law, and J.-Y. Chen (1998). An augmented reduced mechanism for methane oxidation with comprehensive global parametric validation. In *Seventh Symp. (Int'l) on Combust.*, Pittsburgh, pp. (295–304). Combustion Institute.

Van Slooten, P. R., Jayesh, and S. B. Pope (1998). Advances in PDF modeling for inhomogeneous turbulent flows. *Phys. Fluids 10*, 246–265.

Van Slooten, P.R., and S.B. Pope (1999). Application of PDF Modeling to swirling and non-swirling turbulent jets. *Flow, Turbulence and Combust.* (to be published).

Xu, J. and S.B. Pope (1999) Numerical studies of PDF/Monte Carlo methods for turbulent reactive flows. *J. Comp. Phys*, (to be published).

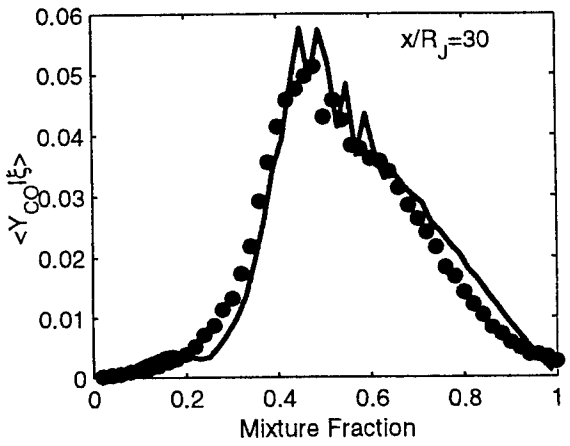


Fig. 1 Mass fraction of CO conditional on mixture fraction. Symbols, experimental data of Barlow & Frank (1998); line, JPDF calculation of Xu & Pope (unpublished).

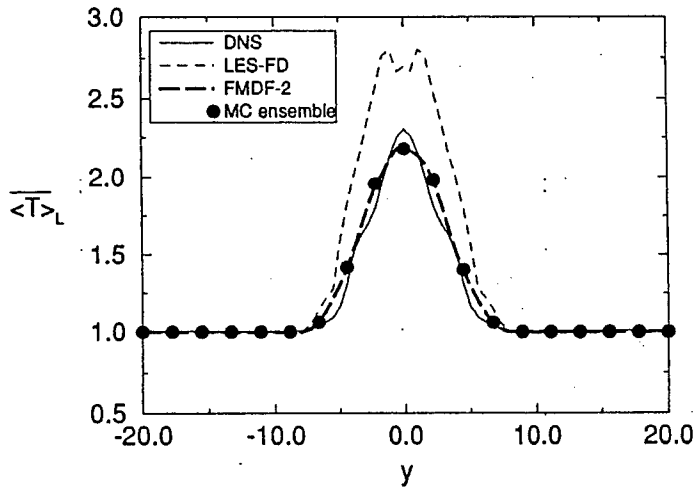


Fig. 2 Mean normalized temperature profiles in a reactive turbulent mixing layer showing the agreement between DNS and LES using PDF methodology (denoted FMDF-2). In LES-FD subgrid-scale fluctuations are neglected. (From Jaberi et al. 1999.)

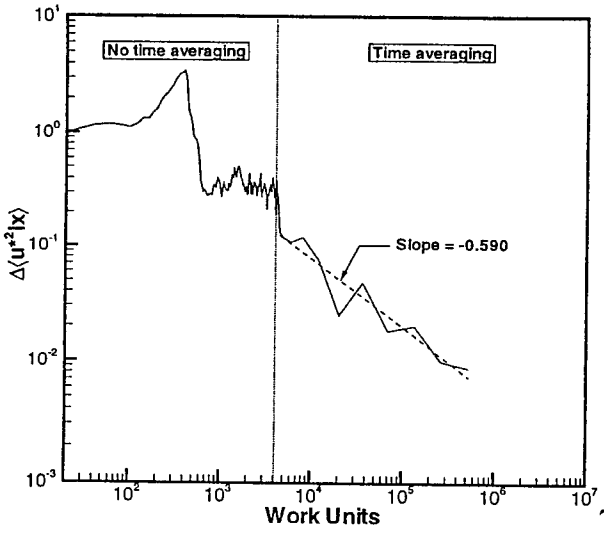


Fig. 3 Change in velocity variance in one iteration, showing the continual convergence of the hybrid PDF method. (From Muradoglu et al. 1999.)

# ENGINE RESEARCH CENTER: ADVANCED DIESEL ENGINE RESEARCH
# CHEMICALLY REACTING SHEAR LAYER-II: A DNS STUDY OF TURBULENT TRANSPORT

(ARO Grant/Contract No. DAAH04-94-G-0328)

Principal Investigators: M. Corradini, P. Farrell, D. Foster, J. Ghandhi, J. Martin, R. Reitz, C. Rutland

Engine Research Center
University of Wisconsin-Madison
1500 Engineering Drive
Madison, Wisconsin 53706

## OVERVIEW

Results from direct numerical simulations (DNS) of turbulent reacting shear layers are reviewed. Time-developing simulations show that pressure dilatation due to heat release is largely responsible for the impaired growth rates observed in reacting shear layers. Results from both non-reacting and reacting spatially-developing simulations are compared with experiments. Growth rates of non-reacting simulations are consistent with the literature. Flame images from reacting simulations are found to qualitatively agree with in-house experiments.

**AUTHORS:** Scott D. Mason and Christopher J. Rutland

## TECHNICAL DISCUSSION

**Code Description.** The DNS code solves non-dimensional transport equations for total mass, momentum, energy, and reactant mass fractions. The main flow assumptions include ideal gas behavior, constant transport coefficients, and negligible radiation, Soret, and Dufour effects. The chemistry is represented by one, single-step, second-order irreversible reaction between a fuel and an oxidizer of equal molecular weights. The molar stoichiometric ratio for the reaction is unity and the reaction rate is given by the Arrhenius expression. The transport equations are solved using a low Mach number approximation such that changes in density due to heat release are supported but acoustic waves are not. Time integration of the transport equations is performed using an explicit third-order Runge-Kutta method; spatial derivatives are calculated using sixth-order compact finite-difference schemes.

**Time-Developing Simulations.** Preliminary two-dimensional, time-developing (streamwise-periodic) simulations were performed to study the effects of reaction on the growth rate as well as the turbulent kinetic energy budget. For these simulations, the streamwise ($x$-direction) component of velocity was initialized with a hyperbolic tangent profile where $U_1 = 0.5$ and $U_2 = -0.5$. Vortex rollup and pairing was expedited by adding spatial perturbations calculated from linear stability theory to the initial base flow. The Reynolds number, $Re$, based on initial vorticity thickness $\delta_{\omega_o}$ and velocity difference $\Delta U$ was 100. The vorticity thickness is defined as $\delta_\omega = \Delta U / \left[\partial \tilde{u} / \partial y\right]_{\max}$, where $\tilde{u}$ is the Favre streamwise-averaged velocity. Both the Prandtl number and the Lewis number were unity.

The global effects of heat release and reaction rate were studied by examining the time evolution of the vorticity thickness. In this work, the heat release is quantified by the non-dimensional parameter:

$$\alpha = \frac{T_{ad} - T_{ref}}{T_{ad}} \tag{1}$$

where $T_{ad}$ is the adiabatic flame temperature and $T_{ref}$ is a reference temperature. The reaction rate is defined by the Damkohler number:

$$Da = \frac{\delta_{\omega_o} / \Delta U}{\left[\frac{B}{W}\rho_{ref} exp\left(-\beta/\alpha\right)\right]^{-1}} \tag{2}$$

where $B$ is the Arrhenius pre-exponential factor, $W$ is the molecular weight of the reactants, $\rho_{ref}$ is a reference density, and $\beta$ is the non-dimensional activation energy (Zeldovich number).

The time evolutions of the mean vorticity thickness are plotted for a range of $\alpha$ with $Da$ = 1 and $\beta$ = 6.4 in Figure 1. Here, the non-dimensional temperature rise varies from $\alpha$ = 0 (non-reacting) to $\alpha$ = 8.5, which is representative of many hydrocarbon combustion systems. As expected, heat release suppresses vortex rollup and pairing. As the heat release increases, the plateau between the first and second pairings becomes less defined and the maximum vorticity thickness decreases. For $\alpha > 0.6$, there is no distinct peak in the vorticity thickness curves and the time evolution, in general, approaches that of an unperturbed shear layer. From this it is evident that heat release alters the unstable modes of the flow.

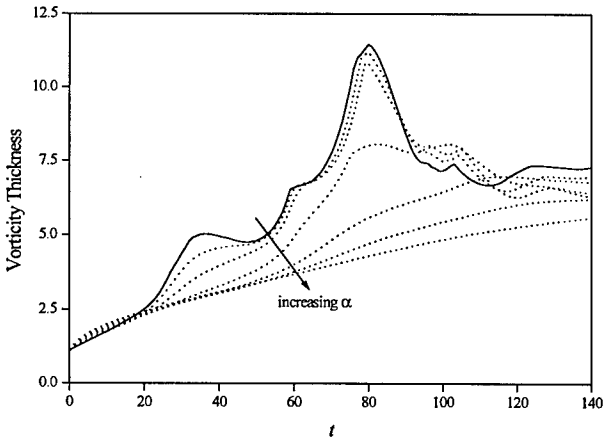


**Figure 1.** Effects of heat release on vorticity thickness for $Da$ = 1. Values of $\alpha$ are 0.0 (top solid line), 0.2, 0.4, 0.6, 0.7, 0.8, and 0.85 (bottom dotted line).

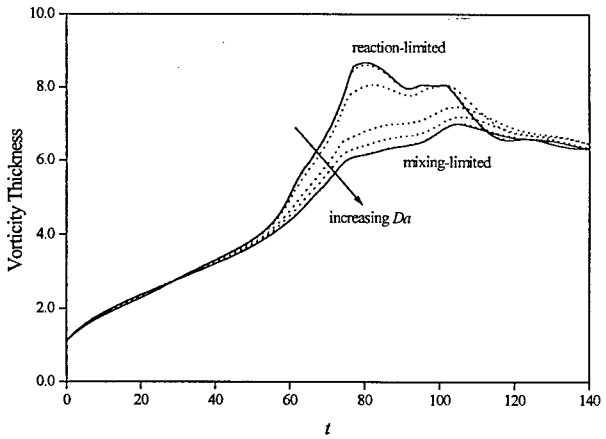


**Figure 2.** Effects of reaction rate on vorticity thickness for $\alpha$ = 0.6. Values of $Da$ are 0.01 (top solid line), 0.1, 1, 5, 10, 50, and 100 (bottom solid line).

For $\alpha$ = 0.6 (moderate heat release) and $\beta$ = 6.4, the effects of reaction rate on the vorticity thickness time evolutions are given in Figure 2. In general, higher reaction rates lead to greater suppression of the shear layer. The plots also reveal that the thickness evolution is bounded by two limits. At $Da \approx 0.01$, the reaction rate is slow compared to the mixing rate and the shear layer is reaction-limited. At $Da \approx 100$, the reaction rate is fast compared to the mixing rates and the layer is mixing-limited. Hydrocarbon combustion is typically characterized by large values of Damkohler number. The limits observed here serve as guidelines for setting the Damkohler number in current simulations.

The effects of heat release are studied further using the turbulent kinetic energy transport equation:

$$\frac{\partial \overline{\rho} K}{\partial t} = -\frac{\partial \overline{\rho} K \widetilde{u}_j}{\partial x_j} - \overline{\rho u_i'' u_j''} \frac{\partial \widetilde{u}_i}{\partial x_j} - \frac{1}{2} \frac{\partial \overline{\rho u_i'' u_i'' u_j''}}{\partial x_j} + \overline{u_i'' \frac{\partial \tau_{i,j}}{\partial x_j}} - \overline{\frac{\partial p u_i''}{\partial x_i}} + \overline{p \frac{\partial u_i''}{\partial x_i}} \qquad (3$$

(i) (ii) (iii) (iv) (v) (vi)

where the turbulence kinetic energy $K$ is defined as:

$$K = \frac{1}{2} \frac{\overline{\rho u_i'' u_i''}}{\overline{\rho}} \qquad (4$$

The terms on the right-hand side of Eq. (4) are: (i) convection, (ii) production, (iii) turbulent transport, (iv) molecular diffusion, (v) pressure transport, and (vi) pressure dilatation.

Representative turbulent kinetic energy budgets for non-reacting and reacting simulations are presented in Figures 3 and 4, respectively. For the non-reacting simulation, the time derivative term is primarily a balance between production, turbulent transport, and pressure transport. At the center, the production is balanced almost equally by the pressure and turbulent transport. Away from the center, positive pressure and turbulent transport combine to form the peaks in the time derivative, which indicate that the thickness of the layer is growing. The time derivative remains positive until the pressure and turbulent transport decay in the free-streams.

For the reacting simulation, the overall balance of terms is quite different. In particular, the pressure transport for the reacting layer is considerably larger than for the non-reacting layer. Furthermore, the turbulent transport is small for all values of $y$. Most importantly, however, the inflated pressure transport is balanced almost exactly everywhere by the pressure dilatation. For the non-reacting layer, growth was related to regions of positive pressure and turbulent transport. Here, in the absence of any turbulent transport, the equalization of pressure transport by the pressure dilatation acts to inhibit growth. This is a direct consequence of the heat release.

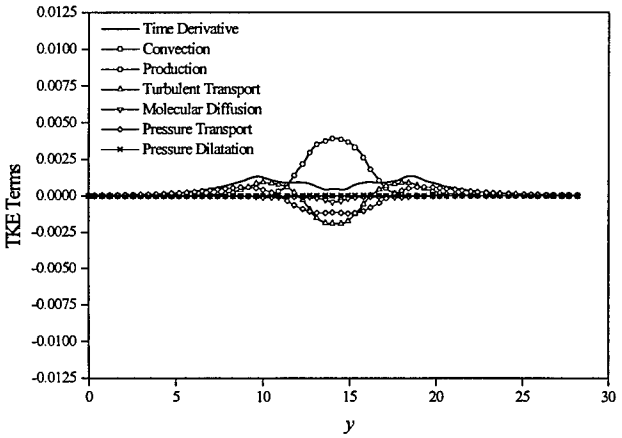


**Figure 3.** Turbulent kinetic energy budget for non-reacting shear layer at $t = 60$. Grid resolution was $128^2$.

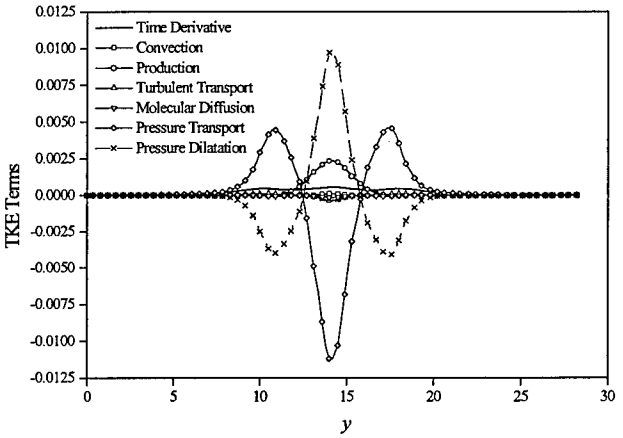


**Figure 4.** Turbulent kinetic energy budget at $t = 60$ for reacting shear layer where $\alpha = 0.6$ and $Da = 1$.

**Spatially-Developing Simulations.** Current work involves spatially-developing simulations, which are physically more realistic than time-developing simulations. In these cases, time-dependent perturbations corresponding to the most unstable mode and its subharmonics are added to the inlet plane to produce rollup and pairing. To simulate a natural shear layer, a random-walk is added to the phase of each subharmonic mode [1]. Preliminary tests have shown this technique to produce time-averaged growth rates consistent with those observed by Brown & Roshko [2].

Two-dimensional, spatially-developing simulations using the random-walk technique have been calculated to compare against non-reacting and reacting (propane/air) shear layer experiments performed by Pickett at the Engine Research Center at the University of Wisconsin-

Madison [3]. Figure 5 is a simulated shadowgraph (contours of $\nabla^2 \rho$) corresponding to a non-reacting experiment where the high-speed stream was preheated 100 K above ambient temperature. Vortex numbers and spacing are consistent with the experimental results. The time-averaged growth rate for the simulation agrees with that suggested by Dimotakis for shear layers with streams of unequal densities [4].

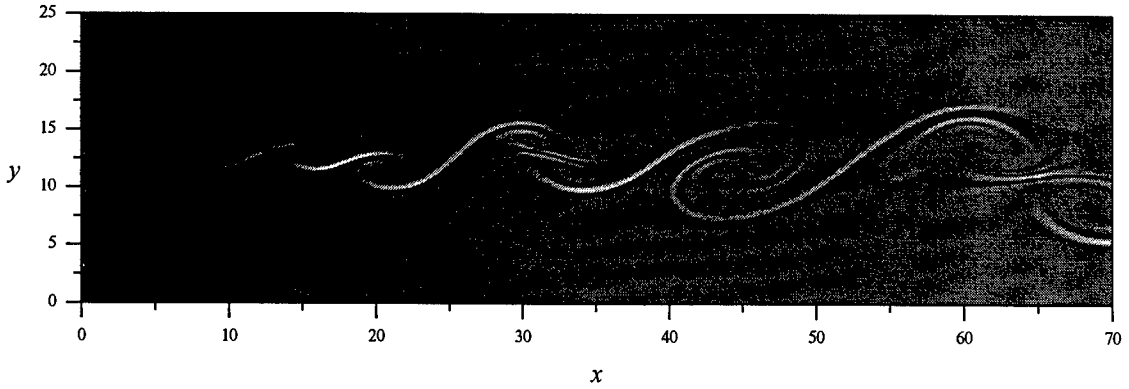


**Figure 5.** Simulated shadowgraph corresponding to non-reacting experiment with preheated high-speed stream. Here, $U_1 = 1.667$, $U_2 = 0.667$, $Re = 480$, $Pr = 0.71$. Grid resolution was 514x172.

Figure 6 shows contours of reaction rate from a simulation corresponding to typical experimental conditions for reacting layers. The insert shows an experimental flame image taken under the same conditions. As is seen, the qualitative agreement is excellent. In future work, three-dimensional, reacting simulations will be used to generate databases for the detailed study of turbulence-flame interactions. The analysis will include a quantitative study using the turbulent kinetic energy and Reynolds stress transport equations. Three-dimensional visualizations of the reaction zone will qualitatively supplement these studies.

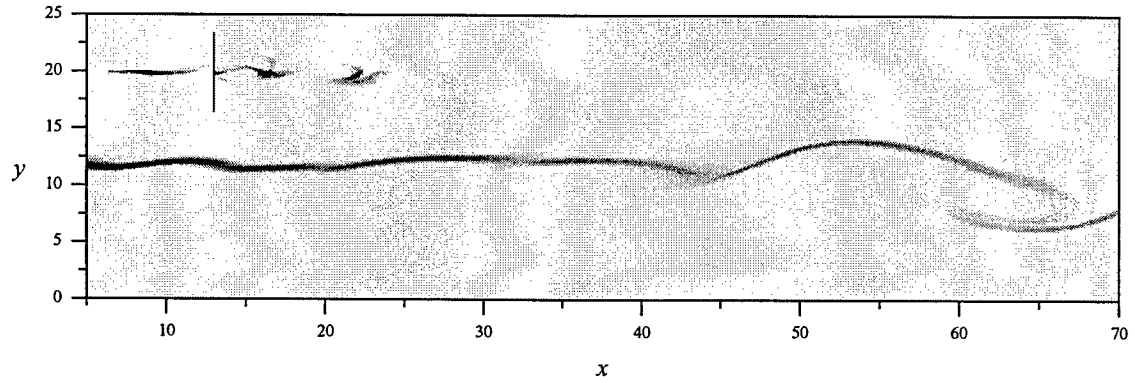


**Figure 6.** Reaction rate contours corresponding to a characteristic reacting shear layer experiment. Here, $U_1 = 1.667$, $U_2 = 0.667$, $Re = 485$, $Pr = 0.82$, $Le = 1.0$, $Da = 50$, $\alpha = 0.85$, $\beta = 6.4$. Grid resolution was 514x172. Insert shows an experimental flame image taken with a high-speed camera.


1. Sandham, N. D., and Reynolds, W. C. (1989), "Some Inlet-Plane Effects on the Numerically Simulated Spatially-Developing Mixing Layer," *Turbulent Shear Flows 6, Sixth Symposium on Turbulent Shear Flows*, September 7-9, Springer-Verlag, Berlin, pp. 441-454.
2. Brown, G. L., and Roshko, A. (1974), "On Density Effects and Large Structures in Turbulent Mixing Layers," *J. Fluid Mech.*, vol. 64, part 4, pp. 775-816.
3. Pickett, L. M., (1998), "The Interaction of Turbulent Mixing and Hydrocarbon Chemistry in a Planar Shear Layer," Ph.D. Preliminary Examination, Dept. of Mechanical Engineering, University of Wisconsin–Madison.
4. Dimotakis, P. E., (1991), "Turbulent Free Shear Layer Mixing and Combustion," S. N. B. Murthy and E. T. Curran, *Progress in Astronautics and Aeronautics*, vol. 137, pp. 265-340.

# EVALUATION OF CLOSURE MODELS OF TURBULENT DIFFUSION FLAMES

(AFOSR Grant No. F49620-97-1-0092)

Principal Investigators: George Kosály and James J. Riley

*Department of Mechanical Engineering*
*University of Washington, Seattle, WA, 98195-2600*

## SUMMARY/OVERVIEW

The long-term objectives of this research are (a) to better understand the coupled physical, chemical, and thermodynamic processes inherent in turbulent diffusion flames, (b) to develop and validate theoretical models for turbulent combustion, as applied in both Reynolds-averaged Navier Stokes (RANS) and large-eddy simulations, and (c) to continue to develop the methodology for applying direct numerical and large-eddy simulations to turbulent combustion. During the past year, there has been emphasis on the validation of models using data from very high resolution direct numerical simulations, and on the testing of the quasi-steady flamelet model.

## TECHNICAL DISCUSSION

*Direct Numerical and Large-eddy Simulations*

A primary objective of the current research is to study how large-eddy simulations (LES) can be used to predict the average species concentrations and reaction rates in non-premixed turbulent combustion. To this end, highly accurate simulated flow fields have been generated by direct numerical simulations (DNS) which give the flow velocity and scalar concentrations as a function of three spatial dimensions and time. Two scalar configurations, one with initial conditions approximating a statistically homogeneous, non-premixed state, and the other an inhomogeneous mixing layer, are convected in an accurate simulation of decaying, isotropic, homogeneous turbulence[1] using numerical domains having as many as $512 \times 512 \times 1024$ grid points. Both isothermal and temperature dependent reactions with a range of reaction rates have been considered. An example of a slice through a high resolution DNS field for the inhomogeneous mixing layer is shown in Fig. 1a.

In isothermal simulations, the reaction zone can be resolved numerically, even with fairly high reaction rates. In temperature dependent reactions, however, the reaction rate gradients can become extremely steep, and the question of numerical resolution is an even more important one. When the simulations are on very high resolution grids, it is not feasible to double the number of grid points in each spatial direction to determine if the simulation is well resolved. In order to better understand the resolution requirements for simulations of non-premixed combustion, a series of direct numerical simulations was conducted over a range of activation temperatures, stoichiometric mixture fractions, and global reaction rates, and various quantitative and qualitative tests performed on the results. High activation temperature was shown to be the parameter most likely to lead to resolution difficulties in the DNS. Fig. 1b shows the reaction rate contours in a poorly resolved DNS.

Next we show DNS and LES data for a scalar mixing layer. This is a fundamental flow that has been the focus of much study in the past, including laboratory experiments with chemical reaction.[2] In this flow, a scalar with a step change in value transverse to the flow is introduced into the velocity field in grid turbulence. Understanding and predicting this flow are important in dealing with more complex flows. The simplicity of the flow encourages the idea that it will evolve in a self-similar manner, but this is not the case in laboratory experiments at moderate Peclet numbers.[3] Experimentalists, however, are limited by the length of the wind tunnels, by difficulties aligning the virtual origins of the velocity and scalar fields, and by the maximum Peclet number that can be achieved. Direct numerical simulations avoid the first two limitations and provide flow data for an almost ideal scalar mixing layer at moderate Peclet number, which can then be used to validate transport theory and closure models; simulation results are compared with laboratory data in Fig. 2. Large-eddy simulations can eliminate the finite Peclet number constraint, and are well suited for examining self-similarity because the large-scale statistics of interest are insensitive to the exact form of the subgrid scale flux models employed.[4] Fig. 3a shows LES results which indicate that a mixing layer with approximately infinite Peclet number does evolve with one length and one time scale. Using LES to predict transport at high Peclet number is an important application of the simulation technique.

In addition to being a valuable research tool, LES can accurately predict species concentrations in reacting flows when used in conjunction with a chemistry model such as the large-eddy laminar flamelet model.[5,6] Fig. 3b shows typical predictions of average filtered product mass fractions for a one-step isothermal reaction. Current research is focusing on testing the predictions of the same model for mass fractions, reaction rates, and temperatures in temperature dependent reactions.

*Quasi-steady Modeling of Diffusion Flames*

Mixture fraction based models[7–9] and pdf (probability density function) approaches[10,11] are the two basic modeling methods in current use for turbulent diffusion flames. A known computational disadvantage of mixture fraction based modeling is the added dimension ($Z$) inherent in the approach. This disadvantage, however, turns into advantage when the "quasi-steady" version of the $Z$-based modeling is applicable.[12]

For computational reasons, the use of the quasi-steady approach is very convenient, and almost unavoidable in three-dimensional, time-dependent cases that require detailed chemical kinetics. Since the LES of any problem in turbulent combustion belongs in this category, the condition of the applicability of quasi-steady modeling is of topic of considerable importance.[5,13,14]

Consider steady, three dimensional burning and let $Q_j(\mathbf{x},\eta)$ $(i = 1, 2, \ldots, N)$ be the average mass fraction of the $i$-th species conditional on a chosen value, $\eta$, of the mixture fraction, and let $Q_j^{qs}(\eta, N_{st})$ be its quasi-steady counterpart. (Here, $N_{st}$ is the average scalar dissipation rate at the average stoichiometric position. $Q_j^{qs}$ depends on the position through $N_{st}$.) The equation defining $Q_j$ is composed of three terms representing convection, mixing, and reaction, and its approximate form is referred to as the CMC-model equation. In the quasi-steady approach, the convection term is neglected.

To investigate the validity of the quasi-steady approach, we have performed RANS computations of a vertical hydrogen jet burning in air.[15] Figures 4 and 5 show the conditional average of OH versus mixture fraction at different distances from the nozzle computed via the two approaches. Figure 4 refers to the true hydrogen case; the results in Fig. 5 were obtained by decreasing the chemical reaction rates used in Fig. 4 by a factor of 36. The quasi-steady and the full results coincide in Fig. 4. (Note that the quasi-steady approach predicts correctly the laboratory data even in this non-equilibrium case.) Comparison of Figs. 4 and 5 demonstrates that the quasi-steady approach is best when the Damköhler number is highest, as can be expected. Since the Damköhler number increases with increasing distance from the nozzle, the naive expectation is that the quasi-steady approach will improve along the axis. Comparison of Figs. 5a and 5b show, however, the opposite tendency. The conclusion is that the validity of the quasi-steady approach is not governed solely by the Damköhler number.

Indeed, theoretical work shows that the condition of quasi-steady behavior can be written as

$$\tau_j^{qs} \equiv \left| \frac{\partial Q_j^{qs}/\partial N_0}{\partial^2 Q_j^{qs}/\partial \eta^2} \right|_{\eta=\xi_{st}}, \qquad \frac{\tau_j^{qs}}{\tau_{N_{st}}} \ll 1 . \tag{1}$$

Here $\tau_j^{qs}$ is related to the characteristic time that governs the relaxation to the quasi-steady solution following an infinitesimal perturbation in $N_{st}$, and $\tau_{N_{st}}$ scales the temporal (axial) change of the scalar dissipation rate. The ratio of the above two characteristic times of $H_2O$ (not shown here) increases with downstream distance for the true hydrogen case and for the artificially slowed chemistry case. The ratio is smaller for the former case, that is, for the case associated with larger values of Da, but it increases along the jet axis. The condition given in Eq. (1) accounts for the behavior seen in Figs. 4 and 5.

## REFERENCES


[1] S. M. de Bruyn Kops and J. J. Riley, Phys. Fluids **10**, 2125 (1998).
[2] R. W. Bilger, L. R. Saetran, and L. V. Krishnamoorthy, J. Fluid Mech. **233**, 211 (1991).
[3] B.-K. Ma and Z. Warhaft, Phys. Fluids **29**, 3114 (1986).
[4] J. R. Chasnov, Phys. Fluids **6**, 1036 (1994).
[5] A. W. Cook, J. J. Riley, and G. Kosály, Combust. Flame **109**, 332 (1997).
[6] A. W. Cook and J. J. Riley, Combust. Flame **112**, 593 (1997).
[7] N. Peters, Combustion Science and Technology **30**, 1 (1983).
[8] R. W. Bilger, Phys. Fluids A **5**, 436 (1993).
[9] V. R. Kuznetsov and V. A. Sabel'nikov, *Turbulence and Combustion*, Hemisphere, New York, 1990.
[10] S. B. Pope, Prog. Energy Combust. Sci. **11**, 119 (1985).
[11] W. Kollmann, in *Turbulent Reacting Flows*, Springer-Verlag, 1989, p. 715.
[12] Y. Y. Buriko, V. R. Kuznetsov, and D. V. Volkov, Combust. Flame **96**, 104 (1996).
[13] A. W. Cook and J. J. Riley, Phys. Fluids **6**, 2868 (1994).
[14] A. W. Cook, Phys. Fluids **9**, 1485 (1997).
[15] R. S. Barlow, N. S. A. Smith, J.-Y. Chen, and R. W. Bilger, Combust. Flame (1999), Accepted for publication.

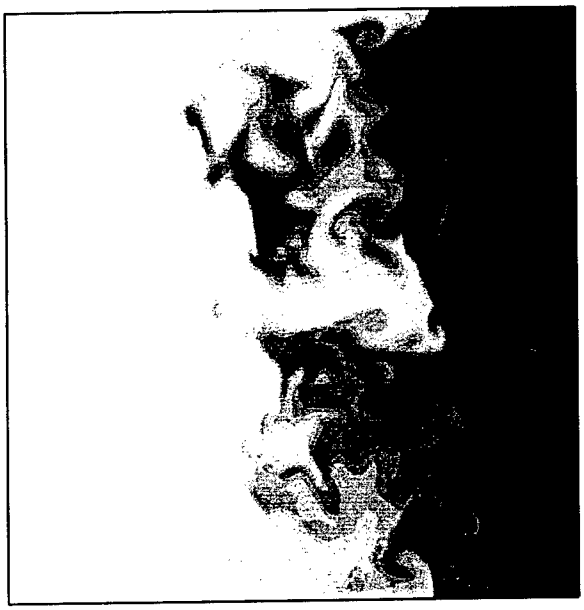

(a) Slice through the mixture fraction field of a well resolved DNS.

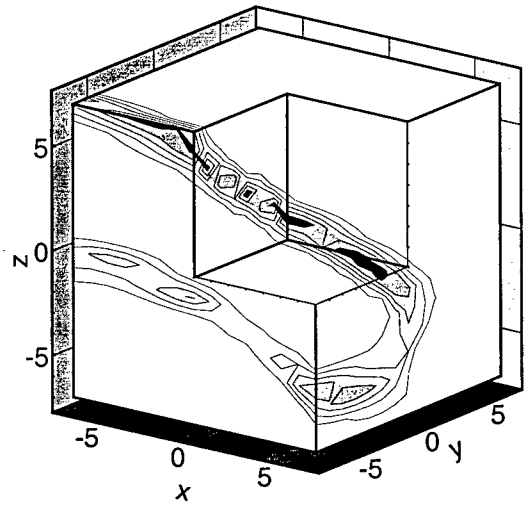


(b) Contour plot showing the reaction rate in a local region of a DNS with the activation temperature of the reaction too high for good resolution. The axes are calibrated in grid points. Note the oscillations in the reaction rate which occur at the highest frequency resolved in the simulations.

Figure 1: DNS provide detailed data for testing models and validating LES.

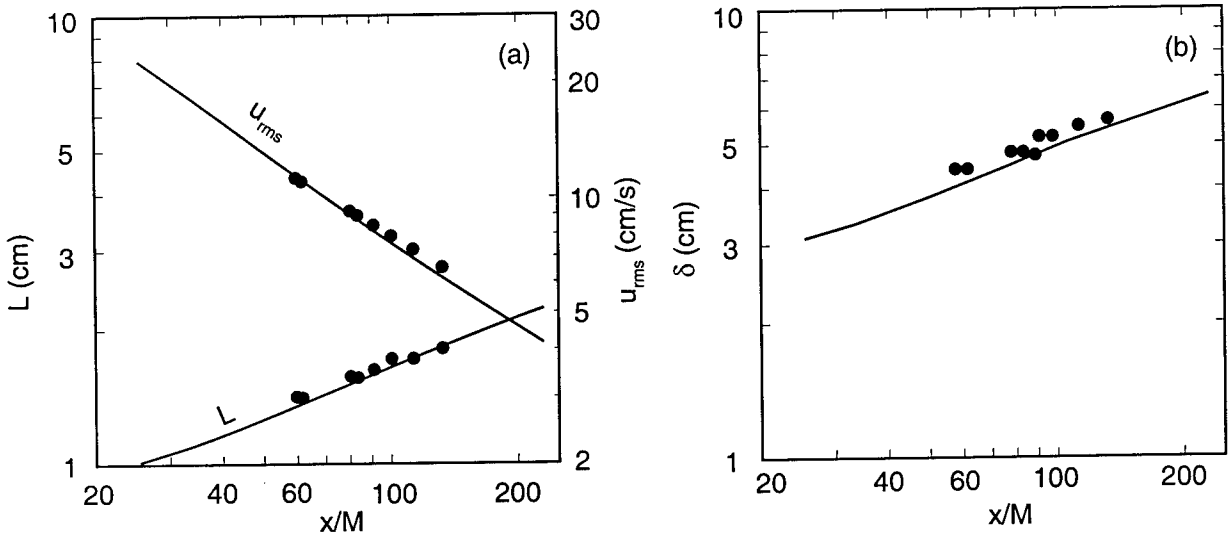


Figure 2: Comparison of DNS (lines) and laboratory[3] data (symbols) show that the DNS is accurate and provides data over a much greater range of downstream distance than the laboratory experiment does. $L$ and $u_{rms}$ are the integral length of the velocity and the rms velocity, $\delta$ is the width of the scalar layer, and $x/M$ is the downstream distance scaled by the turbulence grid size.

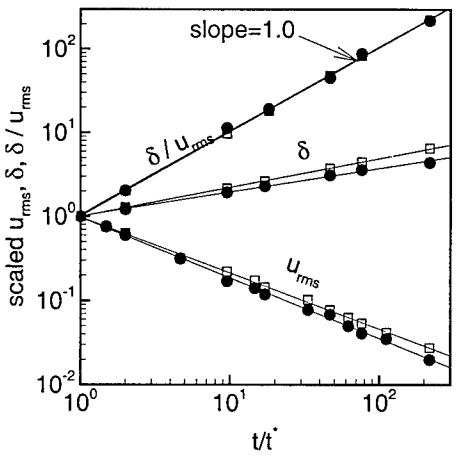


(a) LES data for a mixing layer with infinite Peclet number show that $\delta/u_{rms}$ is proportional to scaled time, regardless of velocity decay rate, consistent with the below being self-similar. Here, $t^*$ is the initial integral time scale, and $\delta$ and $u_{rms}$ are as in Fig. 2.

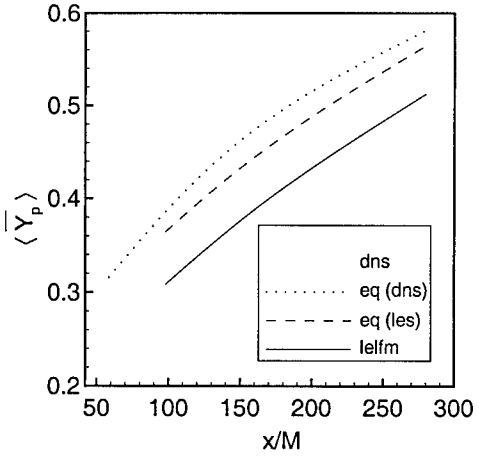


(b) LES predictions of the mean filtered product mass fraction in a one-step, isothermal reaction in grid turbulence. lelfm indicates large-eddy laminar flamelet predictions and eq indicates equilibrium chemistry.

Figure 3: LES is valuable as a research tool for studying large-scale mixing, and as a technique for predicting species concentrations in reacting flows.

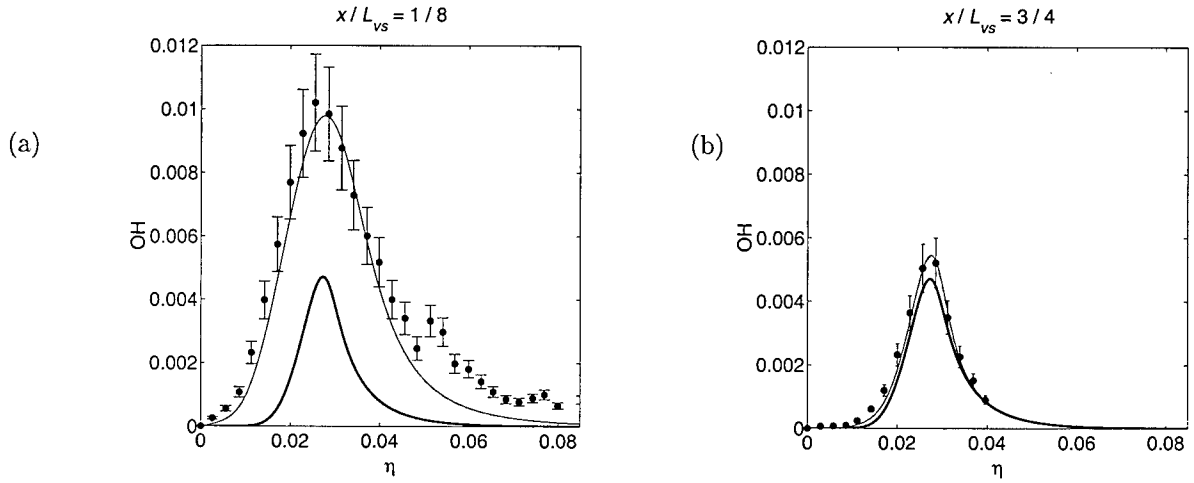


Figure 4: Burning of hydrogen in air. Conditional average of OH versus the mixture fraction at two different axial positions: (a) $x/L_{vs} = 1/8$ and (b) $x/L_{vs} = 3/4$. $L_{vs}$ is the visual flame length. Bold solid line indicates equilibrium chemistry (EQ), solid line indicates CMC, dashed line indicates quasi-steady CMC modeling. Both CMC and quasi-steady modeling yield identical results. Data are from Barlow et. al.[15]

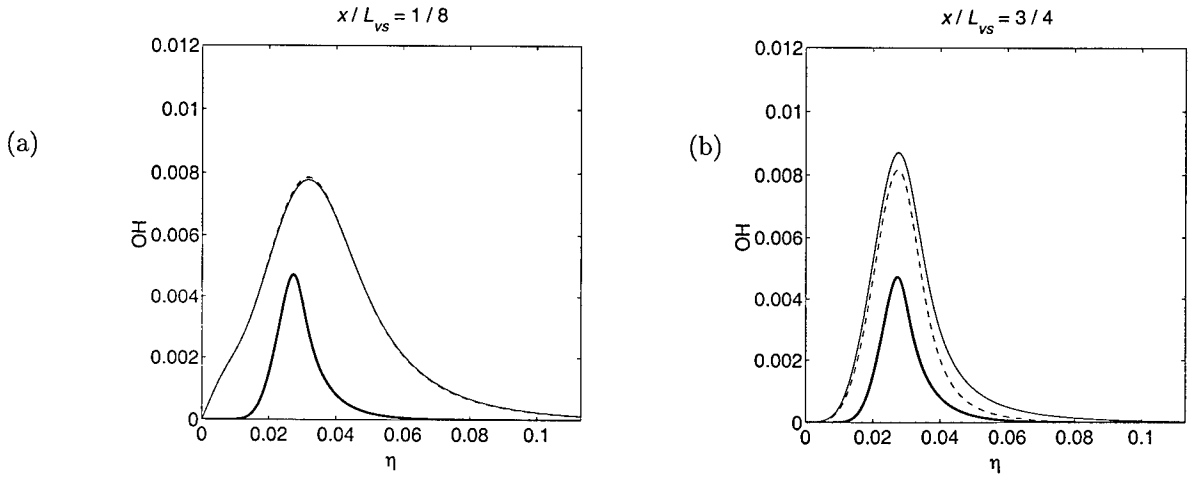


Figure 5: Burning of hydrogen in air with artificially slowed chemistry rates. Notation as in Fig. 4.

# PARALLEL SIMULATIONS OF TURBULENT SPRAY COMBUSTION IN A FULL-SCALE GAS TURBINE COMBUSTOR

**ARO Grant No. DAAH04-96-1-0008**

**Suresh Menon**

**School of Aerospace Engineering**
**Georgia Institute of Technology**
**Atlanta, GA 30332-0150**

SUMMARY/OVERVIEW:

A new parallel two-phase compressible large-eddy simulation (LES) methodology has been developed to study high Reynolds number reacting flows. A key feature of this new solver is the manner in which small-scale turbulent mixing and combustion is simulated. This feature allows for proper and accurate characterization of both large-scale convection and small-scale mixing on the droplet transport and vaporization processes thereby, providing a more accurate prediction of chemical reaction effects in spray flames. Validation of the new approach is carried out using DNS and LES of forced high Re isotropic tubulence and also used to study droplet vaporization and combuston (with infinite and finite-rate kinetics) in mixing layers. Finally, the LES solver is used to simulate a high Reynolds number reacting liquid spray in a co-axial full-scale high swirl combustor. These LES studies in te full-scale combustor are the first such reported studies and preliminary results provide confidence about the new solver. Additional validation and implementation issues for such simulations are also discussed here.

TECHNICAL DISCUSSION:

Desirable features for the next generation gas turbine engines are combustion efficiency, reduced emissions and stable combustion in the lean limit. To reach these goals, current research is focusing on improving the liquid fuel atomization process and to increase fuel-air mixing downstream of the fuel injector. However, the structure of complex three-dimensional, swirling fuel-air mixing layers is very difficult to resolve using current experimental and numerical methods. Since fuel atomization and fuel-air mixing are both highly unsteady, conventional steady state methods cannot be used to elucidate the finer details. On the other hand, although unsteady mixing process can be studied quite accurately using direct numerical simulation (DNS) application of DNS is limited to low to moderate Reynolds numbers (Re), typically of order 1000, due to resolution requirements. Here, an alternative approach using large-eddy simulation (LES) is being developed for high Re (order of 10,000 and more) flows.

In LES modeling of the momentum transport scales larger than the grid size are computed using a time- and space-accurate scheme, while the effect of the unresolved smaller scales (assumed to be mostly isotropic) on the resolved motion is modeled using an eddy viscosity based subgrid model. This approach is acceptable for momentum transport since all the energy containing scales are resolved and all the unresolved scales (that primarily provide for dissipation of the energy transferred from the large scales) can be modeled by using an eddy dissipation subgrid model. However, these arguments cannot be extended to reacting flows since, for combustion to occur, fuel and oxidizer species must first mix at the molecular level. Since, this process is dominated by the mixing process in the small-scales, ad hoc eddy diffusivity concepts cannot be used except under very specialized conditions. To deal with these distinctly different modeling requirements, a new subgrid mixing and combustion model has been developed that allows for proper resolution of the small-scale scalar mixing and combustion effects. This subgrid model is implemented within the framework of a conventional LES based on an Eulerian-Lagrangian Stochastic Separated Flow (SSF) model which has been shown to be

suited for spray modeling since it allows quantitative prediction of the effects of spray. In this approach, the droplets are tracked in a Lagrangian manner within the Eulerian gas flow field. However, a key limitation of this approach is that due to resource constraints only a limited range of droplet sizes are tracked and droplets below an ad hoc (pre-specified) cut-off size are assumed to vaporize instantaneously and to become fully mixed in the gas phase. This approach is demonstrated here to be seriously flawed and it is shown that the new subgrid formulation employed here correctly takes into account the effect of all droplets below the cutoff.

Validation and caliberation of the new formulation is carried out using DNS and LES of relatively high Re stationary isotropic turbulent flows with and without two-phase coupling. Figure 1 shows the kinetic energy and dissipation spectrums predicted using DNS. Results show that two-phase coupling changes the energy and dissipation characteristics at the small scales. This result is consistent with earlier observations except that the present results have been obtained in non-decaying high Re isotropic turbulence. LES is currently being carried out for the same test conditions to caliberate the subgrid closure terms in order to capture the effect of this dynamics in the small scales. These results will be presented.

Further analysis for the subgrid mixing process in two-phase mixing layers has been carried out to investigate the impact of the cutoff size on product formation under both infinite and finite rate conditions. Figure 2 compares the conventional LES predictions with the predictions by the new subgrid based approach. It can be seen that in the conventional case, increasing the cutoff size drastically changes the product formation which is incorrect since the same amount of fuel is being vaporized. However, the new approach (Fig. 2b) consistently predicts the same product formation except when the cutoff siize is increased to very large values. There is a significant computational advantage of this approach since increasing the cutoff size by a factor of 4 descreases the computational cost by a factor of around 4 inspite of the increase in computational effort due to the new subgrid model. This suggests that using an efficient parallel LES two-phase flows could be simulated in a cost effective manner.

To set the stage for such simulations, preliminary LES have been conducted using full-scale test conditions such as in a General Electric high swirl combustor (LM-6000). Figures 3-6 show various axial and cross-stream planes of the flow field in such a combustor. Infinite rate kinetics in the swirling, high Re flow has been simulated with around 65,000 droplet groups on a 101x81x89 grid. Result show qualitative agreement with past observation. It is worth noting that premixed (gas) combustion in an identical combustor showed excellent agreement with data using the same LES code Further analysis of the new two-phase results is underway and will be reported in this presentation.

Using the parallel solver, a typical flow through time can be completed within 10 hours on 120 processors of the Cray T3E. Under the DoD HPC Grand Challenge ARO Project, one flow through can be completed within 24 hours indicating that a full simulation (of around 14 flow through times) can be completed in 2 weeks of real time (assuming consistent availability). It is estimated that on the new SGI (MIPS 12000), using the same number of processors one flow through time will take only around 2-3 hours indicating a full simulation may become feasible in 2 days (assuming 50% availability of the system). These estimates clearly demonstrate that in the near future 3D LES of realistic flows in full-scale combustors may become practical enough for engine manufacturers to use it for limited design studies (a limited such a study is now underway at General Electric using the code developed here). Note that this is only feasible if relatively coarse grid LES (e.g., less than 2 million grid ponts) is carried out. However, in that case, advanced subgrid models such as the one developed here must be used in order to ensure the accuracy of the predictions.

A serious concern in the present development had been the lack of experimental data for code validation under realistic conditions. Recently, however, two sets of data has become available: a large set of non-burning and burning data from NIST and an in-house experimental study of dilute non-vaporizing spray under the present MURI. LES under conditions specified by NIST has already been set up and are underway. Results will be presented during this meeting.

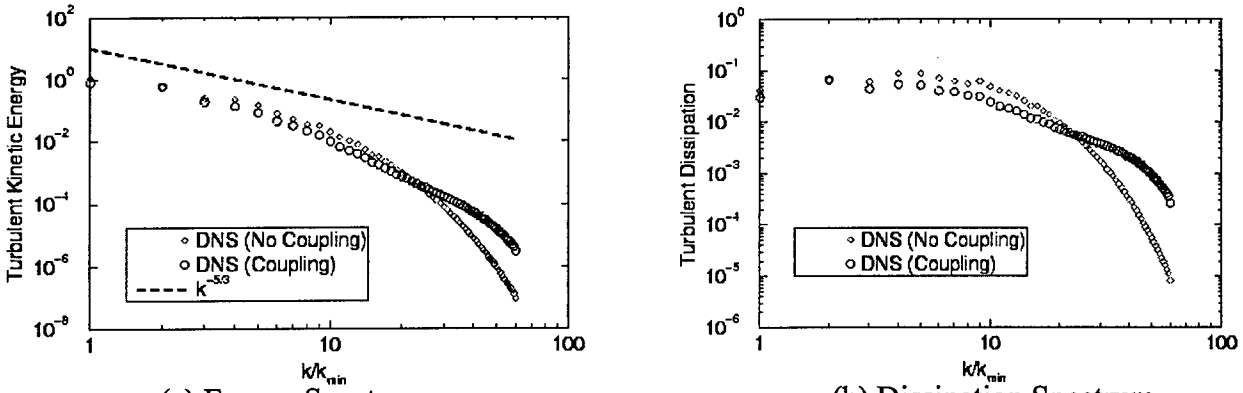


(a) Energy Spectrum (b) Dissipation Spectrum

Figure 1. Energy and dissipation spectrum in high Re stochastically forced isotropic turbulence. The grid resolution is 128x128x128 and 35,000 droplets are tracked. With momentum coupling there are changes in the high wavenumbers. LES models are being developed to account for these changes.

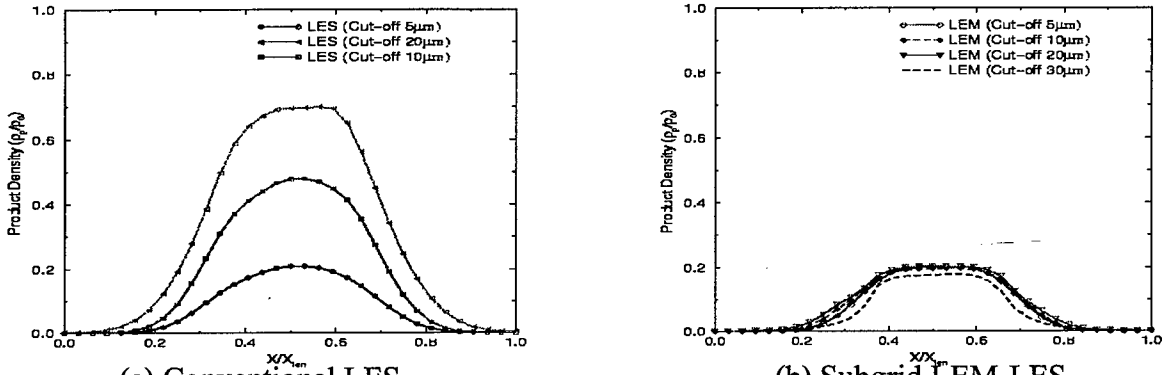


(a) Conventional LES (b) Subgrid LEM-LES

Figure 2. Comparison of conventional and subgrid two-phase model based LES in a turbulent mixing layer. As shown, changing the drop cutoff size in the conventional LES causes gross over-prediction of the product formed.

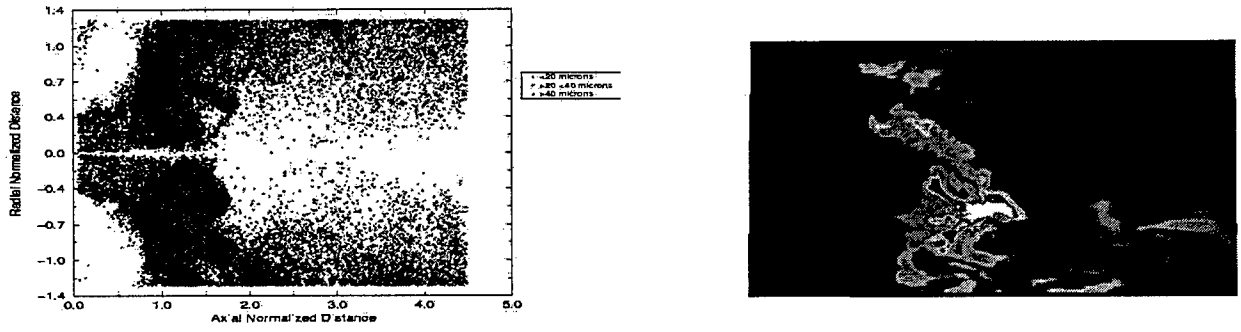


(a) Droplet distribution (a) Product distribution

Figure 3. Instantaneous axial distribution of droplets and product density in a swirling spray jet in a co-axial dump combustor. The configuration is identical to a General Electric LM6000 combustor and the test conditions closely correspond to experimental values. Reynolds number based on the inlet diameter and velocity is 330,000 and the swirl number is 0.56. A spray with a log-normal distribution of droplets is introduced at the inlet and vaporization is included with full two-phase coupling. Grid resolution is 101x81x89 and 65,000 droplet groups have been tracked in the flow field. Infinite-rate kinetics is simulated here.

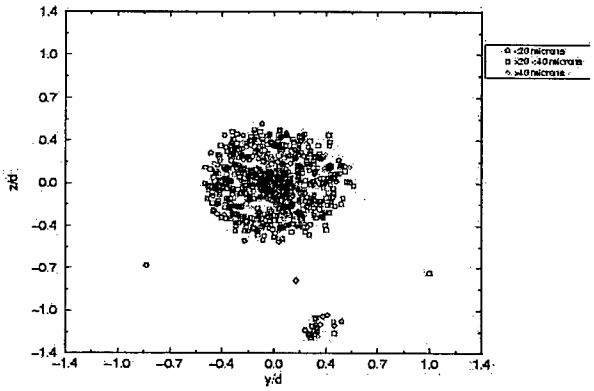


(a) Droplet distribution

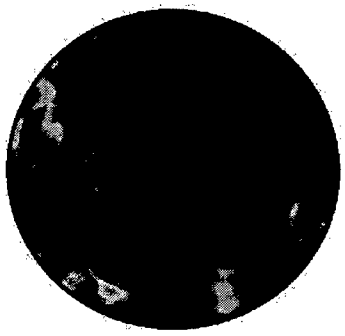

(b) Product distribution

Figure 4. Cross-stream droplet and product distribution in the co-axial combustor at an axial location x/D = 0.05 which is very close to the inlet. At this location the droplets are still following the initial spray pattern and not much product has formed.

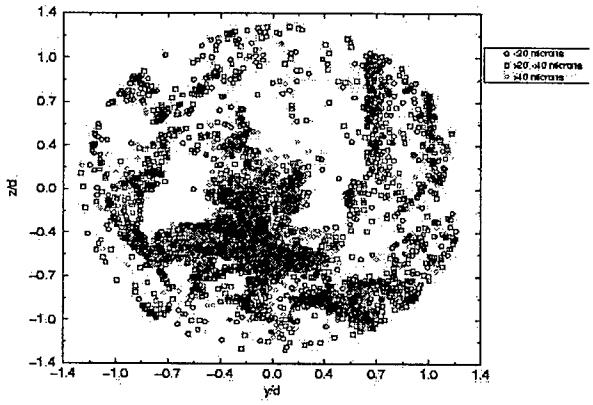


(a) Droplet distribution

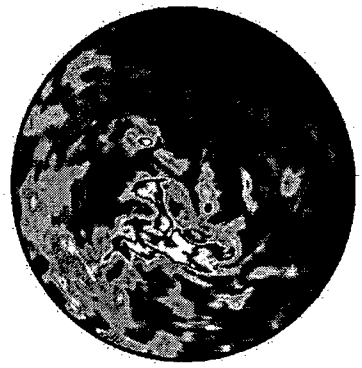

(b) Product distribution

Figure 5. Cross-stream droplet and product distribution in the co-axial combustor at an axial location x/D = 1.5 which is further downstream. By this location, significant dispersion of the droplets has occurred and the vaporized fuel and air has mixed and reacted to form the product.

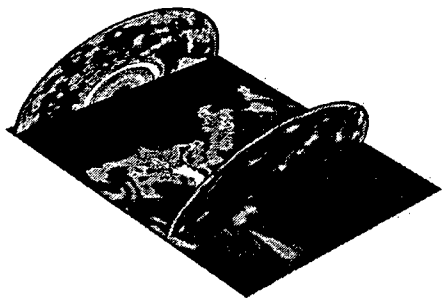

(a) 3D view of the flow in the combustor

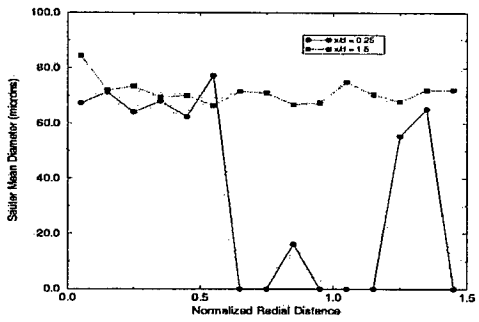


(b) SMD droplet size distribution

Figure 6. 3D view of the swirling shear layer and the Sauter Mean Diameter radial distribution in the combustor. The 3D circular planes show the vorticity magnitude and the spanwise plane shows the product density. The two axial locations in (b) correspond to locations shown in figures 4 and 5.

# COMPRESSIBLE TURBULENT REACTING FLOWS

## (AFOSR Grant No. F49620-96-1-0106)

Principal Investigators: F. A. Williams, P. A. Libby and S. Sarkar

Department of Applied Mechanics and Engineering Sciences
University of California San Diego, La Jolla, CA 92093-0411

## OBJECTIVES

The objective of this research is to advance fundamental understanding of reacting flows relevant to Air Force needs in high-speed airbreathing propulsion. Advanced numerical methods on high-performance computing platforms are applied in order to obtain accurate and detailed descriptions of multidimensional, unsteady combustion processes. Complementary theoretical analysis is performed and predictive models developed using theory and numerical computation. The results obtained here should improve the capability to analyze and design propulsion systems involving high-speed turbulent combustion.

## STATUS OF EFFORT

Specific areas investigated in the past year include direct numerical simulation (DNS) of compressible turbulent combustion, large eddy simulation (LES) and DNS of plane jets, and Reynolds-averaged Navier-Stokes (RANS) modeling of high-speed turbulent Couette and related flows. DNS and theoretical analysis has lead to explanation of inhibited turbulence growth at high speeds and the effect of unequal freestream densities in the shear layer as well as predictive models. Combined density and high-speed effects in supersonic methane-air combustion are currently being studied. LES of the spatially evolving plane jet has been performed and the performance of various models evaluated using our DNS and other experimental data. The dynamic mixed model is found to give good results in both *a priori* tests and *a posteriori* calculations. A new theory of premixed turbulent combustion that accounts for the effect of fluctuating pressure gradients has been developed and shown to give excellent agreement between theory and experiment. Ongoing work in moment closure is aimed at capturing the transition from counter to cogradient transport at large turbulence intensity seen in DNS and experiments.

## ACCOMPLISHMENTS

**The compressible, reacting, shear layer; DNS:** The shear layer between two streams with velocity and density contrasts has been studied using DNS [1, 2]. The Reynolds number based on vorticity thickness is as large as $12,000$, a value large enough for fully-developed turbulence corresponding to laboratory experiments. The compressibility effect of dramatically reduced growth rate as a function of increasing convective Mach number, $M_c$, is observed in the current DNS as shown in Fig. 1. This stabilizing effect of compressibility has been explained and a physics-based turbulence model obtained as described below. DNS shows that the normalized pressure strain term exhibits monotone decrease with increasing $M_c$, which leads to inhibited energy transfer from the streamwise to cross-stream fluctuations, to the reduced turbulence production observed in DNS, and, finally, to reduced growth rate of the shear layer. An analysis of the wave equation for pressure fluctuations that involves two-point, two-time correlations is performed that, in agreement with DNS, predicts that the normalized

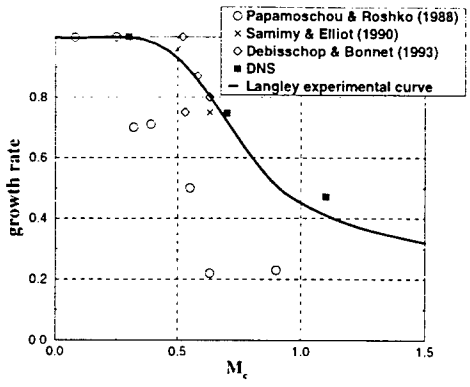


Figure 1: Dependence of normalized shear layer growth rate on $M_c$.

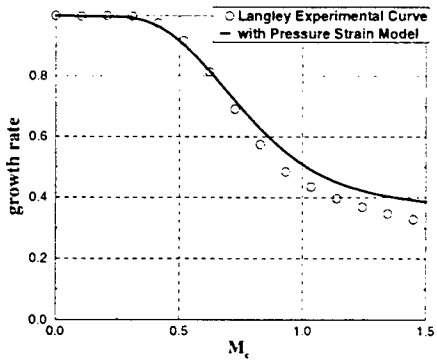


Figure 2: Comparison of new compressibility model (solid line) with the Langley experimental data (circles).

pressure-strain term decreases with increasing $M_c$. Based on our analysis and DNS, we offer the following conceptual mechanism for the stabilizing effect of compressibility. The finite speed of sound in compressible flow causes a time delay, $l/c$, in the communication of pressure signals across a characteristic eddy length $l$ and, thus, causes additional *temporal* decorrelation between adjacent points in an "eddy" that decreases the pressure-strain term. A model for the compressibility effect on the pressure-strain term is also derived which, as shown in Fig. 2, can capture the dependence of the growth rate on $M_c$ that is seen in the experiments.

| $s$ | $\dot{\delta}_\theta/\dot{\delta}_{\theta,1}$, DNS | $1-0.4\lambda(s)a(s)$, Model |
|---|---|---|
| 1 | 1.00 | 1.00 |
| 4 | 0.86 | 0.82 |
| 8 | 0.59 | 0.70 |

Table 1: Density ratio effect on growth rate ratio.

When the ratio of the densities of the free streams is varied in the high-speed regime, $M_c = 0.7$, it is found that, although the vorticity thickness is insensitive to changes in the density ratio $s = \rho_1/\rho_2$, the momentum thickness growth rate decreases. Thus, the hypothesis often made for low-speed flows that the temporal growth rate of the vorticity thickness can be assumed constant, is shown to be true at high speeds. Interestingly, flipping the density ratio to $1/s$ from $s$ has no influence on the growth rate of the temporal mixing layer. The maximum shear stress $\overline{uv}$ is found to remain invariant with $s$; however, its location shifts to the *low-density* side. An analysis is carried out to derive a model that depends on the shift $a(s)$ of the location of maximum shear stress, and the parameter, $\lambda(s) = (s-1)/(1+s)$. Table 1 shows that the model (last column) is a good approximation to the observed effect of density ratio on the momentum thickness growth rate.

The investigation of compressibility effects due to high-speed and those due to density contrasts has been completed. The effect of heat release in high-speed, methane-air combustion is currently being investigated [3]. A four-step mechanism [4] which is well established as a good reduced mechanism for methane-air combustion [5] is used with equations for all member species along with explicit expressions for the reaction rate term. It is probably the

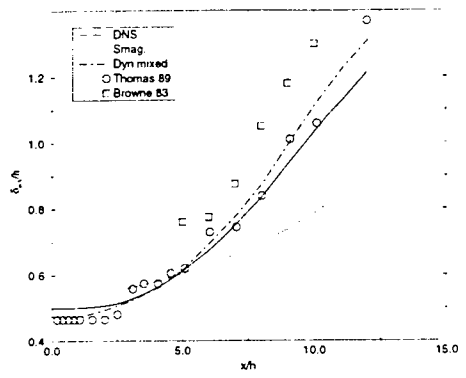


Figure 3: Evolution of the jet half-width in LES.

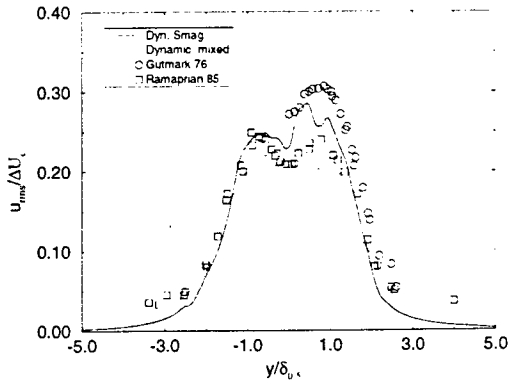


Figure 4: Profiles of streamwise turbulence intensity in LES.

minimal set that gives a flame structure with reasonable representation of major species and temperature in situations with possible extinction where the flame is subjected to a wide variation of strain rates. The generalized flame sheet formulation for methane-air combustion [6] will also be considered. Here, conservation equations are formulated in terms of generalized coupling functions, based on a three-step reduced mechanism. These coupling functions permit nonunity species Lewis numbers as well as finite rate chemistry in the slow recombination of H radicals while retaining the reaction sheet approximation for the oxidation of $CH_4$ to CO.

**The turbulent jet; LES:** LES of a spatially developing jet has been performed [7] and three different subgrid stress models compared: the standard Smagorinsky model, the dynamic Smagorinsky model and the dynamic mixed model. A series of simulations at a low Reynolds number $Re_d = 3,000$ was performed to enable comparisons with our previous DNS [8]. Then the Reynolds number was increased and simulations performed at a high Reynolds number, $Re_d = 30,000$, more typical of engineering applications. Fig. 3 shows the evolution of the jet half-width. The standard Smagorinsky model is much too dissipative while the other two models compare well with both DNS and experiments. Fig. 4 shows that, in the high Reynolds number jet, both, the mixed and dynamic Smagorinsky models give results consistent with experimental data.

Our *a posteriori* tests using the exact subgrid stresses obtained by filtering the DNS jet data, show that the subgrid shear stress is severely underpredicted by the dynamic Smagorinsky model. On the other hand, surprisingly, the dynamic Smagorinsky model provides satisfactory overall results concerning flow statistics as shown by Fig. 3 and Fig. 4. Terms in the equation for streamwise velocity, $U_1$, are examined to understand this apparent contradiction. The dominant balance is found to be between mean convection and the transverse gradient of the *sum* of the resolved Reynolds shear stress and the unresolved SGS stress. After examination of the mean momentum balance, it is found that the sum of the resolved and subgrid shear stress is similar with both models, thus explaining their similar performance.

We are currently evaluating the ability of LES with subgrid scalar transport models to predict the evolution of mean, rms and pdf's of the scalar. Also, our new developments [9] in LES of nonequilibrium turbulent flows will be tested in jets with different coflows, a difficult problem for RANS calculations.

**Couette flows and related studies:** Our study of extinction by wall cooling and the influence of compressibility, heat transfer and shear on the rate of creation of product in laminar

Couette flow[10] has been accepted for publication. In addition to being of fundamental interest this contribution provides the basis for development of extended flamelet models, i.e., models applicable to high speed turbulent reacting flows One of the fundamental problems in the modeling of such flows relates to the treatment of fluctuating pressure gradients which, although neglected in previous theories, have been found to be important in recent DNS studies. In [11] a revised theory of premixed turbulent combustion involving a new model for such fluctuating gradients is developed and applied to turbulent reactant streams impinging on a wall, a flow for which a limited amount of accurate data on first and second moment quantities is available. Excellent agreement between theory and experiment is achieved. Particularly Particularly impressive is the agreement with respect to the mean axial flux.

Suggested by this success is a revisiting of the theory of turbulent flames normal to an oncoming reactant stream. The hope here is that depending on the intensity of the turbulence in that stream relative to the laminar flame speed, a measure of the chemical kinetic rate of the mixture, we shall predict either countergradient or gradient transport. It is now known from both DNS results and experiment that under conditions of intense turbulence the countergradient transport seen so frequently in computations and experiment reverts to gradient form. This transition has never been predicted by a moment method but we hope that the new model for fluctuating pressure gradients will permit us to do so.

As a follow on to these studies we are also currently examining models for the mean rate of creation of products. In the flames in stagnating turbulence that we have been studying we can readily make a separation between the influences of chemistry and turbulence models and thereby assess each chemistry model independently.

# References


[1] C. Pantano and S. Sarkar, "A study of compressibility effects in the high-speed turbulent shear layer using direct simulation, " *J. Fluid Mech.*, submitted (1999).

[2] S. Sarkar, " Contributions of DNS to the investigation of compressible, turbulent shear flows," Joint INI/ERCOFTAC Workshop on Direct and Large-Eddy Simulation, Cambridge University, May 1999, Kluwer (1999).

[3] C. Pantano and S. Sarkar, "Compressibility effects in the high-speed, reacting shear layer," Proceedings, International Symposium on Turbulence and Shear Flow Phenomena, Santa Barbara, September 1999, pp. 8, accepted (1999).

[4] K. Seshadri and N. Peters, "Asymptotic structure and extinction of methane-air diffusion flames, " *Combust. Flame*, **73**, 23.

[5] N. Peters and B. Rogg (Eds.), Reduced kinetic mechanisms for application in combustion systems, Springer-Verlag, Berlin (1993).

[6] F. A. Williams, "Formulations for turbulent diffusion flames with reduced chemistry, *Combust. Sci. Tech.*, Japanese Edition, **6**, 27-46 (1998).

[7] C. Le Ribault, S. Sarkar and S. A. Stanley, "Large eddy simulation of a plane jet," *Phys. Fluids*, submitted (1999).

[8] S. Stanley and S. Sarkar, "A study of the flowfield evolution and mixing in a planar turbulent jet using direct numerical simulation," *J. Fluid Mech.*, submitted (1999).

[9] L. Shao, S. Sarkar, and C. Pantano, "On the relationship between the mean flow and subgrid stresses in LES of turbulent shear flows," *Phys. Fluids*, **11(5)**, 1229-1248 (1999).

[10] K. N. C. Bray, M. Champion and P. A. Libby, "Premixed combustion in laminar Couette flow-extinction and mass burning rate," *Combust. Flame*, in press (1999).

[11] K. N. C. Bray, M. Champion and P. A. Libby, " Premixed flames in stagnating turbulence. Part IV - A new theory for the Reynolds stresses and Reynolds fluxes and exploited in impinging flows, " *Combust. Flame*, submitted (1999).

# LARGE EDDY SIMULATION OF DIESEL COMBUSTION CHANBERS

**ARO Grant No.: DAAH04-96-1-0196**

**I.B. Celik, W.S. Lewellen, J.M. Kuhlman**
**E. Amin, A. Gel, D.C. Lewellen, A. Smirnov, J. Smith, I. Yavuz**

**Department of Mechanical and Aerospace Engineering**
**West Virginia University, Morgantown WV**

## 1.0 OVERVIEW

The objective of this research is to provide via the LES (Large Eddy Simulation) technique information about in-cylinder turbulence in sufficient detail to overcome outstanding turbulence modeling issues. The turbulence data generated from LES can be used to refine combustion and spray models in RANS (Reynolds Averaged Navier-Stokes) codes, which are used for design purposes. Furthermore, investigation of the small scale mixing processes will provide a better understanding of the mechanisms responsible for combustion phenomenon like auto-ignition, pollutant formation, and local flame extinction. To this end the prospects of LES for internal combustion chambers are investigated using a combination of the existing KIVA family of codes (Amsden 1993, 1997), and a WVU/LES code developed for modeling atmospheric turbulence. The KIVA codes, which were designed specifically for internal combustion engines, have been modified for LES of turbulent combustion. The WVU/LES code is used as an initial benchmark code to compare how well KIVA/LES is behaving on incompressible, swirling flow configurations. The main focus of the study has been on engines running under motored conditions. This helped us to identify problems concerning numerical accuracy, grid requirements, and selecting appropriate sub-grid scale (SGS) models as well as understanding mechanics of turbulence generation in IC engines. Currently, simulations are underway aiming at predicting in-cylinder turbulence with combustion.

## 2.0 SUMMARY OF RESULTS

Simulations of in-cylinder flow were performed with relatively fine grid resolution under motored conditions focusing on the compression and expansion strokes first. A comparison of the results using different sub-grid scale models was performed. It was discovered that the simulations that use a quasi-second order upwind scheme for the convective terms with no SGS turbulence model or central differencing scheme with the classical Smagorinsky model produced an energy cascade, derived from a spectral analysis of the fluctuating data, that closely resembled that of experiments. Another goal of this research was to improve existing RANS (Reynolds Averaged Navier Stokes) models when applied to IC-engines. To achieve this, a parallel study was performed on a benchmark flow representing the intake flow of an IC-engine to assess the performance of various RANS turbulence models (see Yavuz and Celik, 1999). As expected, the models do not perform uniformly well over all flow regimes. They show significant variations at higher engine speeds. The deficiencies are currently being evaluated for further refinement.

Initial studies indicated that the KIVA codes were deficient in several areas with respect to performing LES. Considerable effort has been focused on improving these codes. The time accuracy of the code was made fully second-order by implementing a combination of two-stage Runge-Kutta and Adams-Bashforth schemes into the advection phase. Spatial accuracy was improved by introducing an advection scheme where central differencing is used in the momentum equations and quasi-second order upwinding is used in the scalar equations. Efficiency of the single processor version of KIVA was

improved by up to 20% by implementing a more sophisticated preconditioning scheme in the pressure solver (Smith et al. 1999a). The overall computational performance of the code was improved significantly with the distributed-memory implementation of KIVA-3 (KIVA-3/MPI) based on one-dimensional domain decomposition for parallel execution. KIVA-3/MPI has been tested and validated on several hardware platforms including SGI Origin 2000, Cray T3E, and Windows NT based Intel platforms (see Gel & Celik, 1999). The code has been recently ported to the 11-node Beowulf type DEC Alpha Linux cluster built for this project at WVU. The current version is capable of handling fixed grids on any given number of processors. Implementation of piston movement and combustion into KIVA-3/MPI is under progress.

To identify possible problems that would be encountered when running KIVA in LES mode a series of tests were performed on a benchmark problem. One of the benchmark problems was that of a swirling jet which was studied experimentally by Holzapfel (1996). Swirling jets are of particular interest to the internal combustion engine community due to the fact that significant vorticity is induced during the intake stroke to aid in turbulent mixing and combustion inside the engine cylinder. The problem was simulated using both KIVA-3 and another LES code (WVU/LES). It was desired to see if KIVA could reproduce similar results obtained from a well-validated LES code. As presented in detail in Smith et al. (1999b), considerable agreement between the two results was observed in spite of the differences between the codes. Thus it appears that the KIVA code is capable of performing LES. Other interesting results were obtained with the WVU/LES application (Lewellen et al. 1998) that include testing of a new SGS model suitable for swirling flows, work that has significant potential for IC engine modeling.

To investigate the generation of turbulence induced by only the piston/bowl assembly two- and three- dimensional simulations have been performed with various grid arrangements (Yavuz et al. 1998). It was possible to capture flow instabilities, which were sustained over a few compression/expansion cycles. There were noticeable cycle-to-cycle variations and anisotropy in the predictions. The computed root mean square (rms) fluctuations increased linearly with the engine speed in accordance with experimental observations (see Catania et al. 1996). The predicted rms velocity fluctuations were relatively low, but this should be viewed in the light of the fact that turbulence usually decays towards TDC, and any remaining turbulence is either the residual from the intake-generated turbulence and/or the turbulence induced only by the piston/bowl geometry.

In general, most of the turbulence in a real engine is induced during the intake stroke. Simulations of the intake and subsequent expansion and compression strokes were performed for a typical two-valve cylinder assembly. Two sets of runs were performed on grids with different resolution, 220,000 and 440,000 nodes, with different sub-grid scale models. Figure 1 shows the fluctuating velocity component in the radial direction located at a point approximately (5-9) mm below the cylinder head and near the cylinder axis in comparison to measurements (denoted by $u_i$ which is a cycle resolved quantity with a zero mean in Fig. 1b)) of Catania and Spessa (1996). The geometry of Catania's experiment is somewhat different from the computational model in that there is no cylinder bowl in the latter case. Because of that and a slight difference in special locations where the measured and computed velocities were retrieved, it was not possible to predict the mean flow-field exactly. But our aim was to reproduce the main trend in the fluctuating component, which is seen to agree well with experimental data (Fig. 1). The predicted cycle resolved mean velocity (not depicted here) showed roughly the same trend as in experiments but with a lower magnitude. It is noteworthy to see that the velocity fluctuations decrease significantly towards the BDC (~180 CA degree) as observed in the measurements.

One of the early experimental studies demonstrating the decay of turbulence during the expansion stroke is that of Semenov and Sokolik (1958). In these experiments the piston head was flat which corresponds to the computational setup, but the intake valve was located co-axially relative to the

cylinder. A hot wire anemometer was used to obtain the time variation of velocity fluctuations. The comparison (Figure 2, see also Celik et al. 1999) of the measured and computed time dependence of the absolute value of velocity in the plane normal to the cylinder axis showed that the general trend of turbulence decay observed in both cases was in good agreement. Note that the intake valve was closed during the second compression/expansion cycle.

Finally we present the normalized autospectral density function (i.e. energy spectra) in comparison with experiments in Figure 3 at a representative point which roughly corresponds to the measurement point. The agreement of both the energy content and the frequency ranges captured in the present simulations are good in spite of the differences in the cylinder configurations. The calculated spectra looks wavy as compared to the experiments, but this is most probably due to the smoothing effect of the double averaging (including ensemble averages) applied in experiments (see Equation 11, Catania et al. (1996)). More details can be found in Celik et al. (1999).

With the groundwork being laid for performing LES of motored diesel engine cylinders, a parallel study focused on the implementation of combustion models appropriate for LES. The first study (Amin et al. 1998) involved implementing a modified form of an Eddy Breakup (EBU) turbulent combustion model where the model constants are dynamically linked to the reaction surface. The application of the modified EBU model to a direct injected diesel engine using KIVA has shown the importance of this modification on chemistry/turbulence interaction in engines. Further, a validation study of a conserved scalar/assumed pdf turbulent mixing model has been performed (Amin and Celik, 1999). The computations indicate that the conserved scalar/assumed pdf approach can provide a tractable approach to the modeling of turbulent mixing while being an acceptable compromise between accuracy and computational expense. This model has also been implemented into KIVA code and it is being used as a SGS model for combustion.

**REFERENCES**


Amin, E. M., Celik, I. (1999) "A Validation Study for a Turbulent Mixing Model Based on the Probability Density Function Approach" Paper no. 1999-01-0231, SAE International Congress and Exposition Detroit, MI.

Amin, E. M., Celik, I., Yavuz, I., and Smith, J. (1998) "Application of a Variable EBU Coefficient for Turbulent Combustion Modeling in a Direct Injection Diesel Engine," Proceedings of ASME-ICE Spring Tech. Conference, April 26-29, Fort Lauderdale, FL.

Amsden, A.A. (1993) "KIVA-3: A KIVA Program with Block-Structured Mesh for Complex Geometries," Los Alamos National Laboratory, Los Alamos National Laboratory Report LA-12503-MS, UC-361, Los Alamos, New Mexico 87545

Amsden, A.A. (1997) "KIVA-3V: A Block Structured KIVA Program with Vertical or Canted Valves," Los Alamos National Lab. Report No. LA-13313-MS, UC-1412, Los Alamos, New Mexico .

Catania, A., Dongiovanni, C., Mittica, A., Negri, C., and Spessa, E.: (1996), Turbulence Spectrum investigation in a DI Diesel engine with a reentrant combustion bowl and a helical inlet port, *SAE Paper* 962019.

Catania, A.E., and Spessa, E. (1996) "Speed Dependence of Turbulence of Turbulence in a High Squish Automotive Engine Combustion System," SAE Technical Paper # 960268.

Celik, I. Yavuz, I., Smirnov, A., Smith, J., Amin, E., and Gel, A. (1999) "Prediction of in-Cylinder Turbulence for IC Engines," Mediterranean Combustion Symp. Antalya, Turkey, June 20-25.

Gel, A. and Celik, I. (1999) "A Parallel Implementation of a Commonly used internal Combustion Engine Code, KIVA-3," DoD HPC Users Group Conference, Monterey, CA, June.

Holzapfel, F. (1996) "Zur Turbulenzstruktur Freier Und Eingesschlossener Drehstromungen," Dissertation, University of Karlsruhe, Germany.

Lewellen, D., Lewellen, S., and Xia, J. (1998) "Simulation of Turbulence in a Swirling Jet," Submitted to Physics of Fluids.

Semenov, E.S. and Sokolik, A.C. (1958) "Investigation of Turbulence in a cylinder of a Piston Engine," Izvestiya Akademii Nauk. Otd. Tekh. Nauk Vol. 8, pp. 130-134.

Smith, J., Gel, A., and Celik, I. (1999a) "Improvement of the Pressure Solver in KIVA," SAE Paper No. 1999-01-1187.

Smith, J., Celik, I., and Yavuz, I. (1999b) "Investigation of the LES Capabilities of an Arbitrary Lagrangian-Eulerian (ALE) method," AIAA Paper 99-0421.

Yavuz, I. And Celik, I. (1999) "Assessment of Various Turbulence Models for IC-Engine Applications," Submitted to ASME ICE Division's Fall Tech. Conf., Ann Arbor, MI, October 16-20.

Yavuz, I., Celik, I., Smith, J., Gel, A., and Amin, E. (1998) "Bowl Induced Flow Instability in a Typical Engine Cylinder," 1998 ASME-ICE Fall Technical Conference, Clymer, New York Sept. 27-30. Paper No. 98-ICE-139, ICE-Vol. 31-2, pp. 99-106.

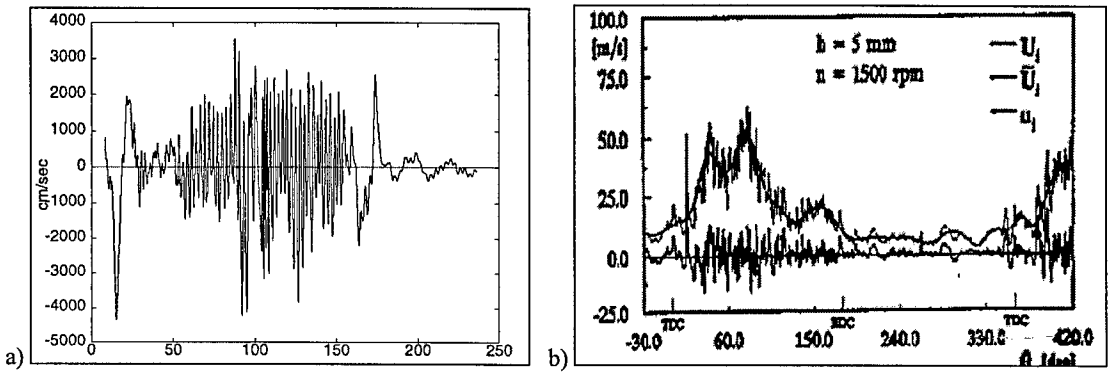


Figure 1. Fluctuating velocity: (a) computed (440000 node case), (b) Catania's data

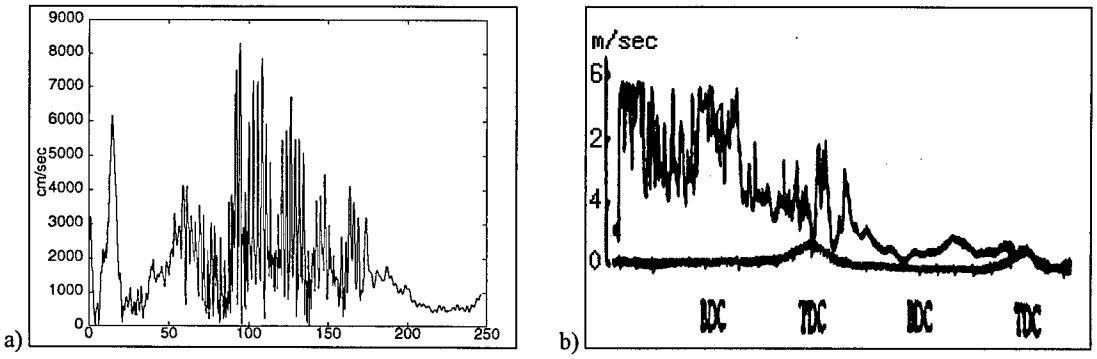


Figure 2. The magnitude of velocity: (a) computed (440000 node case), (b) Semenov's data

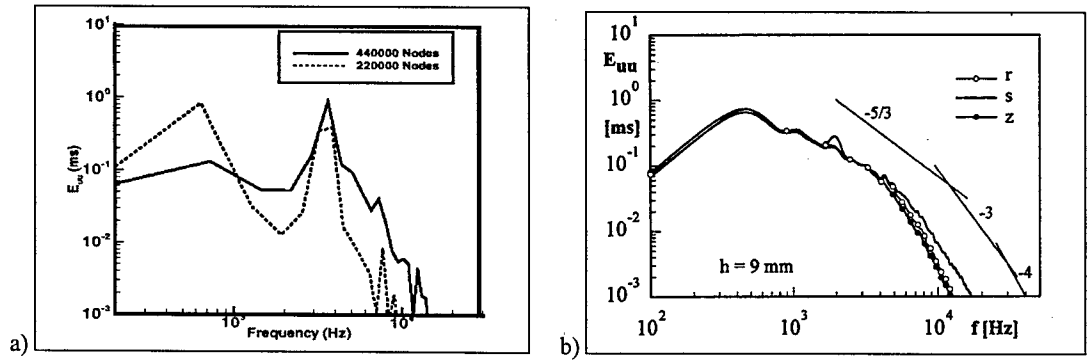


Figure 3. Power density spectra: a) computed (engine without a bowl), b) measured (engine with a bowl): r = radial, s = tangential, z = axial wire

# QUASI-STEADY TWO-ZONE DIESEL FLAME MODEL

ARO Grant DAAG55-98-I-0433

A.M. Mellor*, S.L. Plee, R.J. Tabaczynski

*Box 1592, Station B

Vanderbilt University, Nashville, TN 37215-1592

## SUMMARY/OVERVIEW

The focus of the program is developing engineering models for Diesel emissions and performance that (1) stand alone as preliminary design tools, (2) provide submodels for CFD, spray-marching, and cycle simulations, and (3) offer real-time algorithms for control in smart engines. The models are based on extensive experience with steady-flow gas turbine combustors and were first applied to Diesels twenty years ago at General Motors Research Laboratories. Quasi-steady model equations, derived from first principles, are based on Damköhler numbers describing the predominant pollutant chemistry and fluid flow processes. To date emissions of oxides of nitrogen have received primary emphasis, and both quasi-steady and dynamic analyses demonstrate that the accepted Zeldovich kinetics are inadequate. Development of similar models for particulate emissions and power density continues.

## TECHNICAL DISCUSSION

Analysis of engine data obtained at Ford Scientific Laboratory under a predecessor ARO-funded program showed that semi-logarithmic Arrhenius plots of nitrogen oxides emissions index versus the reciprocal of a temperature based on overall Diesel engine equivalence ratio were linear. Because this temperature can be shown proportional to engine load (bmep), the results suggested that two characteristic temperatures were required to describe such emissions, where the second is the stoichiometric flame temperature used to correlate $NO_x$ emissions from

diffusion-flame gas turbine combustors and Diesel engines, as well as soot emissions from laboratory flames and from Diesels. This finding indicates that the previous quasi-steady one-zone model for Diesel emissions, developed at GM and based only on the stoichiometric temperature, requires modification.

Consequently, a two-zone model for NO emissions is introduced where each zone is characterized by its predominant chemistry at one of these two temperatures. For NO formation (zone 1), the key region is the stoichiometric shear layer formed between each fuel plume and the ambient gas, as in the earlier models for conventional gas turbine combustors and indirect and direct injection Diesel engines. The stoichiometric temperature characterizing this zone is computed based on start-of-combustion conditions in the engine. To account for the observed dependence on a flame temperature that reflects the power output of the Diesel engine, zone 2 is based on an end-of-combustion temperature. In this zone, NO decomposition may proceed, as was suggested from comparison of the GM engine measurements with the one-zone model extended from gas turbine data. It is believed that the traditional $NO_x$/soot trade-off observed with most Diesel engines results from operation in regimes where NO decomposition is significant.

To explore the utility of the new two-zone model, the initial approach is quasi-steady, as in the earlier work. The end-of-combustion temperature is computed from a limited pressure (or dual) cycle fuel/air thermodynamic analysis. In this representation of Diesel combustion, air undergoes a polytropic compression from initial conditions $p_1$, $T_1$ and fuel injection starts prior to the end of compression. State variables are $p_2$, $T_2$ for the appropriate mixture at start of combustion. First law analysis of engine pressure-crank angle information provides premixed burn fraction. With the corresponding value of fuel fraction, constant volume combustion products and state ($p_3$, $T_{3a}$) are evaluated next. The balance of the fuel burns at constant pressure in the vitiated air to the end-of-combustion state variables $p_3$, $T_{3b}$, and this last temperature is used in the quasi-steady model to characterize zone 2.

This conceptually-simplified model for $NO_x$ emissions has been used to evaluate the importance of various mechanisms for NO formation and decomposition in the stoichiometric and lean zones just described. Following extensive kinetic studies for lean-premixed gas turbine engines, it is found that the $N_2O$ route to NO formation cannot be ignored at pressures typical of

combustion in Diesel engines. Likewise, if decomposition occurs, it proceeds via the reverse of the $N_2O$ mechanism. The quasi-steady model also suggests a straightforward dimensionless kinetic parameter that is used to evaluate the importance of decomposition at various engine operating conditions. Results show that increasing engine load can introduce significant NO decomposition, consistent with the experimental results obtained at Ford; however, compression and boost ratios, start-of-combustion temperature and pressure, maximum combustion pressure, properties of typical Diesel fuels, and EGR or water injection are shown to have small or negligible effects. A set of tests involving NO addition to the intake air has been conducted with the collaboration of both Ford and Caterpillar to investigate this aspect of the model.

For the Ford engine, analysis of effects of fuel injector and the remaining engine operating conditions shows that for the top-hat profiles employed in the tests, the fluid flow in the shear layer of zone 1 is dominated by the initial nozzle pressure drop and the engine speed. By using the criterion discussed above to eliminate data with significant decomposition, a closed-form correlation for emissions index of nitrogen oxides (g as $NO_2$/kg fuel) is obtained. Thus, in principle, the designer can estimate the NO formed at a given operating point as well as engine-out $NO_x$ emissions, if decomposition is negligible, with this algebraic equation. Under conditions where decomposition is expected unimportant, the model has been used to predict the emissions from two additional engines of different displacement using different fuel injection profiles, and the results show, as anticipated, both engine size and fuel insertion timing and shape are not yet fully incorporated in the model. Nevertheless, in its present form the model can be used for a given engine to evaluate the effects of EGR or water as diluents for $NO_x$ control; an extensive set of EGR sweeps was performed in the Ford tests, and results of water fumigation studies performed at the University of Wisconsin are accurately predicted. The model also serves as a baseline against which the effectiveness of the Mitsubishi hybrid fuel/water/fuel injector has been evaluated.

Modifications to the model prior to incorporation into CFD or engine simulation codes are nearly complete. Cummins has made available their crank-angle-resolved thermodynamic code in which stoichiometric temperatures are also evaluated so that $NO_x$ and soot emissions can be predicted via their models based on the original GM one-zone framework. Primus of Cummins has also introduced an extremely useful cycle visualization tool with which the

dynamic and quasi-steady models are easily compared. Work to date with the Cummins code reveals (1) the quasi-steady analysis conclusions regarding the importance of NO formation through the $N_2O$ pathway in Diesels are correct and (2) an improvement is required to the cycle model for zone 2 where NO decomposition may occur. Since measured pressure-crank angle histories have been employed in our studies to this point, start-of-combustion timing effects can be explored as well. The comparison of quasi-steady and dynamic simulations has also suggested a means of incorporating timing and burn phasing into the former.

Future efforts are directed towards resolving the effects of engine scale and advanced injection schemes discussed above, as well as refining the quasi-steady model for $NO_x$ emissions. Two- and three-zone soot models are in formulation following the methodology developed with the oxides of nitrogen model. Data for the next phase of the program are forthcoming from Caterpillar, Cummins, Ford, and the University of Wisconsin. Finally, with a complete emissions model, a detailed power density model is envisioned, where effects of fuel injection shape and splits are explicitly described.

TITLE: ADVANCED ENGINE CONTROL FOR INCREASING FUEL EFFICIENCY AND POWER DENSITY WHILE REDUCING OBSERVABLE EMISSIONS FROM MILITARY DIESEL ENGINES

ARO Contract No. DAAG55-98-1-0006

Principal Investigator(s): Dr. Chris Atkinson
Dr. Nigel N. Clark

West Virginia University
Department of Mechanical & Aerospace Engineering
College of Engineering and Mineral Resources
PO Box 6106
Morgantown, WV 26506-6106

SUMMARY:
Military diesel engines used in combat and tactical applications have their own specific engine control requirements that differ from those of commercial heavy-duty vehicles. The implementation of advanced engine control methods in diesel-powered military vehicles can result in an increase in their performance, a reduction in their fuel consumption, a reduction in their observable exhaust emissions and an improvement in their stealth capabilities. Neural network-based engine control has the potential to allow for the simultaneous, optimized control of several engine parameters such as fueling quantity, injection timing, injection pressure and turbocharger boost pressure. Future engines will be considerably more complicated in their control, incorporating such additional technologies as exhaust gas recirculation, variable geometry turbocharging, variable valve timing, multiple injection strategies and exhaust gas aftertreatment. The advanced engine control techniques developed here will facilitate the optimal control of these more sophisticated engines in future military applications.

AUTHORS: C.M. Atkinson, N.N. Clark, G.J. Thompson, T.W. Long and E. Hanzevack

TECHNICAL DISCUSSION:

Modern military diesel engines used for transportation, tactical and combat vehicle propulsion, and power generation are mostly direct injection, four-stroke, turbocharged, aftercooled engines, derived typically from commercial versions of the same engines. However, in terms of their control, military engines have specific requirements that are not adequately addressed in commercial vehicle applications. It would offer a significant strategic advantage under battlefield conditions if these engines offered improved power density (for increased performance), reduced fuel consumption (to increase vehicle range and to reduce refueling requirements), and reduced observable exhaust emissions (to improve their stealth capabilities). These advances can be realized through sophisticated engine management that interfaces with the electronically controlled injection systems present on modern day diesel engines. Moreover, such advanced management will prove essential in optimizing the technology-laden camless diesel engines of the future.

This present work is aimed at the development of artificial neural network (NN)-based techniques for the control of military diesel engines. Artificial NNs attempt to mimic human pattern recognition abilities, with the capacity to learn the associations between given inputs with respect to desired outputs, provided a sufficient amount and scope of data are supplied.

West Virginia University and NeuroDyne, Inc. have demonstrated the efficacy of a NN-based engine modeling system that employs a recurrent neural network structure with error backpropagation. The software, designed by NeuroDyne, Inc., uses three layers and a moving history of information at previous time steps to predict exhaust emissions levels, on-line in real time. The engine modeling or virtual sensor system consists of a predictive engine model (or models) designed to run on a microprocessor in parallel with the engine in real time, taking input signals from the same sensors as the engine itself. The NN model of the engine is able to make highly complex, non-linear and multi-dimensional associations between selected input parameters and outputs in real-time, which allows accurate predictions of engine performance across the full range of engine operation. In compression ignition engines, the NN model takes as inputs the manifold air pressure (MAP) and temperature (MAT), engine speed, engine coolant temperature (ECT), engine oil temperature (EOT), exhaust gas temperature (ExT), injection pressure (ICP), start of injection (SOI), fuel injection pulse width (FIPW), and commanded fueling rate (APS) as a function of time. The NN model of the engine is able to predict real-time torque output [TQ], engine exhaust emissions (unburned hydrocarbon [HC], carbon monoxide [CO], oxides of nitrogen [$NO_x$], and particulate matter [PM] or exhaust opacity [OP] smoke emissions), and fuel consumption (from $CO_2$ emissions) across the full range of engine operation.

During limited dynamometer testing, the NN model learns in real-time and on the fly the precise relationship between all designated inputs and outputs. The NN model assigns global or general weights among all designated inputs (engine operating parameters) and corresponding outputs (torque, fuel consumption, and regulated emissions) based on results learned during engine dynamometer testing. The required breadth of training is on the order of a few hours of highly transient testing. A further (local) set of weights can be allowed to vary in time across the life of the engine in the field, thereby providing a true learning, adaptive prediction system. The resulting NN submodels are able to provide the apparent results from a virtual suite of emissions sensors to the driver, to a smart diagnostic system, or to an engine controller. These virtual sensor results may either be unmeasured or unmeasurable engine parameters, or a duplicate estimation of already measured variables. One immediate application is in the virtual measurement of engine-out $NO_x$ emissions for on-board diagnostics (OBD).

The first year project goals of procuring a heavy duty diesel engine, conducting dynamometer testing for the neural network input, modifying an existing neural network code for the diesel engine, and validating the prediction capabilities of the neural network models with blind data sets have been completed and some of the prediction results are shown below. The (blind) prediction of the emissions from a Navistar T444E direct injection, turbocharged diesel engine measured over the Federal Test Procedure, using limited dynamometer testing to train the NN, is shown to be excellent, and well within the accuracy of the emissions measurement equipment.

The application of the NN-based submodels to predict and control the emissions and torque from a heavy-duty diesel engine to minimize black smoke emissions will be discussed. The continued development of a NN-based emissions predictions system using the existing engine sensors will also be discussed. Applications of the NN-based system as an alternative to map-based engine control, as a diagnostic method and for off-line emissions prediction will be presented. Optimization of the virtual sensing technique to allow high power density operation while minimizing black smoke will also be discussed.

Table 1: Neural Network Engine Model Input and Output Variables

| | Neural Network Submodel Name | | | | | | | |
|---|---|---|---|---|---|---|---|---|
| | Gaseous Emissions | | Particulate Matter | | Exhaust Opacity | | Output Torque | |
| | EM | | PM | | OP | | TQ | |
| | input | output | input | output | input | output | input | output |
| APS (%) | x | | x | | x | | x | |
| SOI ($10^{-6}$ s) | x | | x | | x | | x | |
| FIPW ($10^{-6}$ s) | x | | x | | x | | x | |
| ICP (ADC) | x | | x | | x | | x | |
| MAP (kPa) | x | | x | | x | | x | |
| ECT (°C) | x | | x | | x | | | |
| EOT (°C) | x | | x | | x | | | |
| ExT (°C) | x | | x | | x | | x | |
| IAT (°C) | x | | x | | x | | x | |
| Speed (rpm) | x | | x | | x | | x | |
| Torque (ft-lbf) | | | | | | | | x |
| HC (g/h) | | x | | | | | | |
| CO (g/h) | | x | | | | | | |
| $CO_2$ (g/h) | | x | | | | | | |
| NOx (g/h) | | x | | | | | | |
| PM (g/h) | | | | x | | | | |
| OP (%) | | | | | | x | | |

Table 2: Neural Network Architecture for each Submodel.

| NN Feature | EM | PM | OP | TQ |
|---|---|---|---|---|
| Number of Inputs | 10 | 10 | 10 | 8 |
| Number of Nodes in 1st Hidden Layer | 15 | 15 | 15 | 15 |
| Number of Nodes in 2nd Hidden Layer | 5 | 5 | - | - |
| Number of Outputs | 4 | 1 | 1 | 1 |

Table 3: Neural Network Engine Model Prediction Error versus Measurement Error.

| Output Parameter | Measurement Error | Measurement Error (%) | NN Virtual Sensor Error | NN Virtual Sensor Error (%) |
|---|---|---|---|---|
| Torque (ft-lbf) | 23.21 | 4.38 | 24.75 | 4.67 |
| HC (g/h) | 0.47 | 1.17 | 1.50 | 3.76 |
| CO (g/h) | 16.58 | 1.04 | 24.12 | 1.51 |
| $CO_2$ (g/h) | 1648 | 1.50 | 2219 | 2.02 |
| NOx (g/h) | 14.91 | 1.86 | 25.81 | 3.31 |
| PM (g/h) | 3.09 | 4.41 | 2.69 | 3.85 |
| OP (%) | 0.48 | 2.26 | 0.47 | 2.24 |

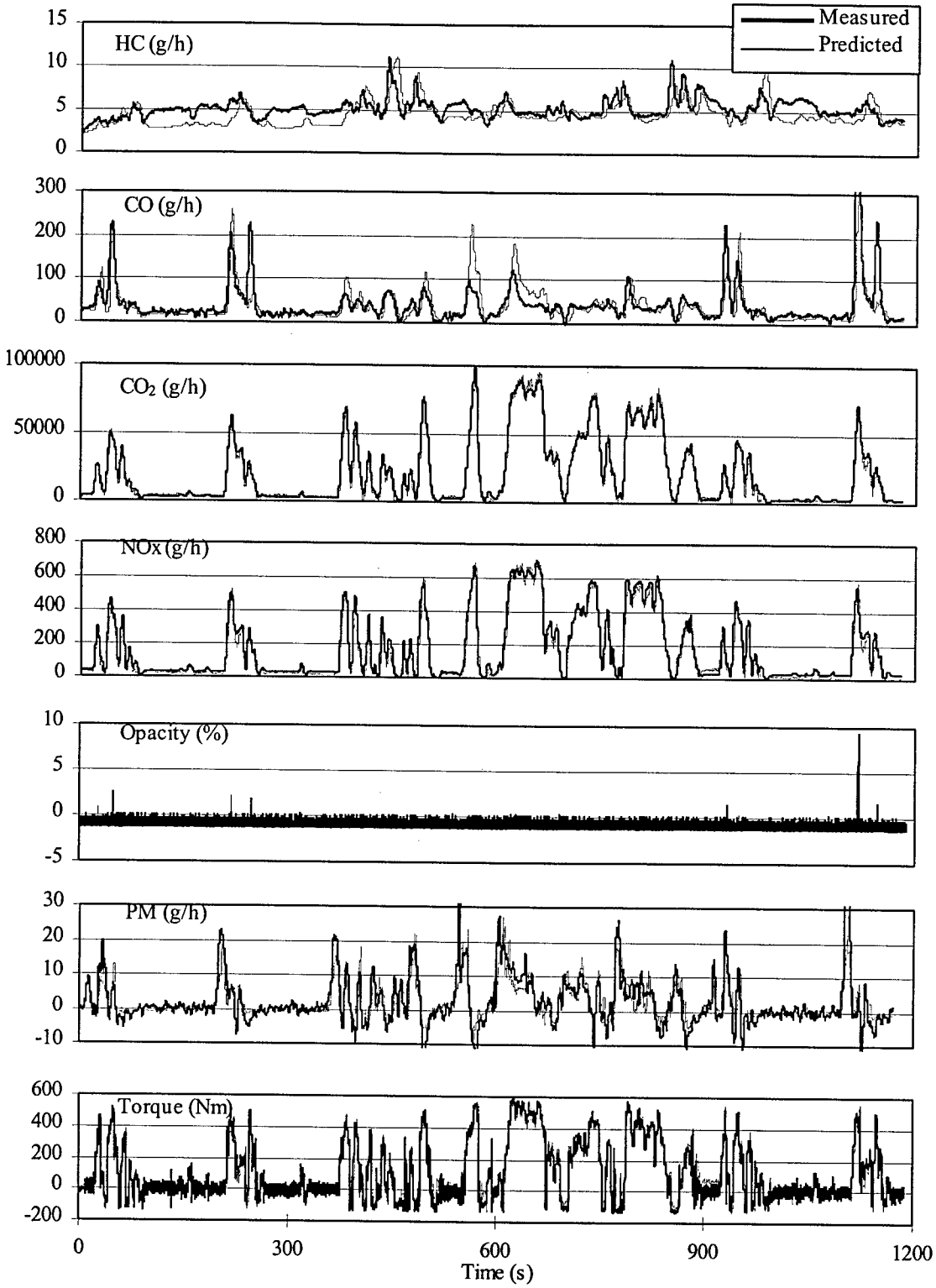


**Figure 1: Predicted versus Measured Performance and Emissions from a Navistar T444 Direct Injection Engine, as tested over the FTP.**

# ABSTRACTS OF WORK UNITS NOT PRESENTED AT THE MEETING

# FUNDAMENTALS OF SOOT FORMATION IN GAS TURBINE COMBUSTORS

AFOSR Contract F49620-98-C-0008

Principal Investigators: M. B. Colket, R. J. Hall, D. Liscinsky and M. Smooke

United Technologies Research Center and Yale University
Silver Lane, E. Hartford, CT 06108 New Haven CT

## SUMMARY/OVERVIEW:

The overall objectives of this work are to obtain necessary fundamental data and to enhance and then validate modeling procedures in order to support modeling of soot production in practical gas turbine combustors. Several focused tasks of this effort include (1) extending measurements of surface growth rate constants to high temperatures, characteristic of rich zones in advanced combustors; (2) modeling of steady, laminar diffusion flames with different fuels to assist in validating the models; (3) advancing the modeling capabilities for describing known physical processes involved in soot production, including carbonization, ageing, and aggregate formation to enable more reliable extrapolation of existing models; and (4) modeling of sooting, transient flames to offer some physical understanding of processes controlling soot formation and destruction in turbulent, diffusion flames.

This year, progress in several areas will be described. First, a brief update of the experimental measurements of surface growth rates is presented. Then subjects related to model advancement are discussed. Some concerns of our prior modeling efforts include (a) limitations in our inception model and (b) an inability to treat non-spherical particles. A separate concern has been the size of the problem that could be considered due to computational restrictions. This latter limitation has recently been resolved due to some new computer acquisitions, with thanks to AFOSR, Yale University and United Technologies Corporation.

### Measurements of Surface Growth Rates at High Temperatures

An important parameter for the prediction of soot production is the surface growth rate. Virtually all fundamental and reliable measurements of this parameter have been obtained over the temperature range of 1500-1950K. Yet for high performance gas turbine combustors the 'sooting' rich zone will be at temperatures well in excess of 2000K. To provide the needed data, a series of fuel-rich, laminar premixed flames are being examined, analogous to several previous studies (see for example, Ref. 1-2) in lower temperature flames. Our efforts, thus far, have been to confirm and validate the experimental methods. Several different methods are being used for particle characterization. Measurements of primary particle size and degree of agglomeration are being made using a computer controlled pneumatic sampling system. This system momentarily inserts a carbon-coated standard 3mm-diameter microscope grid into the flame, which collects particles by thermophoresis. After the grids are exposed for 10 to 30 ms they are examined at 36,000X using transmission electron microscopy (TEM). Samples have been acquired at six

heights in ethylene/oxygen/argon flames with C/O ratios of 0.56 and 0.80. As expected, an increase in degree of agglomeration is observed as a function of height and stoichiometry.

Soot volume fraction is being measured by laser extinction and by thermocouple particle densitometry (TPD). The standard extinction technique, consisting of a chopped HeNe laser beam directed through the flame and monitored with a phase sensitive detector, was used to obtain measurements of soot volume fraction as a function of height for the reference flames. Results are consistent with absorption levels inferred from studies (3) of similar flames. Soot volume fraction as determined using TPD relies on measuring the junction time-temperature history of a fine wire thermocouple rapidly inserted into the flame. The corresponding temperature curve is then fit to a description of the thermophoretic mass transfer (4-5). These results are generally consistent with those from laser extinction.

**PAH/Inception Modeling**

A noticeable discrepancy between our previous model predictions and the experimental data for both the coflow methane and ethylene flames is the underprediction of soot mass along the centerline of the burner. In the case of the methane flame, this discrepancy may be partly explained by low predicted temperatures, but this cannot be argued in the ethylene flame for which our flame model describes the structure, temperatures and gas-phase species concentrations quite well. We believe that the soot growth process along the centerline represents a stretched out version of processes occurring elsewhere in the flame, with a focus on the PAH growth, inception and carbonization, prior to surface growth. Hence, it is desirable to develop a better understanding of the controlling processes of PAH formation and inception along the centerline of the burner. We have explored the possibility that alternative mechanisms contribute to PAH growth. We have compared a variety of PAH growth mechanisms, based on steady-state assumptions of intermediate species and using the computed species profiles from the work described in Refs. 6 and 7. Relative to the net rate of the reaction sequence initiated by phenyl addition to acetylene to form phenylacetylene as described in Ref. 8, we have examined processes initiated by combination of toluene and propargyl, of two cyclopentadienyl radicals, of vinylidene and benzene, and of toluene and phenyl. Of the computed rates for these reaction sequences, none compared favorably with that for original mechanism, except for the toluene reactions in the methane flame. An alternative mechanism that we are exploring is one recently proposed by Moriarty, et al (9) and involves hydrogen migration in the ethenyl-benzene radical. While the net rate of this reaction sequence is still slow near the flame front, its net rate is faster than the original growth mechanism along the centerline of the burner. The total reaction rates are much slower along the centerline (than near the flame front) but longer residence times along the centerline may allow for a slow growth of polyaromatic hydrocarbons.

**Soot Aggregate Modeling**

The extension of the sectional soot formation model to describe the formation of soot aggregates has progressed considerably, and its application to premixed flames has been studied in a preliminary way. The previous model dealt only with coalescing soot spheroids, and was not capable of describing the observed tendency of soot particles to form aggregates of small primary spheroids late in the soot growth process. The new computer model, which is based on an extension of the DISGLOM model (10-11), represents a significant increase in calculational sophistication. The aggregation process is important in soot formation because it affects the particle surface area available for growth, and it is now possible with these improvements in the

algorithm to have a much more realistic description of the growth process. Three types of particles are now treated: incipient or nascent particles which are placed in one or more discrete bins, liquid-like coalescing spheroids which are placed in sectional bins in a way similar to the previous model, and solid sections which consist of chain-like aggregations of small primary particles. The transition from liquid to solid particles occurs at a particle diameter which is an input item. The DISGLOM code did not have provision for surface growth and oxidation arising from gas phase species, and coefficients for these processes were added. Problems with the primary particle balance in the original program were also corrected. Within an aggregate section particles of differing primary particle populations are allowed, but all primary particles within a bin are assumed to be the same size. These primary particles can grow by the conventional acetylene-driven surface growth processes, and also by coalescence with the smaller liquid particles. All collisional processes are now modeled as coalescence or coagulation processes with sticking probabilities that can be independently specified, and there is provision for continuum effects, so the program will be valid for high pressure soot growth as well. It is possible to specify a maximum primary spheroid size beyond which all growth processes affecting the primary spheroids are shut off. This feature represents a heuristic start to modeling surface ageing effects and the tendency of primary spheroids to reach maximum sizes that are largely independent of the type of flame and fuel.

The aggregate model features are illustrated with an application to the premixed ethylene flames of Harris and Weiner (3). In previous studies of these flames (12) profiles of temperature, velocity, and growth/oxidation species concentrations were generated using CHEMKIN. These profiles have now been used to generate new soot growth predictions for these flames on a post-processing basis, assuming that soot growth scrubbing of gas phase species and temperature depression by radiative loss are small. The previous studies were based on the assumption that benzene formation determined the rate-limiting step in nucleation; these calculations are based on the newer nucleation model in which a two ring aromatic species of mass 127 a.mu. ($C_{10}H_7$) is the nucleation species (see Ref. 8). One discrete bin of this mass was included. Five liquid bins terminating at $D_0$ =10 nanometers diameter, where solidification was assumed to begin, were included, followed by seven aggregate bins terminating at a sphere-equivalent diameter of about 1000 nanometers. Two flames were modeled, with C/O ratios of 0.80, and 0.94, as shown in Figure 1. A surface growth rate was employed that is consistent with that reported in Ref. 3. The simulations were first carried out assuming no restriction on the size $D_m$ of the primary spheroids. Significant divergence is observed between experiment and theory in the richer flame beginning at the point where aggregates start to occur, with the model significantly over predicting at the top of the flame. This arises because with solid aggregates no surface area destruction occurs as a result of coagulation, unlike the case for liquid-like particles. For the solid aggregates, surface area increases due to acetylenic surface growth, and the volume fraction grows more rapidly than is observed. The decay of surface growth rate with decreasing temperature at the top of the flame (31.8 kcal activation energy assumed) is insufficient to explain the fall-off in growth. When a more realistic limit on the size of the primary spheroids is imposed ($D_m$ = 20 nanometers), growth is observed to terminate in a way more consistent with experiments. The discontinuity in the growth curves arises from the unrealistic assumption that surface growth truncates sharply at $D_m$ = 20 nanometers; in reality there would be a smoother variation with primary particle diameter. For the C/O=0.80 flame the effects are less pronounced because the particles remain predominately in the liquid sections, with the aggregation effects less important. While the agreement with experiment is not perfect, it is felt to be reasonable in

view of the uncertainties surrounding the spheroid size at which aggregation begins, and the way surface reactivity decays with particle age.

**Planned Work in Modeling of Soot Formation in Diffusion Flames**

Following the work in modeling opposed jet diffusion flames (see Ref. 6-7), we are in the process of code modifications to include such effects as a revised PAH/inception model and agglomeration phenomenon. Just recently, new CPU capabilities have become available to us enlarging the size of the problem that can be considered. We will be shortly be testing out effects such as the sensitivity of the soot solution to the number of soot bins as well as relaxing the assumption of no agglomeration. New problems to be considered include the Santoro flame and variety of perturbations to this flame.

**References**


1. S. Harris, A. Weiner and R. Blint, Combust. Flame **72**, 91 (1988). And references contained therein.
2. P. Sunderland and G. Faeth, C&F **105**, 132 (1996).
3. S.J. Harris and A.M.Weiner, Combustion Science and Technology, **32**, p. 267 (1983).
4. A. D. Eisner and D. E. Rosner, Combust. Flame **61**, 153 (1985).
5. C. S. McEnally, U. O. Koylu, L. D. Pfefferle, and D. E. Rosner, Combust. Flame, **109**, 701 (1997).
6. M. Smooke, C. McEnally, L. Pfefferle, R. Hall, and M. Colket, Combust. Flame, **117**, 117 (1998).
7. C. McEnally, A. Schaffer, M. Long, L. Pfefferle, M. Smooke, M. Colket, and R. Hall, Twenty-Seventh Symposium (International) on Combustion, The Combustion Institute, Pittsburgh, 1497 (1998).
8. R.J.Hall, M.D.Smooke, and M.B.Colket, in *Physical and Chemical Aspects of Combustion, A Tribute to Irvin Glassman* (F.L.Dryer and R.F.Sawyer, Eds.), Gordon and Breach, Amsterdam, (1998)
9. N. Moriaty, N. J. Brown, M. Frenklach, Presentation at the Joint Meeting of the US Sections, Washington, D.C., March (1999).
10. J.J. Wu, Doctoral dissertation, Cal Tech, Pasadena (1986).
11. S.N. Rogak, Doctoral dissertation, Cal Tech, Pasadena (1991).
12. M.B.Colket and R.J.Hall, *Proceedings of the International Workshop on Mechanisms and Models of Soot Formation* (H.Bockhorn, Ed.), Springer-Verlag, Heidelberg, (1994).


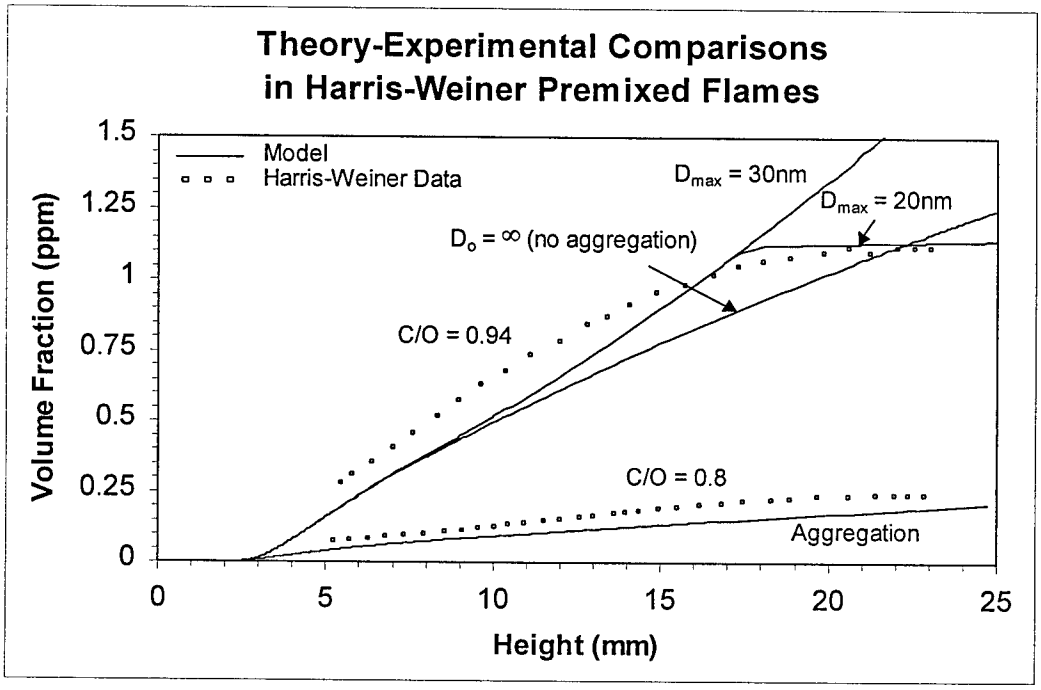

# ADVANCED SUPERCRITICAL FUELS

AFOSR Task # 93WL002

Principal Investigators: Tim Edwards, Jim Gord, Mel Roquemore

Air Force Research Laboratory
AFRL/PRSF Bldg 490
1790 Loop Rd N
Wright Patterson AFB, OH 45433-7103

## SUMMARY/OVERVIEW:

Increases in aircraft and engine performance are increasing the heat load being transferred into an aircraft's primary coolant--the fuel. This research is aimed at understanding the limitations of operation of fuel heated to 480 C (900 F) and beyond. Important issues are expected to be thermal stability, heat transfer/flow instabilities, and injection/combustion properties.

## TECHNICAL DISCUSSION

For fuels that are heated to 900 F and above in use, two pathways of deposit formation are important: thermal-oxidative up to about 600 F (300 C), and pyrolytic above about 800 F (400 C). One fuel target application is "JP-8+225", a JP-8 based fuel that has a thermal stability limit 225 F above JP-8, equivalent to JP-7 (550 F) [1]. The primary obstacle to the use of JP-8+225 is thermal-oxidative degradation. Studies of fuel oxidation and deposition continue [2-5], which have led to several options for reducing fuel deposition from 550 F fuels: high concentrations of dispersants to prevent solid agglomeration/coagulation and hydroperoxide decomposers and other additives to break the fuel oxidation chain reactions [6,7]. Both of these options have shown some success in small-scale research devices (e.g., see Figure 1), but have not been as successful in larger rig tests (e.g., [8-10]). Efforts continue to understand the chemical and physical differences between the various tests, in order to identify the best avenue for deposit reduction. Efforts are also underway to understand a recently identified small subset of JP-8 fuels that create little surface deposits but relatively heavy suspended (bulk) deposits. These deposits clog filters and interfere with fuel controls at high temperatures. Thermal-oxidative fouling modeling efforts also continue [11-15], with a notable result being the ability to predict the effects of mixtures of fuels of varying qualities (Figure 2)[12]. Note the non-linear behavior shown in Figure 2, where the addition of a "good" fuel to a "poor" fuel initially creates larger deposits. This phenomenon is due to the complex interaction between the fuel chain oxidation reactions and the complex, heteroatomic "natural anti-oxidants" present in poor fuels, which slow oxidation but increase deposits. Two significant challenges that remain in the modeling effort are (1) accurately representing the effect of the presence of detergent/dispersant additives, and (2) determining how to account for the wide variations in thermal stability among JP-8 fuels

in field use. Surrogate fuels have been identified that simulate multi-component aviation fuels with a more computationally-tractable number of species [15]. Pyrolytic fouling studies also continue [16-19]. The similarity between the molecular growth that leads to gas phase soot formation and the molecular growth that leads to pyrolytic deposit formation in the supercritical phase (inside the fuel system) is becoming more evident. Supercritical reaction pathways in multi-component fuels are consistent with those identified by Princeton in simpler fuel mixtures [22], where a "caging" effect modifies the reaction pathway under supercritical conditions.

For limited life applications (missiles, rockets), fuels with higher density and higher energy than typical kerosene fuels have important applications. An area that has seen only limited research here is the thermal stability of high energy and/or high density fuels. When used in regeneratively cooled applications, such as high speed vehicles and rockets, the thermal stability of the fuels (inside the cooling passages of the vehicle) becomes important [20]. Because of the expense and availability of these compounds, we have begun the study of the cooling behavior of these fuels in a small-scale, high pressure research flow reactor: the System for Thermal Diagnostic Studies (STDS) [21]. This flow reactor is similar in concept to the Princeton flow reactor [22], and is a high-pressure modification of an instrument that dates back to the 1980's. Initial results show high density fuel JP-10 to be of similar thermal stability to the current kerosene rocket fuel RP-1, while high (strain) energy quadricyclane apparently undergoes isomerization and polymerization reactions at significantly lower temperatures and forms deposits (Figure 3). This is a concern for regeneratively-cooled vehicles, and needs to be followed up on larger-scale test devices under more realistic conditions. Note that the low H/C ratio in high energy fuels tends to cause combustion difficulties also [23]. Efforts continue to follow fuel degradation reactions in situ under high pressure, high temperature conditions [24,25].

[1]. Edwards, T., "Prospects for JP-8+225, A Stepping Stone to JP-900," AIAA 98-3532.

[2]. Balster, W.J., Jones, E. G., "Effects of Temperature on Formation of Insolubles in Aviation Fuels," ASME-97-GT-218, ASME Journal of Engineering for Gas Turbines and Power, Vol. 120(2) pp. 289-293, 1998.

[3]. Pickard, J. M., Jones, E. G., "Liquid-Phase Oxidation Kinetics: Paraffin Blends," Energy & Fuels, Vol. 12(6), pp. 1241-1244, 1998.

[4]. Jones, E. G., Balster, L. M., Balster, W. J., "Autoxidation of Neat and Blended Aviation Fuels," Energy & Fuels, Vol. 12(5), pp. 990-995, 1998.

[5]. Zabarnick, S., Whitacre, S. D., "Aspects of Jet Fuel Oxidation," ASME-97-GT-219, ASME Journal of Engineering for Gas Turbines and Power, Vol. 120(3) pp. 519-525, 1998.

[6]. S. Zabarnick, M. S. Mick, R. C. Striebich, and R. R. Grinstead, "Model Studies of Silylation Agents as Thermal-Oxidative Jet Fuel Additives," *Energy and Fuels*, Vol. 13, pp. 154-159, 1999.

[7]. S. Zabarnick and M.S. Mick, "Studies of Hydroperoxide Decomposing Species for Inhibiting Oxidation in Jet Fuels," ACS Petroleum Chemistry Division Preprints, Vol. 43(3), pp. 349-352, 1998.

[8]. Dieterle, G., Binns, E., and Morris, R., "Evaluation of JP-8+100 Additives in Large Laboratory Test Systems," AIAA Paper 98-3531

[9]. Ervin, J.S., Williams, T., and Hartman, G., "Flowing Studies of Jet Fuel at Supercritical Conditions," AIAA Paper 98-3760.

[10]. J.S. Ervin, T.F. Williams, and G. Hartman, "Effect of Test Period on the Rate of Fouling in a Complex Flowing System," ACS Petroleum Chemistry Division Preprints, Vol. 43(3), pp. 373-377, 1998.

[11]. Ervin, J. S., Heneghan, S. P., "The Meaning of Activation Energy and Reaction Order in Autoaccelerating Systems, ASME-97-GT-224, ASME Journal of Eng. for Gas Turbines and Power, Vol. 120(3) pp. 468-473, 1998.

[12]. Katta, V. R., Jones, E. G., Roquemore, W. M., "Modeling of Deposition Process in Liquid Fuels," Combustion Science and Technology, Vol. 139, pp. 75-111, 1998.

[13]. S. Zabarnick, "Pseudo-Detailed Chemical Kinetic Modeling of Antioxidant Chemistry for Jet Fuel Applications," Energy & Fuels, Vol. 12(3), pp. 547-553, 1998.
[14]. Ervin, J. S., Zabarnick, S., "Computational Fluid Dynamics Simulation of Jet Fuel Oxidation Incorporating Pseudo-Detailed Chemical Kinetics," Energy and Fuels, Vol. 12, pp. 344-352, 1998.
[15]. Edwards, T., Maurice, L. Q., "Surrogate Mixtures to Represent Complex Aviation and Rocket Fuels," AIAA Paper 99-2217, July 1999.
[16]. L. Maurice, L., Striebich, R., Edwards, T., "Formation of Cyclic Compounds in the Fuel Systems of Hydrocarbon High Speed Vehicles," AIAA Paper 98-3534.
[17]. J. C. Sheu, E. G. Jones and V.R. Katta "Thermal Cracking and Fouling of Norpar-13 Fuel under near-critical and supercritical conditions," AIAA 98-3758.
[18]. L.Q. Maurice and R.C. Striebich, "Cyclic Species Formation in the Fuel Systems of High-Speed Vehicles," ACS Petroleum Chemistry Division Preprints, Vol. 43(3), pp. 423-427, 1998.
[19]. Minus, D. K., Corporan, E., "Deposition Effects of Radical Stabilizing Additives in JP-8 Fuel," ," ACS Petroleum Chemistry Division Preprints, Vol. 43(3), pp. 360-363, 1998.
[20]. Maurice, L. Q., Edwards, T., Griffiths, J., "Liquid Hydrocarbon Fuels for Hypersonic Propulsion," invited chapter in AIAA Progress series volume "Scramjet Propulsion", Curran and Murthy, eds.
[21]. Striebich, R. C., Rubey, W. A., "High Pressure, High Temperature Pyrolysis Reactions in the Condensed Phase with In-Line Chemical Analysis," ACS Petroleum Chemistry Div. Preprints, Vol. 43(3), pp. 378-381, 1998.
[22]. Stewart, J., Brezinsky, K., Glassman, I., "Supercritical Methylcyclohexane Pyrolysis: A Flow Reactor Study," ," ACS Petroleum Chemistry Division Preprints, Vol. 43(3), pp. 433-437, 1998.
[23]. Gupta, S. B., Ni, T., Santoro, R. J., "Reduction of Soot Formation in High Energy Density Fuels," CPIA Publication 631, Vol. II, 10/95 JANNAF Combustion Meeting.
[24]. Bunker, C. E., Gord, J. R., Grinstead, K. D., "Spectroscopic Investigations of High-Temperature, High-Pressure Model Aviation Fuels," ," ACS Petroleum Chemistry Division Preprints, Vol. 43(3), pp. 467-470, 1998.
[25]. Steven W. Buckner, Robert A. Forelines, and James R. Gord, "Liquid-Phase Thermometry Based on Fluorescence Lifetimes of Intramolecular Excimers," Appl. Spectrosc. **53**, 115 (1999).

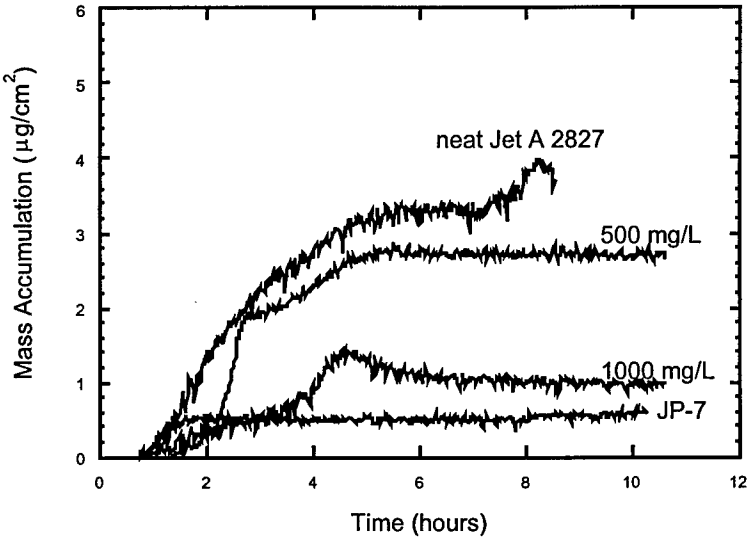


Figure 1 – Quartz crystal microbalance [5] results for two dispersant concentrations. JP-8+100 includes about 200 ppm of this dispersant.

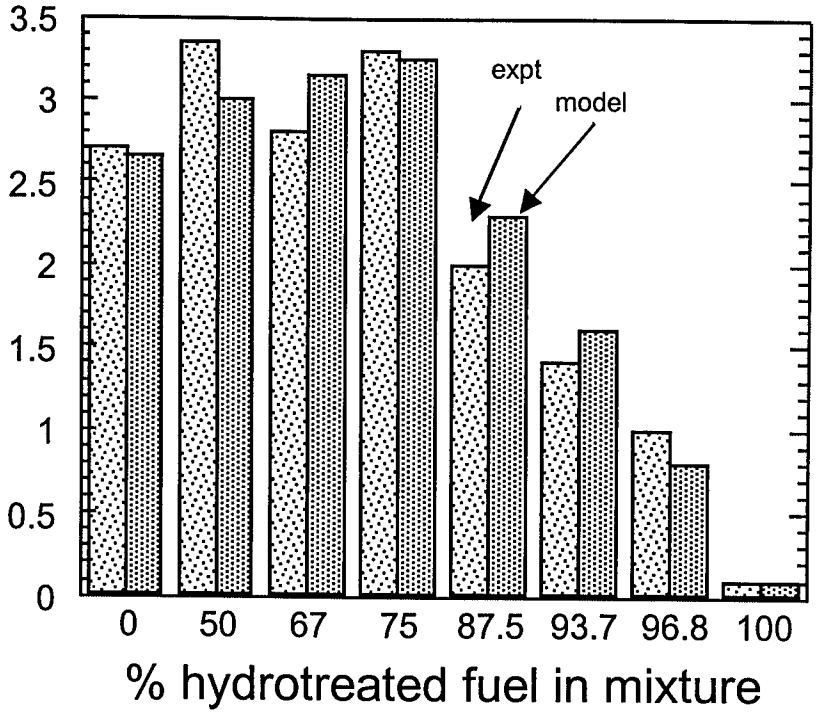


Figure 2 – Model comparison to experim. data for mixtures of two fuels of varying quality [12].

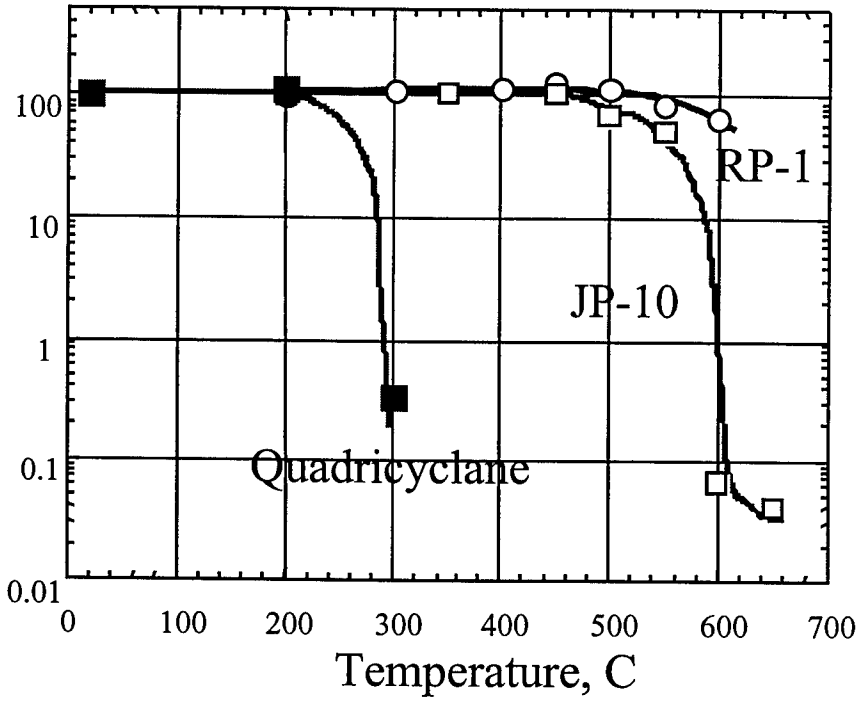


Figure 3 – STDS [21] fuel decomposition results. Conditions: 1.8 sec residence time, 500 psi, deoxygenated fuel.